

Dear editors,

We would like to thank the referees for their careful reading and highly valuable comments that substantially help to raise the quality of our paper. We have made every effort to address their comments and made necessary revisions to the manuscript. Please see below our point-by-point response to referees' comments.

For clarity, referee comments are shown in *italic font*; the response to the comments are shown in **blue color**, the notes and explanations for the changes in the manuscript are shown in **blue with underlines**; the revised contents in the manuscript are shown in **green color**. Our line numbers refer to the updated manuscript, not the original. Detailed corrections can be found in this file after our responses.

Referee #1

General Comment:

This study reports the ice nucleation abilities of three different types of black carbon (BC) particles at thermodynamic conditions relevant to cirrus clouds. The importance of different physicochemical properties such as morphology, size, and SOA coating on the ice nucleation of bare BC particles was evaluated. This is a very interesting topic that nicely fits with the ACP scope. The experiments were carefully performed and the manuscript is well written. The manuscript can be accepted for its publication after the following points are properly addressed.

We thank this referee for accurately summarising and affirming our work. Below, the referee outlines major concerns on our toluene SOA coating experiment data interpretation and SOA coating experiments data representation. We have made substantial revisions which we believe properly address the referee's concerns.

Major comments:

1. From the data shown in Figure 5a, it is concluded that the highly oxidized toluene SOA-coated BC (T-10) reports similar onsets as the bare BC particles. However, it is shown that the slightly oxidized toluene SOA-coated BC (T-3) deactivate the BC particles reporting higher SSI values. A clear explanation about this is missing and needs to be provided.

[Response]: Inferred from the AMS spectra in Fig. 6 and the O/C-H/C in Fig. 7, both T-10 and T-3 coating experiments generated highly oxidized SOA, among which a significant fraction of oligomers might present and induce IN below homogeneous freezing threshold, as stated between L406-431. However, the fraction of oligomers and their phase state cannot be determined from current experiments and data. We can just infer potential SOA formation pathway from the mass spectra and O/C-H/C diagrams. This could be an interesting topic to investigate in future studies since toluene is one of the dominant anthropogenic aromatic emission species. Therefore, we added "BC coated by ~10-15 equivalent days atmospherically

oxidized toluene SOA (*T-3* in Table 2) is less IN active than those coated by highly oxidized toluene SOA (*T-10*) at around -46 °C and -43 °C. This might also be attributed the oxidation level and the corresponding phase state difference between the SOA generated from *T-10* and *T-3* experiments, which is beyond the scope of this study and requires further detailed phase transition study for toluene SOA.” between L422-426. Besides, we tune down the temporary conclusion drawn at the end of this paragraph. More detailed information can be found in the following point-by-point response. The text in Sect. 4 and 5, as well in abstract has been rephrased accordingly.

L406-429: “The higher O/C ratio (Fig. 7) of toluene-derived SOA may enhance the hygroscopicity of the particle (Lambe et al., 2011b; Zhao et al., 2016; Liu et al., 2018) with a potential to form aqueous film on BC surface and reduce the IN ability of BC particles. On the other hand, Hinks et al. (2018) showed that toluene-derived SOA contained a significant amount of oligomers under dry laboratory conditions similar to what we conducted in the PAM chamber in this study. Volkamer et al. (2001) proved that glyoxal, which could facilitate the oligomerization as described by Hinks et al. (2018), can be produced from toluene reaction with OH as highly oxidized products. The slopes of *T-10* and *T-3* in Fig. 7 lie between 0-1 (0.71 and 0.99 for *T-10* and *T-3*, respectively), suggests that oxygen and hydrogen atom addition accompanied by carbon-carbon double bond as well as benzene ring breakage might have happened during the toluene photooxidation experiments. These large oligomers could potentially reduce the hygroscopicity and alter the phase state of toluene SOA to be semi-solid or solid within the temperature range we investigated in this work (DeRieux et al., 2018; Zhang et al., 2018c; Li et al., 2020), under which the SOA can still nucleate ice (Murray et al., 2010; Berkemeier et al., 2014; Zhang et al., 2019b). The toluene SOA in *T-10* with O:C ratio over 1 (Fig. 7) has most likely already transited into solid or semi-solid glassy state at the temperature range we investigated before entering SPIN (DeRieux et al., 2018). Therefore, it is very likely that BC particles are mostly stucked with or embedded in these glassy SOA with some bare BC part exposure. Ice crystals may therefore form on the carbonaceous part of partially coated particles, whose IN onset SS_i should be the same as bare COJ300. At temperatures above -43 °C, toluene SOA-coated BC particles nucleate ice at $SS_i \sim 0.1$ to 0.15 above bare 350 nm COJ300, but still ~ 0.15 below the homogeneous freezing threshold. This might be due to the hygroscopicity enhancement of the toluene SOA-coated BC in *T-10*. BC coated by ~ 10 -15 equivalent days atmospherically oxidized toluene SOA (*T-3* in Table 2) is less IN active than those coated by highly oxidized toluene SOA (*T-10*) at around -46 °C and -43 °C. This might also be attributed the oxidation level and the corresponding phase state difference between the SOA generated from *T-10* and *T-3* experiments, which is beyond the scope of this study and requires further detailed phase transition study for toluene SOA. Overall, two competing effects, i.e. the hygroscopicity enhancement deactivating BC IN ability, together with toluene SOA glass phase transition producing stucked or partly coated BC, may make our toluene SOA coating IN onset move towards but not fully in the homogeneous freezing regime. The toluene SOA coated diesel combustion BC (Kulkarni et al., 2016), however, nucleate ice near the homogeneous threshold, as indicated in Fig. 3(a). This might be due to the much thicker (90 nm) organic coating in their study compared to the 25 nm coating of this work, leading to a complete coverage of BC surface.”

2. In Figure 5 important data is not reported. This information is needed to support the conclusions. a) missing bare BC data above -43°C ; b) missing bare BC data at -40°C , missing D-10 data at -40°C , missing D-3 data below -43°C ; and c) missing bare BC data at -40°C , and missing B-0 data below -44°C .

[Response]: The missing bare BC data in Fig. 5(a) is blocked by the legend. Fig. 5(a) has been modified and the bare BC data above -43°C is now visible.

For consistency, the IN onset was determined from consecutive RH scans. The missing SOA coating experiment data in Fig. 5(b) and 5(c) were excluded on purpose due to instrument issues, such as SPIN inlet clog at the end of the day, during these experiments.

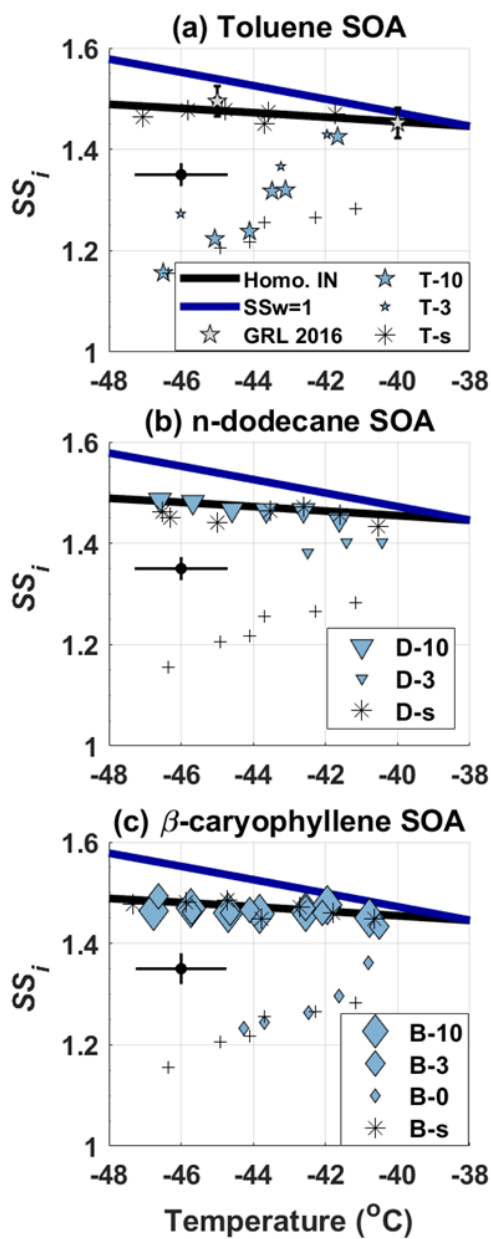


Figure R1 1 Modified Fig. 5

Minor comments:

Line 31: Add "coated BC" after "SOA".

[Response]: Added as suggested.

Lines 32-33: "OH exposure levels of all SOA coating experiments, from an equivalent atmospheric 10 days to 90 days, did not render significant differences in IN potential". This is not true for Toluene SOA.

[Response]: The word ‘all’ has been replaced by “*n*-dodecane and β -caryophyllene”. Besides, we added “Slightly oxidized toluene SOA coating seemed to have a stronger deactivation effect on BC IN ability than highly oxidized toluene SOA, which might be caused by oligomer formation and phase transition of toluene SOA under different oxidation levels.” between L31-32.

L35-36: “OH exposure levels of *n*-dodecane and β -caryophyllene SOA coating experiments, from an equivalent atmospheric 10 to 90 days, did not render significant differences in IN potential.”

Line 62: I suggest to add some key studies in this topic instead of P&K.

[Response]: Reference modified. Added “which is also confirmed by recent heterogeneous IN experiments with various INPs (e.g., Welti et al., 2009; Lüönd et al., 2010; Marcolli, 2014; Mason et al., 2016; Mahrt et al., 2018; Nichman et al., 2019)” after the P&K reference.

IN studies (e.g., Welti et al., 2009; Lüönd et al., 2010; Mason et al., 2016; Mahrt et al., 2018; Nichman et al., 2019) focusing on size effect of ice nucleating particle (INP) have been added.

L69-71: “It is widely acknowledged that larger particles act as more efficient INPs (e.g., Pruppacher and Klett, 2010), which is also confirmed by recent heterogeneous IN experiments with various INPs (e.g., Welti et al., 2009; Lüönd et al., 2010; Marcolli, 2014; Mason et al., 2016; Mahrt et al., 2018; Nichman et al., 2019).”

Line 63: "ice nucleation".

[Response]: Added “ice” before “nucleation”.

We meant to refer to a wider range of nucleation studies apart from ice nucleation because the surface area and active sites theory is a widely accepted nucleation theory in phase transition field with various working fluids other than water here. Since we are talking about ice nucleation in this paper, it is more appropriate and concise to add ice.

Line 64: I suggest to add some key studies in this topic instead of the cited review paper.

[Response]: Reference modified. Rephrased to “Although the mechanism remains uncertain, one common theory is that ice nucleation probability and rate are positively correlated to particle surface area active sites density (Fletcher, 1960, 1969); therefore, an empirical parameter that is relevant to particle size (e.g., Connolly et al., 2009; Kiselev et al., 2017)”.

The classical ice nucleation active sites papers (Fletcher, 1960, 1969) and the surface active sites-particle size correlation papers (e.g., Connolly et al., 2009; Kiselev et al., 2017) have been added.

L71-74: “Although the mechanism remains uncertain, one common theory is that IN ability and rate are positively correlated to particle surface active sites density (Fletcher, 1960, 1969), an empirical parameter that is relevant to particle size (e.g., Connolly et al., 2009; Kiselev et al., 2017).”

Line 88: Add a reference after "weeks".

[Response]: Added (Cape et al., 2012; Lund et al., 2018). Also added “or even months in the tropopause (Pusechel et al., 1992; Yu et al., 2019)”.

L99-101: “These particles can remain suspended in the atmosphere for days to weeks (Cape et al., 2012; Lund et al., 2018), or even months in the tropopause (Pusechel et al., 1992; Yu et al., 2019)...”

Line 89: Can the authors add an older study in addition to Kulkarni et al. (2016).

[Response]: Added (Jacobson, 2001; Zhang et al., 2008; China et al., 2015b; Kulkarni et al., 2016; Zhang et al., 2018b).

L101-103: “...as well as oxidation, can lead to complex secondary organic aerosol (SOA) coatings (Jacobson, 2001; Zhang et al., 2008; China et al., 2015b; Kulkarni et al., 2016; Zhang et al., 2018b).”

Line 102: It should be "-38°C".

[Response]: Corrected.

Line 114: Add a reference after "combustion".

[Response]: Added reference for R2500U (Joyce and Henry, 2006) and Cabot safety datasheet for R330R (Cabot, 2020)().

L126-127: “R2500U and R330R are carbonaceous black pigment powder generated by incomplete combustion (Joyce and Henry, 2006; Cabot).”

Lines 133-134: "β-caryophyllene has been found to be one of the most atmospherically abundant sesquiterpenes". Does it also apply to the upper troposphere (the focus of the present study)? What is its typical concentration at such high altitudes?

[Response]: There is no direct β-caryophyllene observation data available in the tropopause to the authors’ knowledge. However, there is one field observation of β-caryophyllene SOA presence at 1534 m, with a terpene organic carbon concentration of about 0.6 μg m⁻³ (Fu et al., 2009). Besides, previous field studies found that a considerable fraction of ambient organic aerosol is composed of β-caryophyllene SOA (Hu et al., 2008), and the concentrations are highly temperature sensitive (Arey et al., 1991; Helmig et al., 2006; Sakulyanontvittaya et al., 2008),

i.e., tropical areas with stronger convection also have higher β -caryophyllene emission. Therefore, it is reasonable to infer that the strong updrafts in tropical areas or during summer times might bring a significant amount of β -caryophyllene to the upper troposphere or lower stratosphere. Moreover, the β -caryophyllene concentration used in our experiments (2300/5000 PPB) is in line with that used in previous studies (190-200000 ppb) (Grosjean et al., 1993; Jaoui et al., 2007; Jaoui et al., 2013).

L149-157: “Terpenes are biogenic organics emitted by plants, among which β -caryophyllene has been found to be one of the most atmospherically abundant sesquiterpenes originating from agricultural plants and pine trees, as well as other sources (Arey et al., 1991; Ciccioli et al., 1999; Helmig et al., 2006; Sakulyanontvittaya et al., 2008; Guenther et al., 2012; Henrot et al., 2017). Even though the atmospheric abundance of β -caryophyllene is not as significant as other biogenic organics, such as isoprene and α -pinene, its high reactivity towards ozone and hydroxyl radical to form oxidized products with low volatility makes β -caryophyllene an appreciable biogenic SOA source in the atmosphere (Shu and Atkinson, 1995; Calogirou et al., 1997; Hoffmann et al., 1997; Griffin et al., 1999; Helmig et al., 2006; Lee et al., 2006; Jaoui et al., 2007). An up to 7 ng m^{-3} atmospheric concentration of β -caryophyllene tracer during summer time was reported (Jaoui et al., 2007).”

Line 145: *experimental?*

[Response]: Changed to “experimental apparatus”.

Lines 152-154: *"All samples were then neutralized and size selected by a BMI differential mobility analyzer (BMI DMA, Model 2002; Brechtel Manufacturing Inc.) or TSI DMA (Model 3081, Classifier, Model 3082; TSI Inc.) for bare BC and BC-SOA mixing experiments, respectively". Are there any differences in the size selected particles when using the BMI or TSI DMA?*

[Response]: The BMI DMA was used to select 100-400 nm BC particles (i.e., the results showed in Sect. 3.1), while the TSI DMA was used to select 350 nm COJ300 particles during SOA coating experiments (i.e., the results in Sect. 3.2). During the SOA coating experiments, the BMI SMPS was used to confirm the BC size distribution after TSI DMA selection. We consistently used the same experimental apparatus throughout a series of experiments, and therefore the IN onset results shown in Sect. 3.1 and 3.2 are unaffected. Therefore, the difference between size-selected particles is not our concern as long as the particles size distribution peaks around 350 nm.

However, we did calibrate the TSI SMPS and BMI SMPS with 350 nm COJ300 particles. The BMI and TSI SMPSs have been intercompared by scanning 350 nm COJ300. The sheath-to-sample ratio were set to 6:1 for size-selecting DMAs, and the sheath-to-sample ratio were set to 10:1 to perform standard size scans for the SMPSs during instrument intercomparison. There is minor difference between these two systems in terms of particle size selection. The plot below exhibits the instrument intercomparison result.

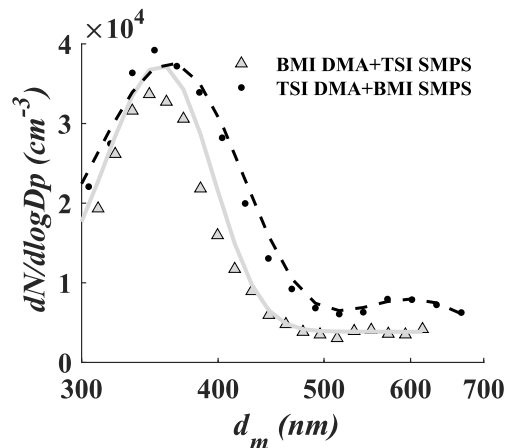


Figure R1 2. Intercomparison of BMI and TSI SMPS by scanning the size distribution of bare 350 nm COJ300.

Line 160: Define "MOUDI".

[Response]: Changed to "Micro-Orifice Uniform Deposit Impactor (MOUDI)".

L185: "...with a Micro-Orifice Uniform Deposit Impactor (MOUDI, Model M135-10; TSI Inc.) ..."

Line 191: "monodisperse BC particles". Based on the data shown in Figures 2 and A3, the particles are not really monodisperse.

[Response]: Changed to "size-selected".

Lines 202-203: Please clarify the type of the AMS used.

[Response]: Changed to "High-Resolution Time-of-Flight Aerosol Mass Spectrometry (HR-ToF-AMS; Aerodyne Research Inc.)".

We used a SP-AMS for SOA coating experiment (Onasch et al., 2012). But only the AMS part was used, i.e. a standard HR-ToF-AMS (DeCarlo et al., 2006). The reference has been modified accordingly.

L232-234: "Chemical composition of the SOA-coated BC particle stream was analyzed online by PALMS and a High-Resolution Time-of-Flight Aerosol Mass Spectrometry (HR-ToF-AMS; Aerodyne Research Inc.). More details about the AMS can be found in literatures (DeCarlo et al., 2006; Onasch et al., 2012), here a brief introduction will be given."

Line 269: Add a reference after "pressure".

[Response]: Added (Borgnakke and Sonntag, 2013; Steane, 2016).

Lines 274-275: "signal (Garimella et al., 2016) was used to classify each particle as an inactivated aerosol or ice crystal over the course of an experiment". Could have liquid droplets been present? How was this evaluated?

[Response]: We have several lines of evidence that allow us to rule out droplet breakthrough during our experiments.

First of all, SPIN was operated in the deposition freezing regime, at temperatures below the threshold for homogeneous freezing and relative humidities below liquid water saturation. Aerosol would therefore be expected to freeze heterogeneously or homogeneously below liquid water saturation.

Secondly, SPIN has an evaporation section before ice crystals entering optical particle counter. The temperature of evaporation section is set so that the droplet will evaporate while ice crystals remain. Besides, the SS_i at which liquid water saturates at our experiment condition is ~1.45-1.57, and liquid droplet breakthrough requires even higher supersaturation beyond the highest SS_i in our experiments (Garimella et al., 2016).

Thirdly, both the laser scattering and polarity signals collected from SPIN OPC were used in this study to train a machine learning algorithm as described in Garimella et al. (2016), to robustly distinguish different phases, as stated between L304-306.

Therefore, we are confident that liquid droplets did not present during our experiments.

Lines 279-281: "SPIN. For the size-selected bare BC experiments, the total particle number concentration was measured by a CPC operating simultaneously with SPIN, while for the SOA coating experiments, the total particle number concentration was integrated from the SMPS measurement." Are there any particle losses during the SMPS analysis?

[Response]: The particle in bins smaller than 200 nm was corrected by using a log-normal fit. We conducted several COJ300 BC scans before injecting organics each day. The difference between integrated SMPS particle concentration during experiments and pure COJ300 BC concentration obtained prior experiments was within $\pm 1\%$.

Lines 285-286: As mentioned above the particles were not truly monodisperse.

[Response]: Panel (b) and (c) of Fig. 3 have been moved to Appendix A and named as Fig. A2 and A3, respectively. Changed the caption of Fig. A3 to "...bare size-selected BC particles with a modal size around 400 nm."

L548-549: "Representative negative-ion PALMS mass spectra of bare size selected (a) R2500U, (b) COJ300, and (c) R330R BC particles with a modal size around 400 nm."

Line 291: Add "(Table 1)" after R2500U.

[Response]: Added as suggested.

Line 308: "The results in Fig. 3A demonstrate that the particle size is relevant to particle IN ability". What has been reported in the literature?

[Response]: Added "ability below homogeneous freezing threshold, consistent with the BC heterogeneous IN ability enhancement triggered by increasing particle size in previous studies (Mahrt et al., 2018; Nichman et al., 2019)".

[The literature discussion was originally placed after the description of our results.](#)

L348-350: “The results in Fig. 3(a) demonstrate that the particle size is relevant to the particle IN ability, consistent with the BC heterogeneous IN ability enhancement triggered by increasing particle size in previous studies (Mahrt et al., 2018; Nichman et al., 2019).”

Lines 346-347: The 350 nm bare BC particles data at temperatures above -43°C on panel a is not shown.

[Response]: Please see our response to the second major comment. The missing bare BC data in Fig. 5(a) was blocked by the legend. Fig. 5(a) has been modified and the bare BC data above -43°C is now visible.

Lines 347-348: The discussed data from the present study was not pure Toluene SOA. It was a mixture of BC/SOA, and the ice nucleation should be attributed to the BC and not the SOA as shown by the pure toluene SOA data. Also, do the authors claim here that all aromatic SOA should behave in the same way?

[Response]: We agree with the referee that our IN data originates from a mixture of bare BC, partially coated BC, fully coated BC, and pure toluene SOA.

The toluene SOA in *T-10* with O:C ratio over 1 (Fig. 7) has most likely already transited into solid or semi-solid glassy state at the temperature range we investigated before entering SPIN (DeRieux et al., 2018). Volkamer et al. (2001) proved that glyoxal, which could facilitate the oligomerization as described by Hinks et al. (2018), can be produced from toluene reaction with OH as highly oxidized products. The slopes of *T-10* and *T-3* in Fig. 7 lie between 0-1 (0.71 and 0.99 for *T-10* and *T-3*, respectively), suggests that oxygen and hydrogen atom addition accompanied by carbon-carbon double bond as well as benzene ring breakage might have happened during the toluene photooxidation experiments. These large oligomers could potentially reduce the hygroscopicity and alter the phase state of toluene SOA to be semi-solid or solid within the temperature range we investigated in this work (DeRieux et al., 2018; Zhang et al., 2018c; Li et al., 2020)

Therefore, it is very likely that BC particles are mostly stucked with or embedded in these glassy SOA with some bare BC part exposure. We hence have modified the discussion statement and attributed the *T-10* IN results to the uncoated bare BC part.

However, slightly oxidized toluene SOA with smaller O:C ratio requires colder glass transition temperature (DeRieux et al., 2018). The toluene SOA generated in *T-3* experiment might still be liquid and entirely enclose BC particles, forming an organic liquid coating film and deactivate BC particles.

The comparison with pure aromatic SOA (Wang et al., 2012) has been modified. Please see the response to major comment #1.

L391-428: “The toluene SOA mass spectrum in Fig. 6(a) exhibits higher $m/z = 44$ (COO^-) and lower $m/z = 43$ (C_3H_7^-) fraction signal, indicating more oxidized organic species were generated during *T-10* and *T-3* experiments (Lambe et al., 2011b), agreeing with the previous study on

toluene SOA (Liu et al., 2018). The higher O/C ratio (Fig. 7) of toluene-derived SOA may enhance the hygroscopicity of the particle (Lambe et al., 2011b; Zhao et al., 2016; Liu et al., 2018) with a potential to form aqueous film on BC surface and reduce the IN ability of BC particles. On the other hand, Hinks et al. (2018) showed that toluene-derived SOA contained a significant amount of oligomers under dry laboratory conditions similar to what we conducted in the PAM chamber in this study. Volkamer et al. (2001) proved that glyoxal, which could facilitate the oligomerization as described by Hinks et al. (2018), can be produced from toluene reaction with OH as highly oxidized products. The slopes of T-10 and T-3 in Fig. 7 lie between 0-1 (0.71 and 0.99 for T-10 and T-3, respectively), suggests that oxygen and hydrogen atom addition accompanied by carbon-carbon double bond as well as benzene ring breakage might have happened during the toluene photooxidation experiments. These large oligomers could potentially reduce the hygroscopicity and alter the phase state of toluene SOA to be semi-solid or solid within the temperature range we investigated in this work (DeRieux et al., 2018; Zhang et al., 2018c; Li et al., 2020), under which the SOA can still nucleate ice (Murray et al., 2010; Berkemeier et al., 2014; Zhang et al., 2019b). The toluene SOA in *T-10* with O:C ratio over 1 (Fig. 7) has most likely already transited into solid or semi-solid glassy state at the temperature range we investigated before entering SPIN (DeRieux et al., 2018). Therefore, it is very likely that BC particles are mostly stucked with or embedded in these glassy SOA with some bare BC part exposure. Ice crystals may therefore form on the carbonaceous part of partially coated particles, whose IN onset SS_i should be the same as bare COJ300. At temperatures above $-43\text{ }^{\circ}\text{C}$, toluene SOA-coated BC particles nucleate ice at $SS_i \sim 0.1$ to 0.15 above bare 350 nm COJ300, but still ~ 0.15 below the homogeneous freezing threshold. This might be due to the hygroscopicity enhancement of the toluene SOA-coated BC in *T-10*. BC coated by ~ 10 - 15 equivalent days atmospherically oxidized toluene SOA (*T-3* in Table 2) is less IN active than those coated by highly oxidized toluene SOA (*T-10*) at around $-46\text{ }^{\circ}\text{C}$ and $-43\text{ }^{\circ}\text{C}$. This might also be attributed the oxidation level and the corresponding phase state difference between the SOA generated from *T-10* and *T-3* experiments, which is beyond the scope of this study and requires further detailed phase transition study for toluene SOA. Overall, two competing effects, i.e. the hygroscopicity enhancement deactivating BC IN ability, together with toluene SOA glass phase transition producing stucked or partly coated BC, may make our toluene SOA coating IN onset move towards but not fully in the homogeneous freezing regime. The toluene SOA coated diesel combustion BC (Kulkarni et al., 2016), however, nucleate ice near the homogeneous threshold, as indicated in Fig. 3(a). This might be due to the much thicker (90 nm) organic coating in their study compared to the 25 nm coating of this work, leading to a complete coverage of BC surface.”

Line 348: "aromatic SOA". Indicate the SOA precursor.

[Response]: The precursor used in (Wang et al., 2012) was naphthalene. We rephrased this paragraph, please see the response to major comment #1 and last comment.

Lines 350-351: I don't get the point of this sentence.

[Response]: Deleted.

Lines 348-361: I do not fully understand the reasoning here. This discussion is useless to understand this (Major comment) as it compares the toluene-SOA with the other two SOA but does not discuss the differences between the slightly and highly oxidized toluene SOA.

[Response]: This whole paragraph has been reformulated. Please see the response to major comment #1 and the comment on L347-348.

Line 370: "between -46 and -42 °C". How about at -40°C?

[Response]: The lamina temperature in Fig. 5(b) was between -46.6 °C to -41.6 °C for *D-10*. We draw a rather conservative conclusion here. Please also see the response to major comment 2.

The data was excluded due to SPIN operating issues that day.

Line 371: "between -43 and -40 °C". How about below -43°C?

[Response]: Please see the response to major comment 2.

The data was excluded due to SPIN operating issues that day.

Line 403: "while β -caryophyllene SOA oxidized by O₃ did not alter the SS_i of the soot particles". Why not? What do the authors think happened here?

[Response]: O₃ addition on β -caryophyllene carbon-carbon double bond leads to formation of organics that have super-low volatility that could be semi-solid or solid (Nguyen et al., 2009; Winterhalter et al., 2009). As with the toluene SOA discussion above, BC particles might be stucked with or embedded in such semi-solid or solid SOA, leaving some bare carbonaceous surface that can nucleate ice in the way bare COJ300 BC particles do.

L465-457: "while β -caryophyllene SOA oxidized by O₃ did not alter the SS_i of the soot particles. In addition, more oxidized SOA (toluene derived SOA from photooxidation) with potentially more oligomer formation, moving IN onset SS_i towards, but still below, homogeneous freezing."

Lines 403-405: this deserved to be deeper discussed.

[Response]: We gratefully thank the referee to suggest us revisit these lines and make the discussion deeper here. The IN onset description has been moved to the end of this paragraph and discussion has been added.

Fig.7 (O/C and R/C plot) was modified by adding B-0 and connect pure β -caryophyllene with B-0. The slope between 0-1 is in compliance with carbon-carbon double bond breakage, and oxygen and hydrogen atoms addition.

L444-450: "However, COJ300 BC coated with O₃ oxidized β -caryophyllene SOA (*B-0* in Table 1) shows no significantly alternation of IN ability, as shown in Fig. 5(c). Unlike OH oxidation of β -caryophyllene where fragmentation happens, O₃-addition is very likely to happen first on the carbon-carbon double bond of β -caryophyllene in *B-0*, leading to formation of semi-solid or solid SOA (Nguyen et al., 2009; Winterhalter et al., 2009). As with the case of *T-10*, such semi-solid

or solid SOA might collide and stick with BC particles, leaving some bare carbonaceous surface that can nucleate ice following the IN pattern of COJ300 BC.”

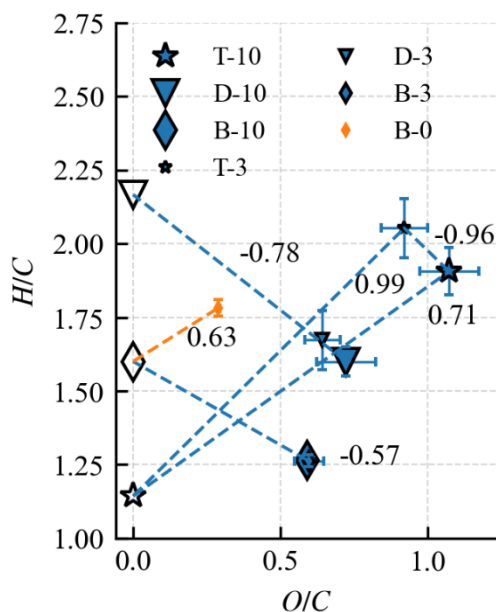


Figure R1 3 Modified Fig.7.

Line 410: "aerosols". How about gasses?

[Response]: Changed to “organic species” to be consistent.

Line 441: are they really monodisperse?

[Response]: Deleted.

To be more cautious and rigorous, the word “monodisperse” has been replaced by “size-selected” throughout the paper.

Figure 2. Why the 350 nm bare BC selected particles did not show a narrow peak at 350 nm?

[Response]: To highlight the modal size shift, the size range of x axis in Fig.2 is 300 to 500 nm, which stretches the figure and makes the size distribution seem very broad. The figure below shows a narrow peak and modal size shift for T-10 and B-10 experiment as examples.

Updated Fig. 2.

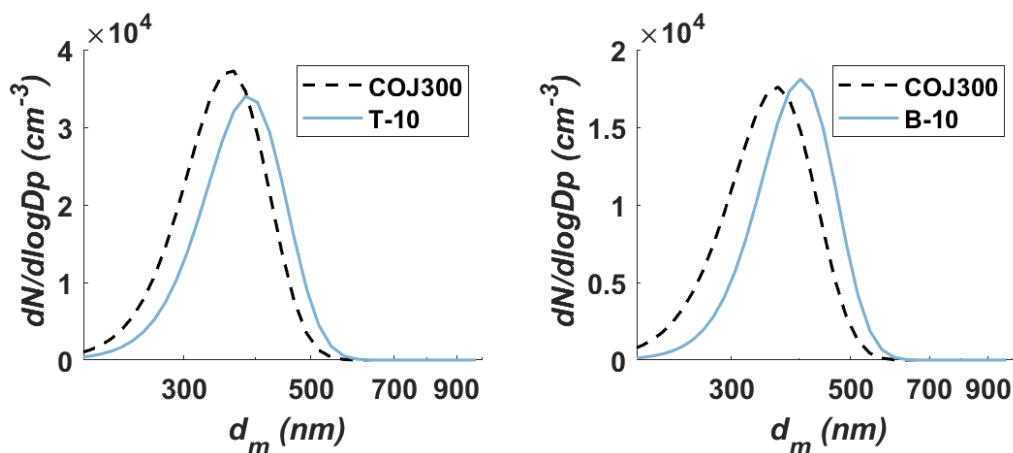


Figure R1 4. Particle size distribution for T-10 and B-10 experiments.

Figures 3 and 5. I am wondering why the authors did not include literature data in both figures.

This will help the readers to directly compare the present results with previous studies.

[Response]: Added the 800 nm R330R and R2500U IN data from (Nichman et al., 2019) in Fig. 3(a) and (b), and toluene SOA coated diesel BC IN data from (Kulkarni et al., 2016) in Fig. 5(a). To the author's knowledge, there is no data available for *n*-dodecane and β -caryophyllene SOA coated BC IN experiments.

Figure 7: I think this figure add very little to the main text, and therefore, it can go to the supplementary material.

[Response]: Please see our response to the comment on L403-405. Fig. 7 is crucial when inferring the atomic change during the experiments. Therefore, we modified Fig. 7 and keep the figure in main text.

Figure A3. Why are the size distribution so polydisperse after size selection?

[Response]: This figure is not the size distribution of BC particles. It is the primary particle (the basic carbonaceous spherules forming BC aggregates) size distribution of size-selected BC aggregates, corresponding to dpp and its standard deviation in Table 1. The primary particle size also obeys normal distribution (Huang and Vander Wal, 2013; Liati et al., 2014)

Figure B1. This figure is not easy to follow. Is it time in the x-axis?

[Response]: This figure is the temporal evolution of particle size distribution, corresponding to the top view of the plots below. Each column of x-axis in Fig. B1 corresponds to a complete BMI SMPS scan, which is equivalent to time. Combining the y-axis and colormap together we can see the size distribution for each scan.

Added "The x axis denotes time. Together with the color map, y axis shows the size distribution for a certain time." in the figure caption.

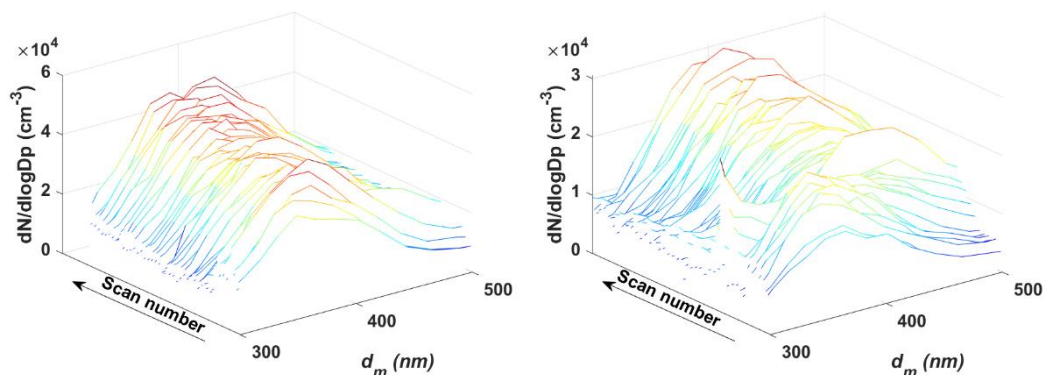


Figure R1 5. BMI SMPS scans for T-10 (left) and B-10 (right) experiments exhibiting modal size shift from 350 nm to 400 nm as a function of scan number.

Figure B2. It is not mentioned/discussed in the text.

[Response]: This figure is placed here to demonstrate that the AMS signals of our SOA results are in line with previous studies.

Referee #2

The work by Zhang et al. presents laboratory data of the ice nucleation ability of different types of black carbon, along with a characterization of the physical and chemical particle properties. The study extends previous laboratory measurements on the ice nucleation ability of soot. This topic fits well within the scope of ACP, and the results are novel and of great interest for the ice nucleation community. Overall, I find the manuscript is well written and structured and the results are presented in a clear way and put into context of previous literature. However, from my point of view there are some aspects, in particular in the discussion of the ice nucleation results, that should be revised. Once the points outlined below are sufficiently addressed, I support publication of the manuscript in ACP.

We thank this referee for recognizing the contribution of our work to the community. Below, the referee outlines major concerns regarding our usage of IN terms and uncertainty discussion. We highlight several substantial revisions which we believe address the referee's concerns properly and sufficiently.

Overall comments and general concerns:

- *The authors do not seem to provide a consistent view of the ice nucleation mechanism of the investigated soot types, which I find in part hard to follow. At various instances throughout the manuscript the authors describe the observed ice nucleation activity to result from deposition nucleation (e.g. L25, 27, 68, 90, 284). At other instances, the authors describe how earlier studies by Nichman et al. (2019; including authors from the present study) and Mahrt et al. 2018 (L80-84) have identified soot to form ice via the pore condensation and freezing (PCF) mechanism at cirrus cloud temperatures, the temperature range studied here. The PCF mechanism is then suggested to explain the observed ice nucleation results (e.g. L228-332) and also used to argue how the coating of the soot particles with secondary organic aerosol (SOA) leads to filling of the pore, which*

renders these pores unable to contribute to ice formation via PCF (e.g. L396-397). This seems to be in stark contradiction to the suggested ice formation via deposition nucleation for some of the bare soot particles. In their discussion (L438-439 and L460) the authors then vaguely talk about “verifying the PCF” mechanism in future studies but it does not become fully clear if the ice nucleation observed in the present study is attributed to PCF or to “classical” deposition nucleation.

I assume that the authors interpret the observed ice formation as PCF and whenever the authors refer to “deposition nucleation”, they refer to ice formation at cirrus temperatures below water saturation (and below homogeneous freezing conditions, to be specific). However, this terminology is confusing for the reader, and suggests a flip-flop between both mechanisms, i.e. classical deposition nucleation and PCF. I would appreciate if the authors could provide a clearer description of the ice nucleation mechanism of the observed ice formation on the investigated soot particles. A relatively simple solution to reduce the in part confusing back and forth would be to use just “IN activity” rather than “deposition IN activity” to describe the ice formation below homogeneous freezing conditions and then provide a comprehensive discussion of both “classical” deposition nucleation and PCF in the results section.

[Response]: We agree with the referee that the mixing usage of deposition IN and PCF might be misleading and confusing. The terms have been checked and replaced throughout the paper. Discussion of IN mechanism has been added where applicable. Please see below the point-to-point response for more details.

- *The title of the presented manuscript suggests that an effect of particle size, morphology and coating on the ice nucleation ability of BC is investigated in this study. While I appreciate the efforts in comprehensively and carefully characterizing the physical and chemical properties of the investigated soot types the associated uncertainties are not sufficiently discussed, which I find problematic. For example, the goodness of the size selection and hence the difference between a 300 nm and a 400 nm R2500U particle are not discussed. Upon revision of the manuscript, the uncertainties of the various measurements of these variables on the dependent variable (ice nucleation activity), should be more clearly emphasized and discussed. As another example, I am not clear whether the O:C ratio of the COJ300 and the R2500U samples are really different.*

[Response]: Added uncertainty and confidence intervals where applicable. The uncertainty of size selection, morphology and chemical composition characterization has been added and discussed. Please see the point-to-point response to comment on Table 1 and the relevant lines for detailed information.

Specific comments:

- L22: Delete “aerosolized”

[Response]: Deleted as suggested.

- L25: Delete “(-24 to -46°C)”

[Response]: Deleted.

- L25,27: “Deposition IN”; please see my general comment above.

[Response]: Replaced “Deposition IN” by “Ice formation at cirrus temperatures below homogeneous freezing thresholds” in L25.

Deleted “deposition” in L27.

- L31: *“We attribute the inhibition of IN ability to the filling of pores on the BC surface by the SOA material coating.” In other words, the IN ability of the uncoated particles results from the pores, i.e. takes place by PCF. This is in contradiction to the “deposition IN” mentioned above and at various other instances in the manuscript. Please see my general comment above.*

[Response]: We agree with the referee. Changes have been made accordingly.

L37-39: “Our study of selected BC types and sizes suggests that increase in diameter, compactness, and/or surface oxidation of BC particles lead to more efficient IN via pore condensation freezing (PCF) pathway, and that the organic coating materials can inhibit the formation of ice.”

- L33: *Delete first “days”*

[Response]: Deleted as suggested.

- L37: *Delete “terrestrial”*

[Response]: Deleted.

- L39,41: *I suggest replacing the given references by primary reference, e.g. the classical textbook by Pruppacher and Klett (1997).*

[Response]: References are replaced by (Pruppacher and Klett, 2010)

- L43: *Why are you only introducing “deposition IN” here and not also PCF?*

[Response]: Added a brief introduction of PCF.

PCF was originally introduced in L83 after description of the experiment results that doubt the classical deposition IN mode.

L47-52: “Deposition IN is one classical heterogeneous IN mode, in which solid ice is formed by direct water vapor deposition on to an INP surface. Recently, laboratory studies demonstrated that ice formation at thermodynamic conditions relevant to classical deposition IN on porous material at cirrus temperature might actually be initiated by homogeneous freezing of liquid water held within the cavities below water saturation due to inverse Kelvin effect (Marcolli, 2014; David et al., 2019; David et al., 2020). This pathway by which porous material might form ice below water saturation below -38 °C is referred to as pore condensation and freezing (PCF, Marcolli, 2014).”

- L45: *Rephrase as: “BC from aircraft emissions may be an ...”*

[Response]: modified as suggested.

- L53: *Delete “simulate the atmospheric environment”*

[Response]: Deleted.

- L59: *Hoose and Möhler (2012) is not a primary reference and I suggest deleting it here.*

[Response]: Deleted as suggested.

- L63-64: *Similarly, the probability of a BC aggregate to contain a pore with the right properties (e.g. pore size and contact angle) increases with increasing aggregate*

diameter, which would favor PCF for larger particles (Mahrt et al., 2018). This could be added.

[Response]: Added as suggested. Since contact angle is a bulk quantity, we replaced the word “contact angle” by “surface hydrophilicity” here to be more rigorous and consistent.

L74-75: “Similarly, the probability of a BC aggregate to contain a pore with the right properties (e.g., pore size and surface hydrophilicity) increases with increasing aggregate diameter, which would favor PCF for larger particles (Mahrt et al., 2018).”

- L68: “*deposition mode*”; see my general comment above.

[Response]: Deleted “deposition” in L77. Replaced “...in deposition...” in L79 by “...at thermodynamic conditions relevant to classical deposition mode at cirrus temperature”.

L78-80: “However, the size threshold below which BC cannot nucleate ice at thermodynamic conditions relevant to classical deposition mode at cirrus temperature and the underlying mechanism is still uncertain.”

- L70: Rephrase to “...during atmospheric aging, leading...”

[Response]: Reworded as suggested.

- L71: Add Bhandari et al. (2019) and Khalizov et al. (2009)

[Response]: Added.

- L80: Delete Kumfer ad Kennedy (2009)

[Response]: Deleted.

- L80-81: This statement is not true and needs to be revised. E.g. see Table 1 and Fig. 3 in Mahrt et al. (2018). The investigated “FS” soot has the second highest surface area, but “LB_RC” shows a similar or higher IN activity.

[Response]: Removed Mahrt et al. (2018). Added “For smaller particles, Mahrt et al. (2018) presented a complex dependence of BC IN activity on particle size, surface area, and BC surface hydrophilicity.” after this sentence.

L92-96: “Nichman et al. (2019) reported a generally positive correlation between BC particle surface area and IN activity for particles with same size. For smaller particles, Mahrt et al. (2018) presented a complex dependence of BC IN activity on particle size, surface area, and BC surface hydrophilicity. They attributed BC IN activity to PCF mechanism (Marcolli, 2014; David et al., 2019; David et al., 2020), in which IN of BC is considered as homogeneous freezing of liquid water taken up in mesopores (2-50 nm) due to capillary effect (Fisher et al., 1981).”

- L82: Delete Koop (2017) and Marcolli (2017). Add David et al. (2020).

[Response]: References modified as suggested.

- L83: Rephrase to: “...in which IN of BC is considered as homogeneous freezing of...”

[Response]: Rephrased as suggested.

- L84: Replace references by Fisher et al. (1981).

[Response]: Modified.

- L90, 100: “*deposition nucleation*”; please see my general comment above

[Response]: Deleted “deposition”.

- L102: “-38°C”

[Response]: Corrected.

- L128: Add: “... in particles of aircraft engine exhaust...”

[Response]: Added.

- L131: Please specify “light” aromatic species

[Response]: Added “such as xylenes, alkylbenzenes, naphthalene, etc.”.

L144: “...a proxy for other light aromatic species (such as xylenes, alkylbenzenes, naphthalene, etc.) in atmospheric aromatic-seeded SOA formation models”

- L133: How representative is β -caryophyllene for biogenic SOA? How does it compare to other major biogenic SOA types such as α -pinene SOA? For the Sect. 2.1.2. more discussion on the atmospheric abundance and relevance of the chosen SOA precursors should be given.

[Response]: There is no direct β -caryophyllene observation data available in the tropopause to the authors’ knowledge. However, there is one field observation of β -caryophyllene SOA presence at 1534 m, with a terpene organic carbon concentration of about $0.6 \mu\text{g m}^{-3}$ (Fu et al., 2009).

In ambient environment, the α -pinene concentration is generally higher than β -caryophyllene. However, due to the high yield of β -caryophyllene, its SOA could still be quite significant (Yee et al., 2018). Previous field studies found that β -caryophyllene SOA comprise a significant fraction of ambient organic aerosol (Hu et al., 2008), and the concentrations are highly temperature sensitive (Arey et al., 1991; Helmig et al., 2006; Sakulyanontvittaya et al., 2008), i.e., tropical areas with stronger convection also have higher β -caryophyllene emission. The deposition ice nucleation of α -pinene SOA has been studied before and the results varies as some studies show α -pinene SOA are not efficient INPs (Ladino et al., 2014; Wagner et al., 2017) while others show they can be relatively good INPs with pre-cooling (Ignatius et al., 2016). This work mainly focuses on β -caryophyllene due to its relative importance in the ambient.

Therefore, it is reasonable to infer that the strong updrafts in tropical areas or during summer times might bring a significant amount of β -caryophyllene to the upper troposphere or lower stratosphere. Moreover, the β -caryophyllene concentration used in our experiments (2300/5000 PPB) lies in the range of that has been used in previous studies (190-200000 ppb) (Grosjean et al., 1993; Jaoui et al., 2007; Jaoui et al., 2013).

Added several lines to address the importance and abundance of n-dodecane and β -caryophyllene in the atmosphere.

L147-157: “Modelling and field studies suggest that such less volatile organic species might be significant anthropogenic SOA precursors in highly populated area (Hodzic et al., 2010; Tsimpidi et al., 2010; Lee-Taylor et al., 2011; Hodzic et al., 2016), among which n-dodecane has

relatively higher emission rate (Lee-Taylor et al., 2011). Terpenes are representative biogenic organics emitted by plants, among which β -caryophyllene has been found to be one of the most atmospherically abundant sesquiterpenes originating from agricultural plants and pine trees, as well as other sources (Arey et al., 1991; Ciccioli et al., 1999; Helmig et al., 2006; Sakulyanontvittaya et al., 2008; Guenther et al., 2012; Henrot et al., 2017). Even though the atmospheric abundance of β -caryophyllene is not as significant as other biogenic organics, such as isoprene and α -pinene, its high reactivity towards ozone and hydroxyl radical to form oxidized products with low volatility makes β -caryophyllene an appreciable biogenic SOA source in the atmosphere (Shu and Atkinson, 1995; Calogirou et al., 1997; Hoffmann et al., 1997; Griffin et al., 1999; Helmig et al., 2006; Lee et al., 2006; Jaoui et al., 2007). An up to 7 ng m⁻³ atmospheric concentration of β -caryophyllene tracer during summer time was reported (Jaoui et al., 2007).”

- L146: Can the authors comment on how the wet dispersion in the atomizer affects the BC particle morphology?

[Response]: We acknowledge that generation method may affect BC morphology because of the surface tension of water. However, based on the SEM observation and shape descriptor derivation in this study, the difference between wet and dry generation BC particles are minor, as showed below. Moreover, a previous study conducted by Nichman et al. (2019) demonstrated that the IN onset for similar BC types was not very much affected by dry vs. wet generation (see their Fig. 5).

Table R2 1. Characteristics of wet and dry generation 400 nm R2500U BC particles

400 nm R2500U	Wet generation	Dry generation
$\overline{d_a}$ (nm)	343.5±106.3	465.0±282.2
\overline{AR}	1.44±0.29	1.53±0.33
$\overline{Roundness}$	0.73±0.09	0.72±0.09
$\overline{Circularity}$	0.61±0.15	0.62±0.25
$\overline{d_{pp}}$ (nm)	34.5±11.4	35.9±8.0
N	343	105
D_f	1.92 [1.68, 2.16]	2.04 [1.81, 2.28]

- L150: The flow reported here (1.5 SLPM) and on L215 (2.2 SLPM) are different. How does this change your flow rate through the DMA and possibly affect your size selection. Please comment in the main text.

[Response]: The statement here might be a little misleading. For clarity, we changed the description in L168-170. We used different flow rate to ensure sufficient BC concentration. Based on the DMA transfer function study by Karlsson and Martinsson (2003), the degradation due to imperfect DMA operation condition becomes less than 5% when the particle size exceeds 100 nm. Please see our response to the next comment for more discussion on DMA difference.

We also added the sheath-to-sample flow rates used in bare BC and BC-SOA mixing experiments and discussed the potential impact of the flow condition on size-selection between L176-180.

L169-171: “The flow rates through the nebulizer was 1.5 SLPM (standard liters per minute) and 2.2 SLPM for bare BC experiments and BC-SOA mixing experiments, respectively, which is controlled by a mass flow controller (MFC, Model MC-2SLPM-D; ALICAT Scientific).”

L176-180: “The sheath-to-sample ratios for bare BC and BC-SOA mixing experiments were respectively ~6:1 and 4:1. Compared with the widely used sheath-to-sample ratio (10:1, Karlsson and Martinsson, 2003), the lower ratios in our experiments might broaden the BC particle size distribution, yet still offering satisfactory number concentration at the target particle size (Fig. 2) because of the large particle size being selected (Karlsson and Martinsson, 2003).”

- L152-153: *Have the TSI and BMI DMA been compared? Can the authors provide a size distribution of the soot types investigated that was size-selected with both DMAs to ensure that there is no difference in the uncoated and coated particles due to the instrumentation used? Please also add the aerosol-to-sheath flow ratios used in the DMAs for aerosol size selection.*

[Response]: The BMI and TSI SMPSs have been intercompared by scanning 350 nm COJ300. The sheath-to-sample ratio were set to 6:1 for size-selecting DMAs, and the sheath-to-sample ratio were set to 10:1 to perform standard size scans for the SMPSs during instrument intercomparison. There is minor difference between these two systems in terms of particle size selection. The plot below exhibits the instrument intercomparison result. To minimize the influence of instrument difference on measured particle number concentration, the BMI DMA and CPC were used in bare BC experiments, and the BMI SMPS (DMA+CPC) was used to measure real-time particle size distribution in SOA coating experiments. Please also see our response to the comment on section 3.1 for more information on doubly-charged BC discussion.

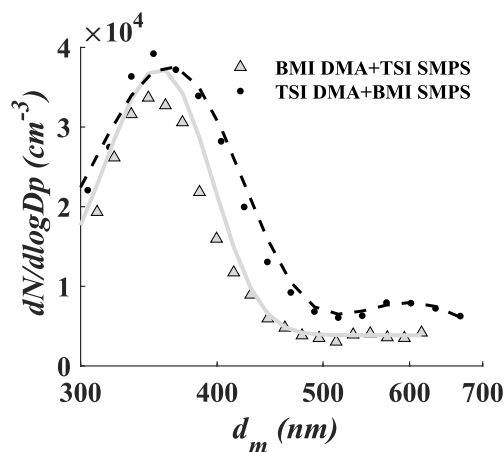


Figure R2 1. Intercomparison of BMI and TSI SMPS by scanning the size distribution of bare 350 nm COJ300. The grey line and black dashed lines represent first-order Gaussian fitting of the scanned particle size distribution.

Table R2 2. Fitting parameters of the scanned particle size distribution with different instrument.

Instrument	Peak	Maximum particle concentration (#/cc)	$d_m \pm \sigma_{d_m}$	R^2	Particle Number (#)
BMI SMPS	1st	3.74E4	360.81 ± 84.78	0.96	5790
	2nd	7.96E3	600.94 ± 129.72	0.89	595
TSI SMPS	1st	3.35E4	353.99 ± 57.18	0.95	3757

There might be some misunderstanding for the results of bare and coated BC here. To clarify: the BMI DMA was only used to select 100-400 nm BC particles (i.e., the results represented in Sect. 3.1) and the particle concentration was monitored with a BMI CPC. The TSI DMA was only used to select 350 nm COJ300 particles during SOA coating experiments (i.e., the results in Sect. 3.2), with the BMI SMPS used to monitor particle size distribution.

Since the same experimental apparatus was used consistently and separately throughout the experiments in Sect. 3.1 and 3.2, we did not mix and intercompare these IN onset results. The 350 nm bare COJ300 results in Sect. 3.2 Fig. 5 was size-selected by TSI DMA and went through PAM chamber. Therefore, the difference between these two DMAs is not our major concern and does not affect our conclusion drawn here as long as the bare COJ300 particles size distribution obtained by BMI SMPS peaks around 350 nm.

Besides, we added “The sheath to sample ratios for bare BC and BC-SOA mixing experiments were respectively ~6:1 and 4:1.” between L176-177.

- L155: *An RH value of 16% seems extremely high. Please comment how this affects your IN measurements that are performed using this air stream (conserving specific humidity) but exposing it to $T < -40$ °C.*

[Response]: Typical ambient *RH* is about 30-80% on the ground. The *RH* is generally above 20% in the tropopause (Ruzmaikin et al., 2014) with exceptions for desert regions around N30° and S30° due to the dry subtropical high. Tropical tropopause layer occupies even higher *RH* at around 13 km. The *RH* in our experiments is at least in-line with, if not lower than, the ambient *RH*.

Besides, when the humidified air stream encounters the sharp temperature gradient at SPIN inlet, the water immediately condense and freeze in the inlet, so the high *RH* in the air stream should have minor effect on the ice formation inside the chamber.

- L160: *Please specify “MOUDI” acronym*

[Response]: Changed to “Micro-Orifice Uniform Deposit Impactor (MOUDI, Model M135-10; TSI Inc.)”.

- L170: *Rephrase as “... by the PALMS.”*

[Response]: Modified as suggested.

- Table 1:

- *da of R2500: Why is the projected area diameter for $d_m = 300$ nm larger than for $d_m = 400$ nm?*

[Response]: This could be possible, because 1) R2500U particles are branched fractal aggregates. The smaller (e.g. 200 and 300 nm) R2500U particles are generally more spherical and compact than the size-selected 400 nm particles, leading to larger projection area without voids; 2) there could be random errors due to manually selection of aggregates to analyse; 3) The particle orientation could affect the projection area. The round aggregates are less affected by particle orientation than the branched ones. Please also see the SEM images in Fig. A3.

Added “400 nm R2500U is more fractal than COJ300 and R330R with the same d_m , as with 300 nm R2500U, which is indicated by D_f . Project area, as well as the derived d_a , are significantly affected by the degree of fractal, since highly fractal particles can have voids affecting project area. COJ300 and R330R, as well as 300 nm R2500U particles, are more spherical and compact than the fractal 400 nm R2500U, leading to larger d_a in comparison with 400 nm R2500U.” between L215-219.

L215-219: “400 nm R2500U is more fractal than COJ300 and R330R with the same d_m , as well as 300 nm R2500U, which is indicated by D_f . Project area, as well as the derived d_a , are significantly affected by the degree of fractal, since highly fractal particles can have voids affecting project area. COJ300 and R330R, as well as 300 nm R2500U particles, are more spherical and compact than the fractal 400 nm R2500U, leading to larger d_a in comparison with 400 nm R2500U.”

- *da: Please comment in the text why the d_a values for $d_m = 400$ nm particles for COJ300 and R330R are significantly larger than for R2500U.*

[Response]: Please see the response to last comment.

- *Roundness: The roundness values for all soot types and mobility sizes are very similar and comparable. Can this be a result of the wet dispersion? Do the authors have data for dry aerosolized BC particles for comparison?*

[Response]: Please see our response to the comment on L146. We did compare the morphology characteristics of both wet and dry generation R2500U BC particles. It shows that generation method has minor impact on particle morphology.

- *Please add the standard deviation values for the reported fractal dimension.*

[Response]: Added the 95% confidence intervals of the fitted D_f , embraced in brackets.

- *Please add the standard deviation for the reported O:C. Why is the median used here and not the mean? Is the difference between 0 (400 nm R2500U) and 0.02 (400 nm COJ300) significant?*

[Response]: Changed to mean O:C ratio and added the standard deviation.

As stated in L221, PALMS can provide qualitative chemical composition information and is operated in a single particle mode. About 21.0% COJ300 negative spectra showed significant $m/z = 16$ signal compared to merely 2.8% for R2500U in this work. The frequency of $m/z = 16$ signal appearance can reflect the probability and abundance of oxygen content in a BC type. The consistent appearance of $m/z = 16$ signals for COJ300 negative spectra is a clear indication of

higher oxygen content in comparison with R2500U. The sparse oxygen signal of R2500U could be either contamination or ion re-combination in PALMS. Therefore, the “*Spectra percentage exhibiting $m/z = -16$ signal*” row is added in Table 1.

Besides, the caption of Fig. A1 has been rephrased.

L527-528: “Generally, the probability of O⁺ signal presence in COJ300 is an order of magnitude higher than R2500U.”

“**Table 1.** Characteristics of selected BC proxies in this study. α_{BET-N_2} is the BET specific surface area based on N₂ adsorption isotherms; d_m is the particle mobility diameter; $\overline{d_a}$ denotes the mean 2-D projected area-equivalent aggregate diameter derived from SEM images; mean aspect ratio (\overline{AR}), roundness ($\overline{Roundness}$) and circularity ($\overline{Circularity}$) are the geometric mean morphology parameters derived from several aggregates and are defined in Sect. 2.2.2; $\overline{d_{pp}}$ denotes the mean geometric diameter of primary particles measured from SEM images, and N the number of primary particles analyzed for each BC type and size; D_f denotes the 3-D fractal dimension derived from 2-D SEM images; d_{va} is the particle vacuum aerodynamic diameter measured by the PALMS; values in parentheses are the corresponding one standard deviations; values in brackets are the 95% confidence intervals of D_f .

BC type	R2500U			COJ300	R330R
Composition	Furnace black			(4-carboxyphenyl)-modified carbon black ^a	Furnace black
CAS No.	1333-86-4			1106787-35-2	1333-86-4
Specific gravity (20 °C)	1.7-1.9 ^a			1.07 (dispersion) ^a	1.7-1.9 ^a
Bulk density (g/cm³)	20-380			-	20-380
pH	7.0 ^b ; 4-11 ^c			7.0-8.6 ^a	6.9 ^b ; 2-11 ^c
Solubility	Insoluble			Insoluble but dispersible	Insoluble
α_{BET-N_2} (m²/g)^{a,d}	270			200	90
d_m (nm)	200	300	400	400	400
$\overline{d_a}$ (nm)	316.9	403.5	343.5	629.4	816.6
($\pm 1\sigma$)	(109.3)	(82.5)	(106.3)	(308.3)	(355.3)
\overline{AR}	1.22	1.36	1.44	1.19	1.33
($\pm 1\sigma$)	(0.16)	(0.27)	(0.29)	(0.17)	(0.28)
$\overline{Roundness}$	0.81	0.77	0.73	0.84	0.75
($\pm 1\sigma$)	(0.06)	(0.08)	(0.09)	(0.08)	(0.10)
$\overline{Circularity}$	0.78	0.64	0.61	0.72	0.53
($\pm 1\sigma$)	(0.18)	(0.14)	(0.15)	(0.20)	(0.16)

$\overline{d_{pp}}$ (nm)	41.9	35.5	34.5	34.2	45.4
($\pm 1\sigma$)	(12.4)	(9.9)	(11.4)	(9.9)	(13.6)
N	242	256	343	139	251
D_f	2.02	1.92	1.92	2.34	2.31
[95% confidence interval]	[1.85, 2.18]	[1.30, 2.53]	[1.68, 2.16]	[2.12, 2.56]	[2.01, 2.61]
Median d_{va} ^e	-	-	608.7	610.6	-
Effective density (g/cm ³) ^f	-	-	1.52	1.44	-
Spectra percentage exhibiting $m/z = 16$ signal	-	-	2.8	21.0	-
Mean O:C ratio ^g	-	-	0.008	0.024	-
($\pm 1\sigma$)	-	-	(0.024)	(0.036)	-

^aInformation offered by manufacturer datasheet. ^bMeasured by Nichman et al. (2019) using VWR pH meter.

^cMeasured by manufacturer in compliance with ASTM 1512. ^dBET specific surface area measured by manufacturers using N₂ adsorption in compliance with ASTM D-4820. ^eConverted from the measured time of flight. ^fCalculated from dividing median d_{va} by d_m (400 nm in this study) and times the reference density 1 g/m³ (Cziczo et al., 2006).

^gCalculated from PALMS spectra area.”

- L178-179: Form Figs. A2 and A3 it remains ambiguous how d_{pp} was determined. More information should be added.

[Response]: Added “manually” in the caption as well as a description paragraph after Fig. A4. A table of the coefficients and goodness of primary particle normal distribution fittings are also added (Table A1).

L553-560: “BC aggregate parameters, including L_{max} and W_{max} , perimeter, and project area, are determined by manually drawing the periphery of the aggregate, as shown in Fig. A4 (a-e). The primary particle diameter is determined by artificially recognizing the boundary of BC primary particle in the SEM image. After manual selection of the start and end points of a primary particle’s length and width respectively, the distance between these points are calculated automatically and recorded. The primary particle diameter equals to the geometric mean of the length and width. Primary particle size distribution of a specific BC type and size can then be obtained by categorizing primary particle diameters into different size bins and count the frequency, as shown in Fig. A5. BC primary particle size distribution obeys normal distribution. The coefficients and goodness of normal distribution fittings are shown in Table A1.”

- L196: Fig. A5 shows a very broad size distribution, even though $d_m = 400$ nm have been sampled. How does d_{va} and d_m relate? Please discuss in the manuscript how the broad, not monodisperse size distribution affect your conclusions for the IN measurements. A similar question arises when looking at Fig. 2.

[Response]: The d_{va} was obtained by calculating particle velocity in PALMS. However, the empirical velocity- d_{va} curve was obtained using PSL particles. For complex particles like BC,

the shape should be taken into account. Omitting shape factors and other factors may introduce bias and lead to wide particle distribution. Kulkarni et al. (2016) also reported larger modal size and broader d_{va} distribution compared with d_m .

The discussion was added between L175-179, please see the response to the comment on L150-153.

- *Please also specify what size threshold was used for the analysis of the SPIN OPC data and discuss this in context of the shown BC size distributions. E.g. Fig. A5 suggest presence of supermicron particles, which could have been miscounted as ice crystals.*

[Response]: We agree with the referee that OPC size threshold is a commonly used criteria to distinguish between ice crystals and aerosols. However, it cannot differentiate water droplets (if there is any) and ice crystals.

Instead, both the laser scattering and polarity signals collected from SPIN OPC were used in this study to train a machine learning algorithm as described in (Garimella et al., 2016), to distinguish different phases, as stated between L305-307.

- *L203: Please add references*

[Response]: Added “More details about the AMS can be found in literatures (DeCarlo et al., 2006; Onasch et al., 2012), here a brief introduction will be given.” after the appearance of AMS, and deleted “More details about AMS can be found in literatures (Jayne et al., 2000; Onasch et al., 2012)” at the end of this paragraph.

L232-238: “Chemical composition of the SOA-coated BC particle stream was analyzed online by PALMS and a High-Resolution Time-of-Flight Aerosol Mass Spectrometry (HR-ToF-AMS; Aerodyne Research Inc.). More details about the AMS can be found in literatures (DeCarlo et al., 2006; Onasch et al., 2012), here a brief introduction will be given. The AMS offers quantitative average mass spectrum of an ensemble of aerosols. Particles entering AMS first go through an aerodynamic lens inlet to form a particle beam. A mechanical chopper is used downstream the inlet to control sampling particle or particle free period. The AMS employs a heated 600 °C tungsten surface to vaporize nonrefractory aerosols. Ionization is achieved using a universal 70 eV electron ionization technique. Ionized species are detected by time of flight mass spectrometry.”

- *L211: Are these number concentrations after size selection? They seem very high.*

[Response]: These are the number concentrations obtained from bare BC experiments size-selected by BMI DMA. We used high flow rate and high concentration in BC-SOA mixing experiments because the particle concentration could drop to a low level and introduce uncertainties after consecutive size-selection by two DMAs when determining particle number and activation fraction.

- *L222: O₃ concentrations of 110 ppm seem very high. Please put this in context of typical tropospheric O₃ concentrations. Can this be used to then report estimates for “Equivalent atmospheric exposure days” of O₃ in your Table 2?*

[Response]: The typical tropopause O₃ mixing ratio ranges between 0.1-1 ppm (Fioletov, 2008; Gettelman et al., 2011). However, the residence time of β -caryophyllene in the ambient environment is much longer than in the PAM reactor (5 min or less). Hence we used a higher concentration of ozone to expediate the reaction that would normally take longer to react in the ambient, which is common for flow tube or oxidation flow reactor related studies (Lambe et al., 2011b; Zhang et al., 2015).

The equivalent atmospheric exposure days are based on OH concentration, which was calculated combining O₃ concentration and UV intensity. The ambient OH concentration was assumed to be $1 \times 10^6 \text{ cm}^{-3}$ (Li et al., 2018) and the OH exposure equivalent time was calculated by using the OH concentration from the PAM and the residence time of the aerosols within the PAM (Zhang et al., 2018a).

Added “The typical O₃ mixing ratio in tropopause ranges between 0.1 to 1 ppm (Fioletov, 2008; Gettelman et al., 2011). The ozone concentration in this study was higher than ambient concentration to expediate the reaction given the short residence time of SOA within the PAM reactor (Lambe et al., 2011b; Zhang et al., 2015).” between L252-255

- L225: Replace “pyrolysis” by “photolysis”

[Response]: Replaced.

- L228: Please specify how the reported “atmospheric aging time” of 10-15 days was calculated.

[Response]: The equivalent atmospheric aging time t_{eq} are calculated using the OH concentration of the PAM reactor c_{OH_PAM} , the residence time of the particles within the PAM, t , and the ambient OH concentration $c_0 = 1 \times 10^6 \text{ cm}^{-3}$ (Li et al., 2018). O₃ concentration and UV intensity, where the OH concentration of the PAM reactor was calculated based on the O₃ concentration, relative humidity (RH), and UV light intensity measured real-time from the PAM reactor (Lambe et al., 2011a; Zhang et al., 2018a). The equation is:

$$t_{eq} = \frac{c_{OH_PAM} \times t}{c_0}$$

L262-265: “The equivalent atmospheric aging time t_{eq} were calculated using the OH concentration of the PAM reactor c_{OH_PAM} , the residence time of the particles within the PAM, t , and the ambient OH concentration $c_0 = 1.0 \times 10^6 \text{ cm}^{-3}$ (Li et al., 2018) following the equation $t = c_{OH_PAM} \times t / c_0$. c_{OH_PAM} was calculated based on O₃ concentration and UV intensity, and RH measured real-time from the PAM reactor (Lambe et al., 2011a; Zhang et al., 2018a).”

- L232: What causes the increase in RH from 16% to 25%?

[Response]: $RH = 25\%$ is the upper RH limit during our experiments. We report the limit to give the readers a better understanding of our experiment condition.

The RH increases gradually during IN experiments because the silica dryers are degraded by the water content in the atomized sample flow. At the end of experiments each day, the RH can reach up to 25% if the ambient humidity is high.

- L236: Please add what the CPC number concentration was after flushing the PAM.

[Response]: Added “The particle concentration measured each day before experiments were below 70 # cc⁻¹.” between L265-266.

- L259: Delete references to Nichman et al. (2019) and Wolf et al. (2019).

[Response]: References removed.

- L263: Specify “centerline” of what?

[Response]: Added “of SPIN chamber”.

L299-300: “Particles fed into SPIN are constrained by a ~9.0 SLPM sheath gas within a lamina near the centerline of SPIN chamber.”

- L276: Specify OPC size threshold used for AF analysis.

[Response]: Please see the response to the last comment on Table 1.

- L277: Please elaborate why different correction factors were applied for R2500U and R330 R and comment in the manuscript.

[Response]: The correction factor to account for aerosol lamina spreading has been extensively characterized in both theory and measurement for the SPIN (Garimella et al., 2017; Wolf et al., 2020). Based on classical fluid dynamics, the turbulence spreading calculation used the spherical particle assumption for simplicity, whose behavior is easier to predict and capture. When it comes to fractal particles, the morphology, dynamic shape factor, and other factors has to be taken into consideration, and the particle behavior are harder to predict. Fractal particles may bear different drag force and not follow the idealized flow trajectory. Therefore, the upper range of correction factors at these SPIN experimental conditions was applied to the more fractal R2500U data, and the lower range of possible correction factors was applied to R330R.

Added “To account for aerosol spreading outside of the lamina where SS_i is the highest (Garimella et al., 2016),... The correction factor was determined by taking the effect of morphology on particle behavior within SPIN lamina into consideration.” between L314-317.

L314-317: “We define the IN onset as 1% of particles activating, i.e. $AF = 1\%$, for a period of 10 seconds as activation. To account for aerosol spreading outside of the lamina where SS_i is the highest (Garimella et al., 2016), correction factor of 3.4 and 2.2 were applied for R2500U and R330R (Wolf et al., 2019). The correction factor was determined by taking the effect of morphology on particle behavior within SPIN lamina into consideration.”

- Section 3.1: Please add the fraction of multiple charged particles in your population of size- selected particles to your Table 1 and discuss a potential impact on your reported IN onsets, using $AF = 1\%$ as threshold.

[Response]: We apologize for leaving this detail in our paper. We actually used a 500 nm impactor at the BMI DMA inlet in our bare BC IN experiments to avoid large doubly-charged particles. Theoretically, at least 50% doubly-charged particle should be removed in the bare 300 and 400 nm BC experiments with the impactor. Since we did not have another DMA or CPMA during bare BC IN experiments, we were not able to determine the doubly-charged population for bare BC.

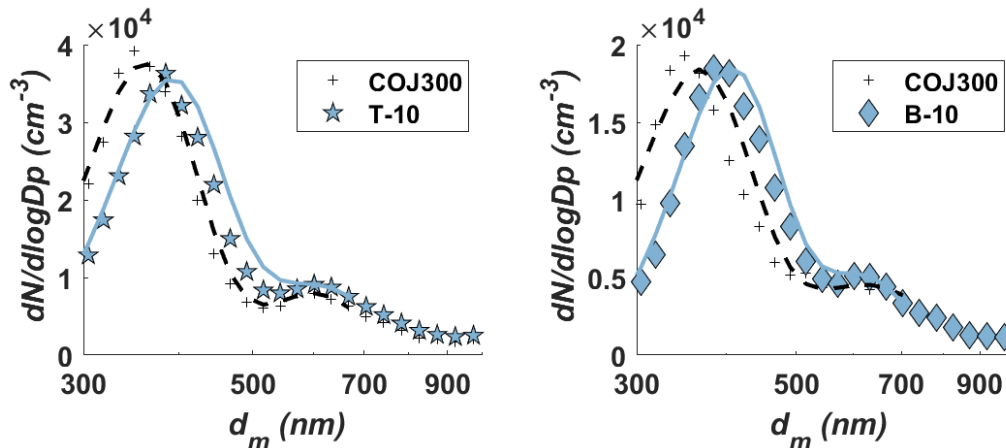


Figure R2 2. The overall particle size distribution of bare COJ300 BC, and toluene and β -caryophyllene SOA coated COJ300 BC. The figure also shows doubly-charged BC particle peaks with modal sizes of ~600 nm.

However, based on the bare BC data in BC SOA coating experiments illustrated above, the number fraction of doubly-charged bare BC particles with a peak around 600 nm are ~13% to 16% of total bare BC particle number, respectively. Therefore, we assume the doubly-charged BC particles made up of 16% of total size-selected BC population, which is quite conservative since the sheath-to-sample ratio in BMI DMA is higher (~6:1) in bare BC experiments than that (~4:1) for the TSI DMA in BC-SOA mixing experiments.

As shown in Fig. 3 (a) and (c), R2500U and R330R did not exhibit IN activity below 300 nm, so we believe doubly-charged particles would affect the 100 and 200 nm COJ300 results most. If the doubly-charged particles who are more IN active did affect the 100 and 200 nm COJ300 results, the -40 °C $AF-SS_i$ activation curve of 100 and 200 nm COJ300 showed below should exhibit a gradual AF increase at $SS_i \approx 1.3$ and grow to about 15%, then with a sudden AF jump to ~100% once SS_i exceeds homogeneous freezing threshold. However, there is no obvious AF growth exceeding 1% at $SS_i \approx 1.3$ in the plot below, and the SS_i approaches homogeneous freezing threshold when the AF approaches 1%. Therefore, we can imply that doubly-charged particles have limited effect on our bare BC IN onset results.

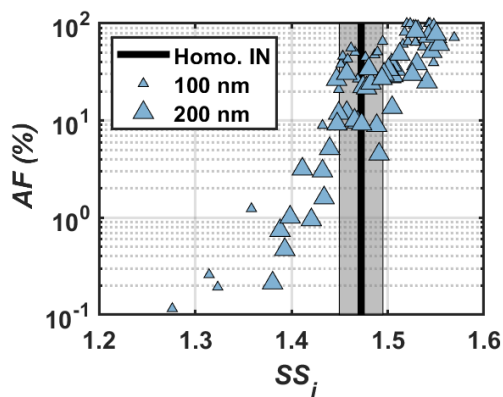


Figure R2 3. Activation curve as a function of SS_i for 100 nm and 200 nm COJ300 particles at -40 °C

For clarity, we modified the statement in Sect. 2.2.1 and added “For bare BC experiments, a BMI differential mobility analyzer (BMI DMA, Model 2002; Brechtel Manufacturing Inc.) was used to size-select particles, with a 500 nm cut-off size impactor installed at the DMA inlet to get rid of large particles.” between L73-175.

- L284: “deposition IN”; please see my general comment above.

[Response]: Deleted “deposition”.

- L286-287: Are the error bars based on theoretical calculations presented in the cited reference or based on measurements; please specify.

[Response]: The error bars are based on measured temperatures. Added “...derived from experimental data for each panel”.

L325-326: “Representative error bars in black lines show one standard deviation of variability for SPIN lamina temperature and SS_i derived from experimental data separately for each panel (Kulkarni and Kok, 2012).”

- L288: I suggest tuning down “substantially” here. Looking at your morphological parameters in Table 1 (AR, roundness, circularity), the values of the different soot types are within uncertainty of each other. Please see also my general comment above.

[Response]: Changed to “the three test BC types exhibit different particle morphology.” Please also see the response to the comment on L146.

- L289: Please use the same precision for the given D_f values as in Table 1, i.e. $D_f = 1.92$.

[Response]: Modified as suggested.

L327-328: “400 nm R2500U has the smallest D_f (~1.92), and COJ300 and R330R have larger D_f (~2.34 and 2.31, respectively);”

- L292: Can this also simply result from uncertainty in the d_{pp} measurements? Please see Anderson et al. (2017).

[Response]: As stated between L341-342 “The larger $\overline{d_{pp}}$ of 200 nm R2500U (Table 1) might result from the blurring of primary particles under high magnification.”

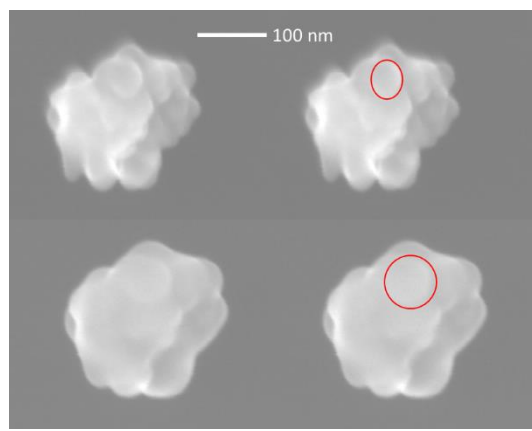


Figure R2 4. Boundary blurring process of BC primary particles under high magnification SEM electron beam when the observation time became longer. The scale bar applies to all panels.

During our SEM observation, the BC particles showed clear boundary at first, but after a few seconds of exposure to electron beam, the boundary of primary particles blurred, resulting in larger primary particle diameter. Such blurring was more severe for 200 nm particles that required higher magnification, and thus stronger electron beam intensity, to see the details of BC primary particles clearly. One possible explanation is that the less conductive part of the BC particles gets surface charging under high intensity electron beam. The SEM detectors will get electrons from multiple sources when the charge dissipation rate is low. As a result, the image becomes less clear the longer we scan at the same spot.

Besides, different magnification level (corresponding to different scales and length of scale bars) can also induce uncertainty in post-processing. To find the optimum balance between magnification level and fusion, we tried our best to use the $\times 30,000$ to $\times 105,000$ SEM images for BC aggregate morphology analysis when possible.

Despite that we cannot exclude the uncertainty caused by manual selection of start and end points when determining d_{pp} (please see our response to the comment on L178-179) apart from the magnification level error mentioned above, such uncertainty is different from the ones raised by automated image processing algorithm in (Anderson et al., 2017).

- Fig. 3:
 - Panel A: Why does the temperature uncertainty change between the subpanels (a), (b) and (c)?

[Response]: Each dot in Fig. 3(A) represents a separate RH scan ramp. To ensure consistency, the IN onsets of a certain BC type was determined from consecutive RH scan ramps in a day. The error bar in Fig. 3 represents the instrument condition during that day calculated following the methodology described in Kulkarni and Kok (2012).

However, the experiments for different BC types were performed on different days. The temperature uncertainty varied slightly between different days.

Besides, we should clarify that the representative uncertainty was calculated using the four coldest thermocouples. In other words, the overall temperature uncertainty is smaller if we take all sixteen thermocouples of SPIN into consideration.

- Panel B: Please specify if the scale bar is valid for all images. The SEM image of COJ300 suggest that this soot type is the most spherical. However, the roundness values reported in Table 1 are similar to e.g. $dm = 200$ nm R2500U. Can the authors provide more SEM images for the Appendix to evaluate the representativeness of the shown images?

[Response]: Moved panel B to Appendix A, numbered as Fig. A2 and added more SEM images. Fig. A2 includes SEM images of (a) 400 nm R2500U, (b) 300 nm R2500U, (c) 200 nm R2500U, (d) 400 nm R330R, and (e) 400 nm COJ300 with separate scale bars for each image. Changed the figure number in Appendix A accordingly.

200 nm R2500U is quite spherical based on the calculated D_f and SEM images. Therefore, there is no surprise that the shape descriptors such as roundness of 200 nm R2500U is close to that of 400 nm COJ300.

- *Panel B: Considering the values of the roundness of the various soot types and $d_m = 400$ nm, suggest that the morphology is the same within experimental uncertainty. In this context, the conclusion drawn that no clear dependence of IN on the particle morphology was found (e.g. L324, 451) is not surprising. However, the COJ300 soot type seems clearly more spherical on the (typical) images depicted in Fig. 3. Interestingly, at the same time this soot type reveals the largest ice nucleation activity. This trend is in-line with recent results of Mahrt et al. (2020), showing that more compacted, round soot aggregates are better ice nucleation particles (INPs) via PCF compared to more fractal soot particles. This provides further evidence that the observed ice nucleation activity in the present study is caused by PCF and might be worthwhile to consider for the discussion of the results. Do the authors have an explanation why the COJ300 aggregates look almost spherical?*

[Response]: According to the technology pathway in the COJ300 patent (Johnson, 1999), the BC particle surface modification was achieved by acid and other solvents washing. The washing and stirring process might shake off BC chains and cause collapse, which may explain why the COJ300 looks so spherical. However, the manufacturer should be contacted for more details about the BC manufacture and modification technology, which should be their core IP.

- *Panel C: It looks like there is also some O ($m/z = 16$) for R2500U, also this is hard to see from the scale. This figure could be improved by moving the PALMS spectra to the SI (they are only mentioned once in the manuscript) and increase the size of the panels showing the IN results, which is the major focus of this work.*

[Response]: Moved panel B and C to Appendix A. Please see the response to the comment on the O:C ratio in Table 1 for PALMS spectra interpretation.

- L308: Add: "... relevant to the particle..."

[Response]: Added.

- L309: "Representative uncertainty" of what?

[Response]: Added "range of SPIN lamina SS_i".

- L310: "deposition IN"; please see my general comment above.

[Response]: Deleted "deposition", added "below homogeneous freezing threshold".

L351-353: "The most spherical and oxidized COJ300 BC particles exhibited IN activity below homogeneous freezing threshold regardless of particle size and temperature in this study."

- L315: Add: "... R330R along the expected homogeneous freezing threshold in Fig..."

[Response]: Added as suggested.

- L316: "...where the IN mode transitions from heterogeneous IN ability to homogeneous freezing..." Please consider revising this statement. During PCF, the formation of ice takes place by homogeneous freezing, i.e. PCF should not be viewed as heterogeneous ice nucleation process (Marcolli, 2020).

[Response]: Rephrased.

L358-360: “We conclude that the lower size threshold where the BC particles exhibit IN activity below homogeneous freezing threshold at thermodynamic conditions relevant to cirrus may well lie between 300-400 nm and 200-400 nm for R2500U and R330R around -46 °C, respectively.”

- L318: “higher” not “warmer” temperature

[Response]: Changed to “higher”.

- L324-326: *You might want to revisit these lines: The number of surface defects and pores for soot particles to form ice via PCF does not necessarily scale with the degree of branching of a soot aggregate. For instance, Mahrt et al. (2020) reported that cloud processes, more compacted (less fractal, even though associated with a higher fractal dimension) soot aggregates were more potent INPs to form ice via PCF. In these more compacted, round soot aggregates the probability of having a pore suitable for PCF is higher. In fact, your results are in-line with these previous findings and further support these. Your Fig. 3 reveals that COJ300 soot is most ice active and also most round based on the SEM image, with the latter being further supported by the roundness and fractal dimension values reported for COJ300.*

[Response]: Reformulated the discussion here.

L366-375: “The IN onset results show no clear dependence on particle fractal level and surface area. Even though the more fractal and branching feature of R2500U BC particles with larger surface area do not clearly exhibit superior IN activity over R330R. Koehler et al. (2009) showed that IN was favored for oxidized hydrophilic BC, but too many hydrophilic active sites may bond water molecules, impeding ice embryo formation and thus impair IN (Pruppacher and Klett, 2010). The surface-modified, highly dispersible and spherical COJ300 with smaller $\overline{d_{pp}}$ shows better IN efficiency than fractal BC, which is consistent with the results of Mahrt et al. (2018) and Nichman et al. (2019) based on PCF mechanism. The physio-chemical properties of COJ300 particles, including oxidized surface, appropriate $\overline{d_{pp}}$, and compacted spherical morphology, may result in higher probability to have cavities with appropriate size and hydrophilicity on particle surfaces to accommodate liquid water below bulk water saturation by the inverse Kelvin effect (Marcolli, 2014; Koop, 2017; David et al., 2019; Marcolli, 2020).”

- L331-332: *Please expand your explanation on this aspect. What you show in Fig. C1 is not the saturation ratio required for pore filling (or onset of PCF), but the negative pressure resulting from keeping water within the cavity; this needs to be revised. Please also comment on how relevant the pore geometries investigated in Marcolli (2020), i.e. cylindrical and wedge-shaped pores are for the BC agglomerates in your study.*

[Response]: We agree that Fig. C1 shows the liquid saturation pressure **drop** due to the presence of cylindrical and wedge-shaped pores, i.e. the difference between saturation pressure over a concave liquid surface and over a plain.

As for the relevance for the BC aggregates and wedge-shape pores, if we assume the primary particles are point connected, the saddle surface between two spheres can be treated like a small wedge if we observe close enough to the contact point, with the first principal radius be a few nanometers between the spheres and the second principal radius be along the circle. The second

principal radius could be an order of magnitude larger than the first principal radius, and thus can be roughly approximated to be infinite.

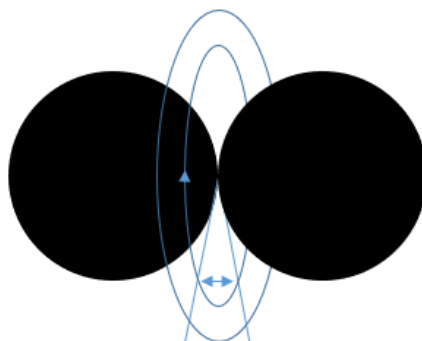


Figure R2 5. Scheme of the wedge-like pore formation between BC primary particles.

We removed Appendix C and this sentence so that we can focus on the IN data and discussion of morphology, hydrophilicity, etc.

L371-375: “The physio-chemical properties of COJ300 particles, including oxidized surface, appropriate $\overline{d_{pp}}$, and compacted spherical morphology, may result in higher probability to have cavities with appropriate size and hydrophilicity on particle surfaces (Mahrt et al., 2020). Such cavities can accommodate liquid water below bulk water saturation and initiate homogeneous freezing of liquid water via PCF pathway (Marcolli, 2014; David et al., 2019; David et al., 2020).”

- *Figs. 3 (and 5): Does each dot correspond to a single RH-scan?*

[Response]: Each dot in Fig. 3 and 5 represents a separate RH scan ramp. To ensure consistency, the IN onset of a certain BC type was determined from consecutive RH scan ramps in a day.

- *Sect. 3.2: Can you determine the coating thickness from your measurements. Adding an estimate of the coating thickness to this section would be helpful, in order to estimate for what coating thickness ice nucleation by PCF becomes inhibited.*

[Response]: We can infer a coating thickness of 25 nm from the d_m modal size shift. For detailed surface coverage information, SEM observation would be required, which is our future study scope.

Kulkarni et al. (2016) reported a 120 nm to 280 nm diesel BC modal size shift after α -pinene SOA coating. Combining their results and our data together, a very rough estimation can be obtained using d_m modal size shift as evidence: coating thickness of 25 nm for n -dodecane and β -caryophyllene SOA can inhibit PCF of COJ300.

- *L337: “deposition IN”; please see my general comment above*

[Response]: Changed to “ice formation below homogeneous freezing threshold”.

L379-380: “IN onset SS_i of pure SOA particles are shown as an asterisk separately to rule out the possible ice formation below homogeneous freezing threshold induced by pure SOA.”

- L346-347: *It looks like the onset of toluene SOA-coated BC particles and bare BC particles is still within uncertainty.*

[Response]: We modified the discussion here and attributed the *T-10* results to potential toluene SOA phase state transition.

L389-429: “The toluene SOA mass spectrum in Fig. 6(a) exhibits higher $m/z = 44$ (COO^-) and lower $m/z = 43$ (C_3H_7^-) fraction signal, indicating more oxidized organic species were generated during *T-10* and *T-3* experiments (Lambe et al., 2011b), agreeing with the previous study on toluene SOA (Liu et al., 2018). The higher O/C ratio (Fig. B2) of toluene-derived SOA may enhance the hygroscopicity of the particle (Lambe et al., 2011b; Zhao et al., 2016; Liu et al., 2018) with a potential to form aqueous film on BC surface and reduce the deposition IN ability of BC particles. On the other hand, Hinks et al. (2018) showed that toluene-derived SOA contained a significant amount of oligomers under dry laboratory conditions similar to what we conducted in the PAM chamber in this study. These large oligomers could potentially reduce the hygroscopicity and alter the phase state of toluene SOA to be semi-solid or solid within the temperature range we investigated in this work (DeRieux et al., 2018; Zhang et al., 2018c; Li et al., 2020), under which the SOA can still nucleate ice (Murray et al., 2010; Berkemeier et al., 2014; Zhang et al., 2019b). The toluene SOA in *T-10* with O:C ratio over 1 (Fig. B2) has most likely already transited into solid or semi-solid glassy state at the temperature range we investigated before entering SPIN (DeRieux et al., 2018). Therefore, it is very likely that BC particles are mostly stucked with or embedded in these glassy SOA with some bare BC part exposure. Ice crystals may therefore form on the carbonaceous part of partially coated particles, whose IN onset SS_i should be the same as bare COJ300. At temperatures above -43°C , toluene SOA-coated BC particles nucleate ice at $SS_i \sim 0.1$ to 0.15 above bare 350 nm COJ300, but still ~ 0.15 below the homogeneous freezing threshold. This might be due to the hygroscopicity enhancement of the toluene SOA-coated BC in *T-10*. BC coated by ~ 10 - 15 equivalent days atmospherically oxidized toluene SOA (*T-3* in Table 2) is less IN active than those coated by highly oxidized toluene SOA (*T-10*) at around -46°C and -43°C . This might also be attributed the oxidation level and the corresponding phase state difference between the SOA generated from *T-10* and *T-3* experiments, which is beyond the scope of this study and requires further detailed phase transition study for toluene SOA. Overall, two competing effects, i.e. the hygroscopicity enhancement deactivating BC IN ability, together with toluene SOA glass phase transition producing stucked or partly coated BC, may make our toluene SOA coating IN onset move towards but not fully in the homogeneous freezing regime. The toluene SOA coated diesel combustion BC (Kulkarni et al., 2016), however, nucleate ice near the homogeneous threshold, as indicated in Fig. 3(a). This might be due to the much thicker (90 nm) organic coating in their study compared to the 25 nm coating of this work, leading to a complete coverage of BC surface.”

- L349: *10-15 days is longer than the average tropospheric lifetime of soot particles. This should be reflected in your discussion.*

[Response]: We agree with the referee that the typical life time of BC particles in the troposphere can be days to weeks (Cape et al., 2012; Lund et al., 2018). However, the life time of BC particles in the tropopause can be extended to months (Pusechel et al., 1992; Yu et al., 2019).

- Fig. 6: Showing difference spectra between each panel and the bare soot shown in Fig. 6d would facilitate showing the differences between the coatings.

[Response]: Added BG-10 for each plot, denoted as grey bars to show the difference clearly.

- L369: Rephrase to: “The IN onset...” ... “... in Fig. 5b show that these particles nucleate ice ...”

[Response]: Rephrased as suggested.

- L373: Can you provide a difference AMS spectra of the OH and the O3 oxidized β -caryophyllene coated BC particles?

[Response]: Added B-0 spectra in Fig. 6(c3).

- L384: “form” instead of “forms”

[Response]: Modified.

- Fig. 7:
 - o It would be helpful to add the H/C and the O/C values of the O3 oxidized β -caryophyllene soot here as well.

[Response]: Added. Please see our response to the next comment.

- o Please verify that the suggested slope for the toluene coated SOA is correct. From your legend it looks like you should connect the white start in the lower left corner to the blue star in the middle right. If that is the case, you need to revise your statement in L378-380.

[Response]: We gratefully thank the referee for making us revisit this figure and think deeper.

We noted that the O/C and H/C ratio in Fig. 7 is closer to glyoxal SOA rather than toluene SOA (Lambe et al., 2011b), which is also true for the f_{44}/f_{43} plot in modified Fig. B2. It is reported that toluene photolysis can produce glyoxal (Volkamer et al., 2001), which may lead to oligomerization under dry condition (Hinks et al., 2018). The slopes between pure toluene (hollow symbols at lower left) and T-10 and T-3 are 0.71 and 0.99 in Fig. 7, respectively. This suggests that benzene ring or carbon-carbon double bond breakage accompanied by oxygen and hydrogen atoms addition might have happened during the experiments, which is compliant with the glyoxal formation pathway in Volkamer et al. (2001). Therefore, we believe that the toluene SOA in T-10 and T-3 experiments represent the highly oxidized late generation products with oligomer formation.

The statement between L438-440, however, represents early stage OH oxidation reactions for *n*-dodecane and β -caryophyllene. OH oxidation of toluene has already passed the stage and the SOA in T-10 and T-3 experiments can be treated as oxidation products of toluene SOA.

Fig. 7 was modified by adding lines connecting pure toluene and T-10 and T-3, and a line connecting pure β -caryophyllene and B-0, respectively.

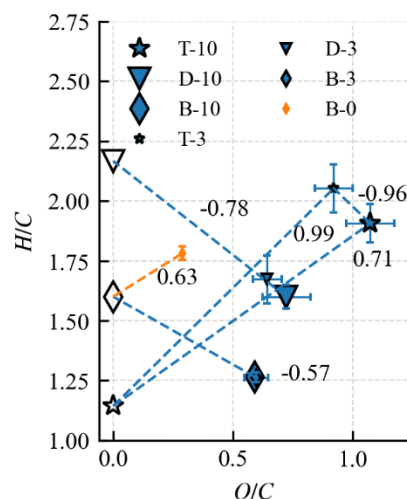


Figure R2 6 Modified Fig. 7

Added “Volkamer et al. (2001) proved that glyoxal, which could facilitate the oligomerization as described by Hinks et al. (2018), can be produced from toluene reaction with OH as highly oxidized products. The slopes of T-10 and T-3 in Fig. 7 lie between 0-1 (0.71 and 0.99 for T-10 and T-3, respectively), suggests that oxygen and hydrogen atom addition accompanied by carbon-carbon double bond as well as benzene ring breakage might have happened during the toluene photooxidation experiments.” between L407-411.

L404-416: “The higher O/C ratio (Fig. 7) of toluene-derived SOA may enhance the hygroscopicity of the particle (Lambe et al., 2011b; Zhao et al., 2016; Liu et al., 2018) with a potential to form aqueous film on BC surface and reduce the IN ability of BC particles. On the other hand, Hinks et al. (2018) showed that toluene-derived SOA contained a significant amount of oligomers under dry laboratory conditions similar to what we conducted in the PAM chamber in this study. Volkamer et al. (2001) proved that glyoxal, which could facilitate the oligomerization as described by Hinks et al. (2018), can be produced from toluene reaction with OH as highly oxidized products. The slopes of T-10 and T-3 in Fig. 7 lie between 0-1 (0.71 and 0.99 for T-10 and T-3, respectively), suggests that oxygen and hydrogen atom addition accompanied by carbon-carbon double bond as well as benzene ring breakage might have happened during the toluene photooxidation experiments. These large oligomers could potentially reduce the hygroscopicity and alter the phase state of toluene SOA to be semi-solid or solid within the temperature range we investigated in this work (DeRieux et al., 2018; Zhang et al., 2018c; Li et al., 2020), under which the SOA can still nucleate ice (Murray et al., 2010; Berkemeier et al., 2014; Zhang et al., 2019b). The toluene SOA in *T-10* with O:C ratio over 1 (Fig. 7) has most likely already transited into solid or semi-solid glassy state at the temperature range we investigated before entering SPIN (DeRieux et al., 2018)”

- L392: Add: “In these studies shifts from...”

[Response]: Rephrased.

- L394-396: *I do not think that it is the volatility that changes and allows a SOA particle to become glassy, but the phase state (here viscosity). Please reformulate.*

[Response]: Changed “volatility” to “phase state”.

- L396-398: *If the suppression of the ice nucleation results from filling of the pores, the ice nucleation mechanism of the bare/uncoated particles would likely be best described by PCF, not? Please see my general comment above.*

[Response]: Yes, you are right.

L458-460: “The suppression of BC IN ability by organic coating was attributed to coverage of surface-active sites and filling of pores on BC surface when the volatility of the organic coating is relatively high and might present in liquid phase.”

- L401: *Please give details about the mass loadings used in the PAM and briefly comment on typical tropospheric SOA mass loadings.*

[Response]: Change to “...with 200 to 4000 folds of typical tropospheric SOA (Tsigaridis and Kanakidou, 2003; Heald et al., 2008; Hodzic et al., 2016) mass loading in PAM chamber (~2000 to 4000 $\mu\text{g m}^{-3}$)...”

L462-465: “Our results suggest that less oxidized SOA (*n*-dodecane and β -caryophyllene derived SOA from photooxidation), with 200 to 4000 folds of typical tropospheric SOA (Tsigaridis and Kanakidou, 2003; Heald et al., 2008; Hodzic et al., 2016) mass loading in PAM chamber (~2000 to 4000 $\mu\text{g m}^{-3}$), are more likely to condense on seed particle and form fully coated BC particles, moving IN onset SS_i to the homogeneous regime...”

- L412-415: *This discussion should be expanded and more specific examples are needed to make the claim that the characteristics of the investigated BC types is similar to ambient soot.*

[Response]: Reformulated and added specific literature examples.

L474-485: “The morphological characteristics are within the value range of typical BC emitted from combustion sources, and those collected in field observation (e.g., Lapuerta et al., 2007; China et al., 2013; China et al., 2014; Vander Wal et al., 2014; China et al., 2015b; Zhang et al., 2019a). BC primary particle size range in this study lies between 10 to 70 nm with a modal size around 25 to 40 nm, being consistent with previous primary particle studies on combustion BC (e.g., Smekens et al., 2005; Liati et al., 2016; Joo et al., 2018). Previous field observation of transportation emission and biomass burning reported that ambient BC occupied d_a , circularity and roundness in the range of 130 to 940 nm, 0.19 to 0.55 and 0.32 to 0.6, respectively (China et al., 2013; China et al., 2014; China et al., 2015a; China et al., 2015b), overlapping with the range in this work. R2500U is similar to the fresh BC emitted from B737 at medium power burning conventional jet fuel in terms of morphology characteristics (Vander Wal et al., 2014). The primary particle size is consistent with BC emitted from prevalent gas turbine engines (Huang and Vander Wal, 2013). Findings in this study can be relevant to airborne aircraft emissions and ground emissions carried by updrafts to tropopause.”

- L419: *The reported threshold of “ $dm < 200 \text{ nm}$ ” seems rather high and is misleading. For instance, Moore et al. (2017) report mode sizes of around 30 nm. While Kittelson*

(1998) report soot aggregates up to 200 nm (see their Fig. 11) a more profound literature search should be done here to support the given threshold.

[Response]: Rephrased to "...which are generally fractal and smaller than 200 nm with modal size ranging from 20 to 100 nm (Kittelson, 1998; Wey et al., 2006; Anderson et al., 2011; Wang et al., 2016; Moore et al., 2017; Awad et al., 2020)."

We meant to say that freshly emitted BC particles from transportation are typically smaller than 200 nm.

L488-490: "This is important for freshly emitted BC from aircraft engines and ground transportation, which are generally fractal and smaller than 200 nm with modal size ranging from 20 to 100 nm (Kittelson, 1998; Wey et al., 2006; Anderson et al., 2011; Wang et al., 2016; Moore et al., 2017; Raza et al., 2018; Awad et al., 2020)."

- L423: Change to: "However, IN ability of small BC particles... may collapse forming PCF favoring..."

[Response]: Changed as suggested.

- L424-425: Why do you mention "surfaces" here and then talk about the "mesopores" in the next sentence.

[Response]: Reorganized the sequences. Please see the response to next comment.

- L425: The connection between the primary particle size and the mesopores is unclear and should be further elaborated.

[Response]: Rephrased and emphasis the importance of d_{pp} .

L494-499: "Apart from the most spherical morphology, the smaller d_{pp} of COJ300 may also offer higher probability to form smaller mesopores with appropriate size to accommodate ice crystal formation below water saturation, with particles down to 100 nm can act as efficient INP. Pores formed by BC with larger d_{pp} might be too wide to accommodate liquid water at our experimental conditions. Besides, the COJ300 IN results imply that ice crystal formation may favor oxidized hydrophilic surfaces, confirming the importance of surface hydrophilicity for pore filling in PCF mechanism (David et al., 2019; David et al., 2020)."

- L426: I suggest tuning down: "This suggest that long-lived...INPs."

[Response]: Changed as suggested.

- L433: Specify as: "... growth, SOA-coated soot particles..."

[Response]: Specified as suggested.

- L441: Delete "monodisperse", your Fig. 2 indicates a more polydisperse sample.

[Response]: Deleted.

- L444: Why is the R330R sample "atmospheric compacted"? The COJ300 is the most round according to your Fig. 3B and Table 1.

[Response]: It is correct that COJ300 is the most spherical one. However, R330R is also relatively spherical based on Fig. A3 and Table 1, even though not as spherical as COJ300. With its modified surface, we prefer to refer COJ300 as "atmospheric compacted and oxidized", because oxidation may also modify the BC particle surface and make it more spherical.

Changed the description of COJ300 to “atmospheric compacted and oxidized”.

L517-519: “...freshly emitted (R2500U), atmospheric compacted (R330R), and atmospheric compacted and oxidized (COJ300).”

- L449: “*deposition nucleation*”; please see my general comment above. I think that in particular in the summary section you need to be careful on how to describe the ice nucleation mechanism, as in the same section (L456 and L461), you imply some ice formation via PCF.

[Response]: Replaced the terms accordingly.

L522: “The onset of some IN below homogeneous freezing threshold, as opposed to ...”

- L451-452: See my earlier comment. The study by Mahrt et al. (2020) found more compacted soot particles to be better INP (via the PCF mechanism) compared to less compacted soot.

[Response]: Rephrased.

L523-525: “We conclude that BC IN favors larger, spherical particles with oxidized hydrophilic surface. The highly fractal BC particles did not necessarily act as superior deposition INP over more spherical ones as would normally be anticipated from surface area. This could be attributed to PCF occurring in the pores and cavities with appropriate size offered by compacted BC particles.”

Reference

- Anderson, B. E., Beyersdorf, A. J., Hudgins, C. H., Plant, J. V., Thornhill, K. L., Winstead, E. L., Ziemba, L. D., Howard, R., Corporan, E., Miake-Lye, R. C., Herndon, S. C., Timko, M., Woods, E., Dodds, W., Lee, B., Santoni, G., Whitefield, P., Hagen, D., Lobo, P., Knighton, W. B., Bulzan, D., Tacina, K., Wey, C., VanderWal, R., and Bhargava, A.: Alternative Aviation Fuel Experiment (Aafex), National Aeronautics and Space Administration, Langley Research Center. NASA/TM-2011-217059., Hanover, 2011.
- Anderson, P. M., Guo, H., and Sunderland, P. B.: Repeatability and Reproducibility of Tem Soot Primary Particle Size Measurements and Comparison of Automated Methods, *Journal of Aerosol Science*, 114, 317-326, <https://doi.org/10.1016/j.jaerosci.2017.10.002>, 2017.
- Arey, J., Winer, A. M., Atkinson, R., Aschmann, S. M., Long, W. D., Morrison, C. L., and Olszyk, D. M.: Terpenes Emitted from Agricultural Species Found in California's Central Valley, *Journal of Geophysical Research: Atmospheres*, 96, 9329-9336, 10.1029/91JD00447, 1991.
- Awad, O. I., Ma, X., Kamil, M., Ali, O. M., Zhang, Z., and Shuai, S.: Particulate Emissions from Gasoline Direct Injection Engines: A Review of How Current Emission Regulations Are Being Met by Automobile Manufacturers, *Science of The Total Environment*, 718, 137302, <https://doi.org/10.1016/j.scitotenv.2020.137302>, 2020.
- Berkemeier, T., Shiraiwa, M., Pöschl, U., and Koop, T.: Competition between Water Uptake and Ice Nucleation by Glassy Organic Aerosol Particles, *Atmospheric Chemistry and Physics*, 14, 12513-12531, 10.5194/acp-14-12513-2014, 2014.
- Borgnakke, C., and Sonntag, R. E.: Thermodynamic Relations, in: *Fundamentals of Thermodynamics*, 8th ed., Wiley, New York, 557, 2013.
- Cabot Corporation: <https://www.cabotcorp.com/search/?query=regal+330R>, last access: 9 October, 2020.
- Calogirou, A., Kotzias, D., and Kettrup, A.: Product Analysis of the Gas-Phase Reaction of B-Caryophyllene with Ozone, *Atmospheric Environment*, 31, 283-285, [https://doi.org/10.1016/1352-2310\(96\)00190-2](https://doi.org/10.1016/1352-2310(96)00190-2), 1997.
- Cape, J. N., Coyle, M., and Dumitrean, P.: The Atmospheric Lifetime of Black Carbon, *Atmospheric Environment*, 59, 256-263, <https://doi.org/10.1016/j.atmosenv.2012.05.030>, 2012.
- China, S., Kulkarni, G., Scarnato, B. V., Sharma, N., Pekour, M., Shilling, J. E., Wilson, J., Zelenyuk, A., Chand, D., Liu, S., Aiken, A. C., Dubey, M., Laskin, A., Zaveri, R. A., and Mazzoleni, C.: Morphology of Diesel Soot Residuals from Supercooled Water Droplets and Ice Crystals: Implications for Optical Properties, *Environmental Research Letters*, 10, 114010, 10.1088/1748-9326/10/11/114010, 2015a.
- China, S., Mazzoleni, C., Gorkowski, K., Aiken, A. C., and Dubey, M. K.: Morphology and Mixing State of Individual Freshly Emitted Wildfire Carbonaceous Particles, *Nature communications*, 4, 2122, 10.1038/ncomms3122, 2013.
- China, S., Salvadori, N., and Mazzoleni, C.: Effect of Traffic and Driving Characteristics on Morphology of Atmospheric Soot Particles at Freeway on-Ramps, *Environmental Science & Technology*, 48, 3128-3135, 10.1021/es405178n, 2014.

- China, S., Scarnato, B., Owen, R. C., Zhang, B., Ampadu, M. T., Kumar, S., Dzepina, K., Dziobak, M. P., Fialho, P., Perlinger, J. A., Hueber, J., Helmig, D., Mazzoleni, L. R., and Mazzoleni, C.: Morphology and Mixing State of Aged Soot Particles at a Remote Marine Free Troposphere Site: Implications for Optical Properties, *Geophysical Research Letters*, 42, 1243-1250, doi:10.1002/2014GL062404, 2015b.
- Ciccioli, P., Brancaleoni, E., Frattoni, M., Di Palo, V., Valentini, R., Tirone, G., Seufert, G., Bertin, N., Hansen, U., Csiky, O., Lenz, R., and Sharma, M.: Emission of Reactive Terpene Compounds from Orange Orchards and Their Removal by within-Canopy Processes, *Journal of Geophysical Research: Atmospheres*, 104, 8077-8094, 10.1029/1998jd100026, 1999.
- Connolly, P. J., Möhler, O., Field, P. R., Saathoff, H., Burgess, R., Choularton, T., and Gallagher, M.: Studies of Heterogeneous Freezing by Three Different Desert Dust Samples, *Atmos. Chem. Phys.*, 9, 2805-2824, 10.5194/acp-9-2805-2009, 2009.
- Cziczo, D. J., Thomson, D. S., Thompson, T. L., DeMott, P. J., and Murphy, D. M.: Particle Analysis by Laser Mass Spectrometry (Palms) Studies of Ice Nuclei and Other Low Number Density Particles, *International Journal of Mass Spectrometry*, 258, 21-29, 10.1016/j.ijms.2006.05.013, 2006.
- David, R. O., Fahrni, J., Marcolli, C., Mahrt, F., Brühwiler, D., and Kanji, Z. A.: The Role of Contact Angle and Pore Width on Pore Condensation and Freezing, *Atmos. Chem. Phys.*, 20, 9419-9440, 10.5194/acp-20-9419-2020, 2020.
- David, R. O., Marcolli, C., Fahrni, J., Qiu, Y., Perez Sirkin, Y. A., Molinero, V., Mahrt, F., Brühwiler, D., Lohmann, U., and Kanji, Z. A.: Pore Condensation and Freezing Is Responsible for Ice Formation Below Water Saturation for Porous Particles, *Proceedings of the National Academy of Sciences*, 116, 8184-8189, 10.1073/pnas.1813647116, 2019.
- DeCarlo, P. F., Kimmel, J. R., Trimborn, A., Northway, M. J., Jayne, J. T., Aiken, A. C., Gonin, M., Fuhrer, K., Horvath, T., Docherty, K. S., Worsnop, D. R., and Jimenez, J. L.: Field-Deployable, High-Resolution, Time-of-Flight Aerosol Mass Spectrometer, *Analytical Chemistry*, 78, 8281-8289, 10.1021/ac061249n, 2006.
- DeRieux, W. S. W., Li, Y., Lin, P., Laskin, J., Laskin, A., Bertram, A. K., Nizkorodov, S. A., and Shiraiwa, M.: Predicting the Glass Transition Temperature and Viscosity of Secondary Organic Material Using Molecular Composition, *Atmos. Chem. Phys.*, 18, 6331-6351, 10.5194/acp-18-6331-2018, 2018.
- Fioletov, V. E.: Ozone Climatology, Trends, and Substances That Control Ozone, *Atmosphere-Ocean*, 46, 39-67, 10.3137/ao.460103, 2008.
- Fisher, L. R., Gamble, R. A., and Middlehurst, J.: The Kelvin Equation and the Capillary Condensation of Water, *Nature*, 290, 575-576, 10.1038/290575a0, 1981.
- Fletcher, N. H.: Nucleation and Growth of Ice Crystals Upon Crystalline Substrates, *Australian Journal of Physics*, 13, 408-418, 1960.
- Fletcher, N. H.: Active Sites and Ice Crystal Nucleation, *Journal of the Atmospheric Sciences*, 26, 1266-1271, 10.1175/1520-0469(1969)026<1266:asaicn>2.0.co;2, 1969.
- Fu, P. Q., Kawamura, K., Pochanart, P., Tanimoto, H., Kanaya, Y., and Wang, Z. F.: Summertime Contributions of Isoprene, Monoterpenes, and Sesquiterpene Oxidation to the Formation of Secondary Organic Aerosol in the Troposphere over Mt. Tai, Central

- East China During Mtx2006, *Atmos. Chem. Phys. Discuss.*, 2009, 16941-16972, 10.5194/acpd-9-16941-2009, 2009.
- Garimella, S., Kristensen, T. B., Ignatius, K., Welti, A., Voigtländer, J., Kulkarni, G. R., Sagan, F., Kok, G. L., Dorsey, J., Nichman, L., Rothenberg, D. A., Rösch, M., Kirchgäßner, A. C. R., Ladkin, R., Wex, H., Wilson, T. W., Ladino, L. A., Abbatt, J. P. D., Stetzer, O., Lohmann, U., Stratmann, F., and Cziczo, D. J.: The Spectrometer for Ice Nuclei (Spin): An Instrument to Investigate Ice Nucleation, *Atmospheric Measurement Techniques*, 9, 2781-2795, 10.5194/amt-9-2781-2016, 2016.
- Garimella, S., Rothenberg, D. A., Wolf, M. J., David, R. O., Kanji, Z. A., Wang, C., Rösch, M., and Cziczo, D. J.: Uncertainty in Counting Ice Nucleating Particles with Continuous Flow Diffusion Chambers, *Atmos. Chem. Phys.*, 17, 10855-10864, 10.5194/acp-17-10855-2017, 2017.
- Gottelman, A., Hoor, P., Pan, L. L., Randel, W. J., Hegglin, M. I., and Birner, T.: The Extratropical Upper Troposphere and Lower Stratosphere, *Reviews of Geophysics*, 49, 10.1029/2011RG000355, 2011.
- Griffin, R. J., Cocker III, D. R., Seinfeld, J. H., and Dabdub, D.: Estimate of Global Atmospheric Organic Aerosol from Oxidation of Biogenic Hydrocarbons, *Geophysical Research Letters*, 26, 2721-2724, 10.1029/1999gl900476, 1999.
- Grosjean, D., Williams, E. L., Grosjean, E., Andino, J. M., and Seinfeld, J. H.: Atmospheric Oxidation of Biogenic Hydrocarbons: Reaction of Ozone With .Beta.-Pinene, D-Limonene and Trans-Caryophyllene, *Environmental Science & Technology*, 27, 2754-2758, 10.1021/es00049a014, 1993.
- Guenther, A. B., Jiang, X., Heald, C. L., Sakulyanontvittaya, T., Duhl, T., Emmons, L. K., and Wang, X.: The Model of Emissions of Gases and Aerosols from Nature Version 2.1 (Megan2.1): An Extended and Updated Framework for Modeling Biogenic Emissions, *Geosci. Model Dev.*, 5, 1471-1492, 10.5194/gmd-5-1471-2012, 2012.
- Heald, C. L., Henze, D. K., Horowitz, L. W., Feddema, J., Lamarque, J. F., Guenther, A., Hess, P. G., Vitt, F., Seinfeld, J. H., Goldstein, A. H., and Fung, I.: Predicted Change in Global Secondary Organic Aerosol Concentrations in Response to Future Climate, Emissions, and Land Use Change, *Journal of Geophysical Research: Atmospheres*, 113, 10.1029/2007JD009092, 2008.
- Helmig, D., Ortega, J., Guenther, A., Herrick, J. D., and Geron, C.: Sesquiterpene Emissions from Loblolly Pine and Their Potential Contribution to Biogenic Aerosol Formation in the Southeastern Us, *Atmospheric Environment*, 40, 4150-4157, <https://doi.org/10.1016/j.atmosenv.2006.02.035>, 2006.
- Henrot, A. J., Stanelle, T., Schröder, S., Siegenthaler, C., Taraborrelli, D., and Schultz, M. G.: Implementation of the Megan (V2.1) Biogenic Emission Model in the Echam6-Hammoz Chemistry Climate Model, *Geosci. Model Dev.*, 10, 903-926, 10.5194/gmd-10-903-2017, 2017.
- Hinks, M. L., Montoya-Aguilera, J., Ellison, L., Lin, P., Laskin, A., Laskin, J., Shiraiwa, M., Dabdub, D., and Nizkorodov, S. A.: Effect of Relative Humidity on the Composition of Secondary Organic Aerosol from the Oxidation of Toluene, *Atmos. Chem. Phys.*, 18, 1643-1652, 10.5194/acp-18-1643-2018, 2018.

- Hodzic, A., Jimenez, J. L., Madronich, S., Canagaratna, M. R., DeCarlo, P. F., Kleinman, L., and Fast, J.: Modeling Organic Aerosols in a Megacity: Potential Contribution of Semi-Volatile and Intermediate Volatility Primary Organic Compounds to Secondary Organic Aerosol Formation, *Atmos. Chem. Phys.*, 10, 5491-5514, 10.5194/acp-10-5491-2010, 2010.
- Hodzic, A., Kasibhatla, P. S., Jo, D. S., Cappa, C. D., Jimenez, J. L., Madronich, S., and Park, R. J.: Rethinking the Global Secondary Organic Aerosol (Soa) Budget: Stronger Production, Faster Removal, Shorter Lifetime, *Atmos. Chem. Phys.*, 16, 7917-7941, 10.5194/acp-16-7917-2016, 2016.
- Hoffmann, T., Odum, J. R., Bowman, F., Collins, D., Klockow, D., Flagan, R. C., and Seinfeld, J. H.: Formation of Organic Aerosols from the Oxidation of Biogenic Hydrocarbons, *Journal of Atmospheric Chemistry*, 26, 189-222, 10.1023/A:1005734301837, 1997.
- Hu, D., Bian, Q., Li, T. W. Y., Lau, A. K. H., and Yu, J. Z.: Contributions of Isoprene, Monoterpenes, B-Caryophyllene, and Toluene to Secondary Organic Aerosols in Hong Kong During the Summer of 2006, *Journal of Geophysical Research: Atmospheres*, 113, 10.1029/2008jd010437, 2008.
- Huang, C.-H., and Vander Wal, R. L.: Effect of Soot Structure Evolution from Commercial Jet Engine Burning Petroleum Based Jp-8 and Synthetic H₂ and Ft Fuels, *Energy & Fuels*, 27, 4946-4958, 10.1021/ef400576c, 2013.
- Ignatius, K., Kristensen, T. B., Järvinen, E., Nichman, L., Fuchs, C., Gordon, H., Herenz, P., Hoyle, C. R., Duplissy, J., Garimella, S., Dias, A., Frege, C., Höppel, N., Tröstl, J., Wagner, R., Yan, C., Amorim, A., Baltensperger, U., Curtius, J., Donahue, N. M., Gallagher, M. W., Kirkby, J., Kulmala, M., Möhler, O., Saathoff, H., Schnaiter, M., Tomé, A., Virtanen, A., Worsnop, D., and Stratmann, F.: Heterogeneous Ice Nucleation of Viscous Secondary Organic Aerosol Produced from Ozonolysis of α -Pinene, *Atmos. Chem. Phys.*, 16, 6495-6509, 10.5194/acp-16-6495-2016, 2016.
- Jacobson, M. Z.: Strong Radiative Heating Due to the Mixing State of Black Carbon in Atmospheric Aerosols, *Nature*, 409, 695-697, 10.1038/35055518, 2001.
- Jaoui, M., Kleindienst, T. E., Docherty, K. S., Lewandowski, M., and Offenberg, J. H.: Secondary Organic Aerosol Formation from the Oxidation of a Series of Sesquiterpenes: α -Cedrene, B-Caryophyllene, α -Humulene and α -Farnesene with O₃, OH and NO₃ Radicals, *Environmental Chemistry*, 10, 178-193, <https://doi.org/10.1071/EN13025>, 2013.
- Jaoui, M., Lewandowski, M., Kleindienst, T. E., Offenberg, J. H., and Edney, E. O.: B-Caryophyllinic Acid: An Atmospheric Tracer for B-Caryophyllene Secondary Organic Aerosol, *Geophysical Research Letters*, 34, 10.1029/2006GL028827, 2007.
- Jayne, J. T., Leard, D. C., Zhang, X., Davidovits, P., Smith, K. A., Kolb, C. E., and Worsnop, D. R.: Development of an Aerosol Mass Spectrometer for Size and Composition Analysis of Submicron Particles, *Aerosol Science and Technology*, 33, 49-70, 10.1080/027868200410840, 2000.
- Joo, P. H., Gigone, B., Griffin, E. A., Christensen, M., and Gülder, Ö. L.: Soot Primary Particle Size Dependence on Combustion Pressure in Laminar Ethylene Diffusion Flames, *Fuel*, 220, 464-470, <https://doi.org/10.1016/j.fuel.2018.02.025>, 2018.

- Joyce, G. A., and Henry, W. M.: Modeling the Equilibrium Compressed Void Volume of Carbon Black, *Rubber Chemistry and Technology*, 79, 735-764, 10.5254/1.3547964, 2006.
- Karlsson, M. N. A., and Martinsson, B. G.: Methods to Measure and Predict the Transfer Function Size Dependence of Individual Dmas, *Journal of Aerosol Science*, 34, 603-625, [https://doi.org/10.1016/S0021-8502\(03\)00020-X](https://doi.org/10.1016/S0021-8502(03)00020-X), 2003.
- Kiselev, A., Bachmann, F., Pedevilla, P., Cox, S. J., Michaelides, A., Gerthsen, D., and Leisner, T.: Active Sites in Heterogeneous Ice Nucleation-the Example of K-Rich Feldspars, *Science*, 355, 367-371, 10.1126/science.aai8034, 2017.
- Kittelson, D. B.: Engines and Nanoparticles: A Review, *Journal of Aerosol Science*, 29, 575-588, [https://doi.org/10.1016/S0021-8502\(97\)10037-4](https://doi.org/10.1016/S0021-8502(97)10037-4), 1998.
- Koehler, K. A., DeMott, P. J., Kreidenweis, S. M., Popovicheva, O. B., Petters, M. D., Carrico, C. M., Kireeva, E. D., Khokhlova, T. D., and Shonija, N. K.: Cloud Condensation Nuclei and Ice Nucleation Activity of Hydrophobic and Hydrophilic Soot Particles, *Physical Chemistry Chemical Physics*, 11, 7906-7920, 10.1039/B905334B, 2009.
- Koop, T.: Crystals Creeping out of Cracks, *Proceedings of the National Academy of Sciences*, 114, 797-799, 10.1073/pnas.1620084114, 2017.
- Kulkarni, G., China, S., Liu, S., Nandasiri, M., Sharma, N., Wilson, J., Aiken, A. C., Chand, D., Laskin, A., Mazzoleni, C., Pekour, M., Shilling, J., Shutthanandan, V., Zelenyuk, A., and Zaveri, R. A.: Ice Nucleation Activity of Diesel Soot Particles at Cirrus Relevant Temperature Conditions: Effects of Hydration, Secondary Organics Coating, Soot Morphology, and Coagulation, *Geophysical Research Letters*, 43, 3580-3588, 10.1002/2016gl068707, 2016.
- Kulkarni, G. R., and Kok, G. L.: Mobile Ice Nucleus Spectrometer, ; Pacific Northwest National Lab. (PNNL), Richland, WA (United States)PNNL-21384; Other: 600306000 United States 10.2172/1071991 Other: 600306000 PNNL English, Medium: ED; Size: PDFN, 2012.
- Ladino, L. A., Zhou, S., Yakobi-Hancock, J. D., Aljawhary, D., and Abbatt, J. P. D.: Factors Controlling the Ice Nucleating Abilities of A-Pinene Soa Particles, *Journal of Geophysical Research: Atmospheres*, 119, 9041-9051, 10.1002/2014JD021578, 2014.
- Lambe, A. T., Ahern, A. T., Williams, L. R., Slowik, J. G., Wong, J. P. S., Abbatt, J. P. D., Brune, W. H., Ng, N. L., Wright, J. P., Croasdale, D. R., Worsnop, D. R., Davidovits, P., and Onasch, T. B.: Characterization of Aerosol Photooxidation Flow Reactors: Heterogeneous Oxidation, Secondary Organic Aerosol Formation and Cloud Condensation Nuclei Activity Measurements, *Atmos. Meas. Tech.*, 4, 445-461, 10.5194/amt-4-445-2011, 2011a.
- Lambe, A. T., Onasch, T. B., Massoli, P., Croasdale, D. R., Wright, J. P., Ahern, A. T., Williams, L. R., Worsnop, D. R., Brune, W. H., and Davidovits, P.: Laboratory Studies of the Chemical Composition and Cloud Condensation Nuclei (Ccn) Activity of Secondary Organic Aerosol (Soa) and Oxidized Primary Organic Aerosol (Opoa), *Atmos. Chem. Phys.*, 11, 8913-8928, 10.5194/acp-11-8913-2011, 2011b.
- Lapuerta, M., Martos, F. J., and Herreros, J. M.: Effect of Engine Operating Conditions on the Size of Primary Particles Composing Diesel Soot Agglomerates, *Journal of Aerosol Science*, 38, 455-466, <https://doi.org/10.1016/j.jaerosci.2007.02.001>, 2007.

- Lee-Taylor, J., Madronich, S., Aumont, B., Baker, A., Camredon, M., Hodzic, A., Tyndall, G. S., Apel, E., and Zaveri, R. A.: Explicit Modeling of Organic Chemistry and Secondary Organic Aerosol Partitioning for Mexico City and Its Outflow Plume, *Atmos. Chem. Phys.*, 11, 13219-13241, 10.5194/acp-11-13219-2011, 2011.
- Lee, A., Goldstein, A. H., Kroll, J. H., Ng, N. L., Varutbangkul, V., Flagan, R. C., and Seinfeld, J. H.: Gas-Phase Products and Secondary Aerosol Yields from the Photooxidation of 16 Different Terpenes, *Journal of Geophysical Research: Atmospheres*, 111, 10.1029/2006jd007050, 2006.
- Li, M., Karu, E., Brenninkmeijer, C., Fischer, H., Lelieveld, J., and Williams, J.: Tropospheric Oh and Stratospheric Oh and Cl Concentrations Determined from Ch₄, Ch₃cl, and Sf₆ Measurements, *npj Climate and Atmospheric Science*, 1, 29, 10.1038/s41612-018-0041-9, 2018.
- Li, Y., Day, D. A., Stark, H., Jimenez, J. L., and Shiraiwa, M.: Predictions of the Glass Transition Temperature and Viscosity of Organic Aerosols from Volatility Distributions, *Atmos. Chem. Phys.*, 20, 8103-8122, 10.5194/acp-20-8103-2020, 2020.
- Liati, A., Brem, B. T., Durdina, L., Vogtli, M., Dasilva, Y. A., Eggenschwiler, P. D., and Wang, J.: Electron Microscopic Study of Soot Particulate Matter Emissions from Aircraft Turbine Engines, *Environmental science & technology*, 48, 10975-10983, 10.1021/es501809b, 2014.
- Liati, A., Schreiber, D., Dimopoulos Eggenschwiler, P., Arroyo Rojas Dasilva, Y., and Spiteri, A. C.: Electron Microscopic Characterization of Soot Particulate Matter Emitted by Modern Direct Injection Gasoline Engines, *Combustion and Flame*, 166, 307-315, 10.1016/j.combustflame.2016.01.031, 2016.
- Liu, T., Huang, D. D., Li, Z., Liu, Q., Chan, M., and Chan, C. K.: Comparison of Secondary Organic Aerosol Formation from Toluene on Initially Wet and Dry Ammonium Sulfate Particles at Moderate Relative Humidity, *Atmos. Chem. Phys.*, 18, 5677-5689, 10.5194/acp-18-5677-2018, 2018.
- Lund, M. T., Samset, B. H., Skeie, R. B., Watson-Parris, D., Katich, J. M., Schwarz, J. P., and Weinzierl, B.: Short Black Carbon Lifetime Inferred from a Global Set of Aircraft Observations, *npj Climate and Atmospheric Science*, 1, 31, 10.1038/s41612-018-0040-x, 2018.
- Lüönd, F., Stetzer, O., Welte, A., and Lohmann, U.: Experimental Study on the Ice Nucleation Ability of Size-Selected Kaolinite Particles in the Immersion Mode, *Journal of Geophysical Research: Atmospheres*, 115, 10.1029/2009jd012959, 2010.
- Mahrt, F., Kilchhofer, K., Marcolli, C., Grönquist, P., David, R. O., Rösch, M., Lohmann, U., and Kanji, Z. A.: The Impact of Cloud Processing on the Ice Nucleation Abilities of Soot Particles at Cirrus Temperatures, *Journal of Geophysical Research: Atmospheres*, 125, e2019JD030922, 10.1029/2019jd030922, 2020.
- Mahrt, F., Marcolli, C., David, R. O., Gronquist, P., Meier, E. J. B., Lohmann, U., and Kanji, Z. A.: Ice Nucleation Abilities of Soot Particles Determined with the Horizontal Ice Nucleation Chamber, *Atmospheric Chemistry and Physics*, 18, 13363-13392, 10.5194/acp-18-13363-2018, 2018.

- Marcolli, C.: Deposition Nucleation Viewed as Homogeneous or Immersion Freezing in Pores and Cavities, *Atmospheric Chemistry and Physics*, 14, 2071-2104, 10.5194/acp-14-2071-2014, 2014.
- Marcolli, C.: Technical Note: Fundamental Aspects of Ice Nucleation Via Pore Condensation and Freezing Including Laplace Pressure and Growth into Macroscopic Ice, *Atmos. Chem. Phys.*, 20, 3209-3230, 10.5194/acp-20-3209-2020, 2020.
- Mason, R. H., Si, M., Chou, C., Irish, V. E., Dickie, R., Elizondo, P., Wong, R., Brintnell, M., Elsasser, M., Lassar, W. M., Pierce, K. M., Leaitch, W. R., MacDonald, A. M., Platt, A., Toom-Sauntry, D., Sarda-Estève, R., Schiller, C. L., Suski, K. J., Hill, T. C. J., Abbatt, J. P. D., Huffman, J. A., DeMott, P. J., and Bertram, A. K.: Size-Resolved Measurements of Ice-Nucleating Particles at Six Locations in North America and One in Europe, *Atmos. Chem. Phys.*, 16, 1637-1651, 10.5194/acp-16-1637-2016, 2016.
- Moore, R. H., Thornhill, K. L., Weinzierl, B., Sauer, D., D'Ascoli, E., Kim, J., Lichtenstern, M., Scheibe, M., Beaton, B., Beyersdorf, A. J., Barrick, J., Bulzan, D., Corr, C. A., Crosbie, E., Jurkat, T., Martin, R., Riddick, D., Shook, M., Slover, G., Voigt, C., White, R., Winstead, E., Yasky, R., Ziemba, L. D., Brown, A., Schlager, H., and Anderson, B. E.: Biofuel Blending Reduces Particle Emissions from Aircraft Engines at Cruise Conditions, *Nature*, 543, 411-415, 10.1038/nature21420, 2017.
- Murray, B. J., Wilson, T. W., Dobbie, S., Cui, Z., Al-Jumur, S. M. R. K., Möhler, O., Schnaiter, M., Wagner, R., Benz, S., Niemand, M., Saathoff, H., Ebert, V., Wagner, S., and Kärcher, B.: Heterogeneous Nucleation of Ice Particles on Glassy Aerosols under Cirrus Conditions, *Nature Geoscience*, 3, 233-237, 10.1038/ngeo817, 2010.
- Nguyen, T. L., Winterhalter, R., Moortgat, G., Kanawati, B., Peeters, J., and Vereecken, L.: The Gas-Phase Ozonolysis of B-Caryophyllene (C₁₅H₂₄). Part II: A Theoretical Study, *Physical Chemistry Chemical Physics*, 11, 4173-4183, 10.1039/B817913A, 2009.
- Nichman, L., Wolf, M., Davidovits, P., Onasch, T. B., Zhang, Y., Worsnop, D. R., Bhandari, J., Mazzoleni, C., and Cziczo, D. J.: Laboratory Study of the Heterogeneous Ice Nucleation on Black-Carbon-Containing Aerosol, *Atmos. Chem. Phys.*, 19, 12175-12194, 10.5194/acp-19-12175-2019, 2019.
- Onasch, T. B., Trimborn, A., Fortner, E. C., Jayne, J. T., Kok, G. L., Williams, L. R., Davidovits, P., and Worsnop, D. R.: Soot Particle Aerosol Mass Spectrometer: Development, Validation, and Initial Application, *Aerosol Science and Technology*, 46, 804-817, 10.1080/02786826.2012.663948, 2012.
- Pruppacher, H. R., and Klett, J. D.: *Microphysics of Clouds and Precipitation*, 2 ed., Atmospheric and Oceanographic Sciences Library, 18, Springer Netherlands, XXII, 954 pp., 2010.
- Pusechel, R. F., Blake, D. F., Snetsinger, K. G., Hansen, A. D. A., Verma, S., and Kato, K.: Black Carbon (Soot) Aerosol in the Lower Stratosphere and Upper Troposphere, *Geophysical Research Letters*, 19, 1659-1662, 10.1029/92GL01801, 1992.
- Raza, M., Chen, L., Leach, F., and Ding, S.: A Review of Particulate Number (P_n) Emissions from Gasoline Direct Injection (Gdi) Engines and Their Control Techniques, *Energies*, 11, 10.3390/en11061417, 2018.

- Ruzmaikin, A., Aumann, H. H., and Manning, E. M.: Relative Humidity in the Troposphere with AIRS, *Journal of the Atmospheric Sciences*, 71, 2516-2533, 10.1175/JAS-D-13-0363.1, 2014.
- Sakulyanontvittaya, T., Duhl, T., Wiedinmyer, C., Helmig, D., Matsunaga, S., Potosnak, M., Milford, J., and Guenther, A.: Monoterpene and Sesquiterpene Emission Estimates for the United States, *Environmental Science & Technology*, 42, 1623-1629, 10.1021/es702274e, 2008.
- Shu, Y., and Atkinson, R.: Atmospheric Lifetimes and Fates of a Series of Sesquiterpenes, *Journal of Geophysical Research: Atmospheres*, 100, 7275-7281, 10.1029/95JD00368, 1995.
- Smekens, A., Godoi, R. H. M., Berghmans, P., and Van Grieken, R.: Characterisation of Soot Emitted by Domestic Heating, Aircraft and Cars Using Diesel or Biodiesel, *Journal of Atmospheric Chemistry*, 52, 45-62, 10.1007/s10874-005-6903-7, 2005.
- Steane, A. M.: Phase Change, in: *Thermodynamics: A Complete Undergraduate Course*, Oxford University Press, 2016.
- Tsigaridis, K., and Kanakidou, M.: Global Modelling of Secondary Organic Aerosol in the Troposphere: A Sensitivity Analysis, *Atmos. Chem. Phys.*, 3, 1849-1869, 10.5194/acp-3-1849-2003, 2003.
- Tsimpidi, A. P., Karydis, V. A., Zavala, M., Lei, W., Molina, L., Ulbrich, I. M., Jimenez, J. L., and Pandis, S. N.: Evaluation of the Volatility Basis-Set Approach for the Simulation of Organic Aerosol Formation in the Mexico City Metropolitan Area, *Atmos. Chem. Phys.*, 10, 525-546, 10.5194/acp-10-525-2010, 2010.
- Vander Wal, R. L., Bryg, V. M., and Huang, C.-H.: Aircraft Engine Particulate Matter: Macro-Micro- and Nanostructure by Hrtm and Chemistry by Xps, *Combustion and Flame*, 161, 602-611, 10.1016/j.combustflame.2013.09.003, 2014.
- Volkamer, R., Platt, U., and Wirtz, K.: Primary and Secondary Glyoxal Formation from Aromatics: Experimental Evidence for the Bicycloalkyl-Radical Pathway from Benzene, Toluene, and p-Xylene, *The Journal of Physical Chemistry A*, 105, 7865-7874, 10.1021/jp010152w, 2001.
- Wagner, R., Höhler, K., Huang, W., Kiselev, A., Möhler, O., Mohr, C., Pajunoja, A., Saathoff, H., Schiebel, T., Shen, X., and Virtanen, A.: Heterogeneous Ice Nucleation of α -Pinene Soa Particles before and after Ice Cloud Processing, *Journal of Geophysical Research: Atmospheres*, 122, 4924-4943, 10.1002/2016jd026401, 2017.
- Wang, B., Lambe, A. T., Massoli, P., Onasch, T. B., Davidovits, P., Worsnop, D. R., and Knopf, D. A.: The Deposition Ice Nucleation and Immersion Freezing Potential of Amorphous Secondary Organic Aerosol: Pathways for Ice and Mixed-Phase Cloud Formation, *Journal of Geophysical Research: Atmospheres*, 117, n/a-n/a, 10.1029/2012jd018063, 2012.
- Wang, Y., Liu, H., and Lee, C.-F. F.: Particulate Matter Emission Characteristics of Diesel Engines with Biodiesel or Biodiesel Blending: A Review, *Renewable and Sustainable Energy Reviews*, 64, 569-581, <https://doi.org/10.1016/j.rser.2016.06.062>, 2016.

- Welti, A., Lüönd, F., Stetzer, O., and Lohmann, U.: Influence of Particle Size on the Ice Nucleating Ability of Mineral Dusts, *Atmos. Chem. Phys.*, 9, 6705-6715, 10.5194/acp-9-6705-2009, 2009.
- Wey, C., Anderson, B., Hudgins, C., Wey, C., Li-Jones, X., Winstead, E., Thornhill, L., Lobo, P., Hagen, D., and Whitefield, P.: Aircraft Particle Emissions Experiment (Apex), 2006.
- Winterhalter, R., Herrmann, F., Kanawati, B., Nguyen, T. L., Peeters, J., Vereecken, L., and Moortgat, G. K.: The Gas-Phase Ozonolysis of B-Caryophyllene (C₁₅H₂₄). Part I: An Experimental Study, *Physical Chemistry Chemical Physics*, 11, 4152-4172, 10.1039/B817824K, 2009.
- Wolf, M. J., Coe, A., Dove, L. A., Zawadowicz, M. A., Dooley, K., Biller, S. J., Zhang, Y., Chisholm, S. W., and Cziczo, D. J.: Investigating the Heterogeneous Ice Nucleation of Sea Spray Aerosols Using *Prochlorococcus* as a Model Source of Marine Organic Matter, *Environmental science & technology*, 53, 1139-1149, 10.1021/acs.est.8b05150, 2019.
- Wolf, M. J., Goodell, M., Dong, E., Dove, L. A., Zhang, C., Franco, L. J., Shen, C., Rutkowski, E. G., Narducci, D. N., Mullen, S., Babbitt, A. R., and Cziczo, D. J.: A Link between the Ice Nucleation Activity of Sea Spray Aerosol and the Biogeochemistry of Seawater, *Atmos. Chem. Phys. Discuss.*, 2020, 1-28, 10.5194/acp-2020-416, 2020.
- Yee, L. D., Isaacman-VanWertz, G., Wernis, R. A., Meng, M., Rivera, V., Kreisberg, N. M., Hering, S. V., Bering, M. S., Glasius, M., Upshur, M. A., Gray Bé, A., Thomson, R. J., Geiger, F. M., Offenberg, J. H., Lewandowski, M., Kourtchev, I., Kalberer, M., de Sá, S., Martin, S. T., Alexander, M. L., Palm, B. B., Hu, W., Campuzano-Jost, P., Day, D. A., Jimenez, J. L., Liu, Y., McKinney, K. A., Artaxo, P., Viegas, J., Manzi, A., Oliveira, M. B., de Souza, R., Machado, L. A. T., Longo, K., and Goldstein, A. H.: Observations of Sesquiterpenes and Their Oxidation Products in Central Amazonia During the Wet and Dry Seasons, *Atmos. Chem. Phys.*, 18, 10433-10457, 10.5194/acp-18-10433-2018, 2018.
- Yu, P., Toon, O. B., Bardeen, C. G., Zhu, Y., Rosenlof, K. H., Portmann, R. W., Thornberry, T. D., Gao, R.-S., Davis, S. M., Wolf, E. T., de Gouw, J., Peterson, D. A., Fromm, M. D., and Robock, A.: Black Carbon Lofts Wildfire Smoke High into the Stratosphere to Form a Persistent Plume, *Science*, 365, 587-590, 10.1126/science.aax1748, 2019.
- Zhang, R., Khalizov, A. F., Pagels, J., Zhang, D., Xue, H., and McMurry, P. H.: Variability in Morphology, Hygroscopicity, and Optical Properties of Soot Aerosols During Atmospheric Processing, *Proc Natl Acad Sci U S A*, 105, 10291-10296, 10.1073/pnas.0804860105, 2008.
- Zhang, Y., Chen, Y., Lambe, A. T., Olson, N. E., Lei, Z., Craig, R. L., Zhang, Z., Gold, A., Onasch, T. B., Jayne, J. T., Worsnop, D. R., Gaston, C. J., Thornton, J. A., Vizuete, W., Ault, A. P., and Surratt, J. D.: Effect of the Aerosol-Phase State on Secondary Organic Aerosol Formation from the Reactive Uptake of Isoprene-Derived Epoxydiols (Iepox), *Environmental Science & Technology Letters*, 5, 167-174, 10.1021/acs.estlett.8b00044, 2018a.
- Zhang, Y., Favez, O., Canonaco, F., Liu, D., Močnik, G., Amodeo, T., Sciare, J., Prévôt, A. S. H., Gros, V., and Albinet, A.: Evidence of Major Secondary Organic Aerosol Contribution to Lensing Effect Black Carbon Absorption Enhancement, *npj Climate and Atmospheric Science*, 1, 47, 10.1038/s41612-018-0056-2, 2018b.

- Zhang, Y., Katira, S., Lee, A., Lambe, A. T., Onasch, T. B., Xu, W., Brooks, W. A., Canagaratna, M. R., Freedman, A., Jayne, J. T., Worsnop, D. R., Davidovits, P., Chandler, D., and Kolb, C. E.: Kinetically Controlled Glass Transition Measurement of Organic Aerosol Thin Films Using Broadband Dielectric Spectroscopy, *Atmos. Meas. Tech.*, 11, 3479-3490, 10.5194/amt-11-3479-2018, 2018c.
- Zhang, Y., Liu, F., Clavel, D., Smallwood, G. J., and Lou, C.: Measurement of Soot Volume Fraction and Primary Particle Diameter in Oxygen Enriched Ethylene Diffusion Flames Using the Laser-Induced Incandescence Technique, *Energy*, 177, 421-432, <https://doi.org/10.1016/j.energy.2019.04.062>, 2019a.
- Zhang, Y., Nichman, L., Spencer, P., Jung, J. I., Lee, A., Heffernan, B. K., Gold, A., Zhang, Z., Chen, Y., Canagaratna, M. R., Jayne, J. T., Worsnop, D. R., Onasch, T. B., Surratt, J. D., Chandler, D., Davidovits, P., and Kolb, C. E.: The Cooling Rate- and Volatility-Dependent Glass-Forming Properties of Organic Aerosols Measured by Broadband Dielectric Spectroscopy, *Environmental Science & Technology*, 53, 12366-12378, 10.1021/acs.est.9b03317, 2019b.
- Zhang, Y., Sanchez, M. S., Douet, C., Wang, Y., Bateman, A. P., Gong, Z., Kuwata, M., Renbaum-Wolff, L., Sato, B. B., Liu, P. F., Bertram, A. K., Geiger, F. M., and Martin, S. T.: Changing Shapes and Implied Viscosities of Suspended Submicron Particles, *Atmos. Chem. Phys.*, 15, 7819-7829, 10.5194/acp-15-7819-2015, 2015.
- Zhao, D. F., Buchholz, A., Kortner, B., Schlag, P., Rubach, F., Fuchs, H., Kiendler-Scharr, A., Tillmann, R., Wahner, A., Watne, Å. K., Hallquist, M., Flores, J. M., Rudich, Y., Kristensen, K., Hansen, A. M. K., Glasius, M., Kourtchev, I., Kalberer, M., and Mentel, T. F.: Cloud Condensation Nuclei Activity, Droplet Growth Kinetics, and Hygroscopicity of Biogenic and Anthropogenic Secondary Organic Aerosol (Soa), *Atmos. Chem. Phys.*, 16, 1105-1121, 10.5194/acp-16-1105-2016, 2016.

The effects of morphology, mobility size and SOA material coating on the ice nucleation activity of black carbon in the cirrus regime

Cuiqi Zhang^{1,2}, Yue Zhang^{3,4,5}, Martin J. Wolf², Leonid Nichman⁶, Chuanyang Shen^{2,7}, Timothy B. Onasch^{4,5}, Longfei Chen¹, and Daniel J. Cziczo^{2,8,9}

¹School of Energy and Power Engineering, Beihang University, Beijing, China

²Department of Earth, Atmospheric, and Planetary Sciences, Massachusetts Institute of Technology, Cambridge, MA 02139, United States

³Department of Environmental Sciences and Engineering, University of North Carolina at Chapel Hill, Chapel Hill, NC 27599, United States

⁴Aerodyne Research Incorporated, Billerica, MA 01821, United States

⁵Department of Chemistry, Boston College, Chestnut Hill, MA 02467, United States

⁶National Research Council Canada, Flight Research Laboratory, Ottawa, ON, K1V 9B4, Canada

⁷Department of Atmospheric and Oceanic Sciences, Peking University, Beijing, China

⁸Department of Civil and Environmental Engineering, Massachusetts Institute of Technology, Cambridge, MA 02139, United States

⁹Department of Earth, Atmospheric, and Planetary Sciences, Purdue University, West Lafayette, IN 47907, United States

Correspondence to: Longfei Chen (chenlongfei@buaa.edu.cn)

Abstract. There is evidence that black carbon (BC) particles may affect cirrus formation and hence global climate by acting as potential ice nucleating particles (INPs) in the troposphere. Nevertheless, the ice nucleation (IN) ability of bare BC and BC coated with secondary organic aerosol (SOA) material remains uncertain. We have systematically examined the IN ability of 100–400 nm size-selected BC particles with different morphologies and different SOA coatings representative of anthropogenic (toluene and *n*-dodecane) and biogenic (β -caryophyllene) sources in the cirrus regime (–46 to –38 °C). Several ~~aerosolized~~-BC proxies were selected to represent different particle morphologies and oxidation levels. Atmospheric aging was further replicated with exposure of SOA-coated BC to OH. The results demonstrate that the 400 nm hydrophobic BC types nucleate ice only at or near the homogeneous freezing threshold (~~–42 to –46 °C~~). ~~Deposition-IN~~Ice formation at cirrus temperatures below homogeneous freezing thresholds, as opposed to purely homogeneous freezing, was observed to occur for some BC types between 100–200 nm within the investigated temperature range. More fractal BC particles did not consistently act as superior ~~deposition~~-INPs over more spherical ones. SOA coating generated by oxidizing β -caryophyllene with O₃ did not seem to affect BC IN ability, probably due to an SOA phase state transition. However, SOA coatings generated from OH oxidation of various organic species did exhibit higher IN onset supersaturation ratio with respect to ice (*SS_i*) compared with bare BC particles, with toluene SOA coating showing an increase of *SS_i* by 0.1–0.15 while still below the homogeneous freezing threshold. Slightly oxidized toluene SOA coating seemed to have a stronger deactivation effect on BC IN ability than highly oxidized toluene SOA, which might be caused by oligomer formation and phase state transition of toluene SOA under different oxidation levels. *n*-dodecane and β -caryophyllene-derived SOA coated BC only froze in the homogeneous regime. We attribute the inhibition of IN ability to the filling of the pores on the BC surface by the SOA material coating. OH exposure levels of *n*-

dodecane and β -caryophyllene all SOA coating experiments, from an equivalent atmospheric 10 days to 90 days, did not render significant differences in IN potential. Our study of selected BC types and sizes suggests that increase in diameter, compactness, and/or surface oxidation of BC particles lead to more efficient IN via pore condensation freezing (PCF) pathway, and that coatings of common SOA materials can inhibit the formation of ice. Our study suggests that BC particles with large sizes and/or oxidized surfaces generally exhibit better IN ability, and that the organic coating materials can inhibit ice formation.

1 Introduction

Cirrus clouds affect the global energy balance predominantly by more effectively trapping ~~terrestrial~~ long-wave terrestrial radiation than reflecting solar energy (e.g., Kärcher et al., 2007; Heymsfield et al., 2017; Kärcher, 2018). In cirrus clouds, ice crystals can form via two pathways, i.e. homogeneous and heterogeneous ice nucleation (IN) (Pruppacher and Klett, 2010). Homogeneous freezing is the spontaneous freezing of solution droplets without any foreign surfaces aiding the process (Pruppacher and Klett, 2010). Heterogeneous IN occurs more readily than homogeneous IN due to the presence of an ice nucleating particle (INP) at a lower supersaturation with respect to ice (SS_i) or warmer temperature (DeMott et al., 2003; Vali et al., 2015; Kanji et al., 2017). Deposition IN is one ~~classical~~ heterogeneous IN mode, in which solid ice is formed by direct water vapor deposition on to an INP surface. Recently, laboratory studies demonstrated that ice formation at thermodynamic conditions relevant to classical deposition IN on porous material at cirrus temperature (below -38 °C) might actually be initiated by homogeneous freezing of liquid water held within the cavities below water saturation due to inverse Kelvin effect (Marcolli, 2014; David et al., 2019; David et al., 2020). This pathway by which porous material might form ice below water saturation below -38 °C is referred to as pore condensation and freezing (PCF, Marcolli, 2014).

Black carbon (BC) particles from Aircraft emissions, especially those containing black carbon (BC) aerosols, may be an important direct source of anthropogenic INPs to the tropopause (Petzold et al., 1998; Seinfeld, 1998; Popovicheva et al., 2004; Burkhardt and Kärcher, 2011; Kärcher, 2018). Global mass-based aviation BC emission rates are estimated to range between 2-20 Gg year⁻¹ (Bond et al., 2004; Lee et al., 2010; Bond et al., 2013; Zhang et al., 2019a), while the number-based aviation BC emission rate is estimated to be equivalent to ~1.3 % of total ground anthropogenic BC emissions (Zhang et al., 2019a). Aviation fuel usage is projected to increase 2-4 fold in the next few decades (Lee et al., 2009; Lee et al., 2010), simultaneously increasing aircraft-induced cloudiness (Petzold et al., 1998; Seinfeld, 1998; Popovicheva et al., 2004; Burkhardt and Kärcher, 2011; Kärcher, 2018). However, the role of BC aerosol-cloud-climate interactions in cirrus formation remains highly uncertain (IPCC, 2013).

Laboratory experiments have been carried out to ~~simulate the atmospheric environment to~~ study the effects of isolated processes on BC IN ability in detail. Both well-characterized commercially available BC (e.g., DeMott et al., 1999; Fornea et al., 2009; Brooks et al., 2014; Mahrt et al., 2018; Nichman et al., 2019) and soot particles from combustion sources (e.g., Diehl

and Mitra, 1998; Möhler et al., 2005b; Dymarska et al., 2006; Kanji and Abbatt, 2006; Koehler et al., 2009; Crawford et al., 2011; Friedman et al., 2011; Kanji et al., 2011; Kulkarni et al., 2016; Mahrt et al., 2018; Nichman et al., 2019) have been used to investigate the IN ability of BC particles, with a particular focus on ~~the deposition-IN-mode~~IN below -38 °C. According to previous studies (e.g., Koehler et al., 2009; Friedman et al., 2011; Kulkarni et al., 2016; Mahrt et al., 2018; Nichman et al., 2019), the following physicochemical properties of particles may play vital roles in determining BC ~~deposition~~-IN activity: a) mobility diameter (d_m), b) morphology, c) surface oxidation state, and d) organic material coating. It is widely acknowledged that larger particles act as more efficient INPs (e.g., Pruppacher and Klett, 2010), which is also confirmed by recent heterogeneous IN experiments with various INPs (e.g., Welti et al., 2009; Lüönd et al., 2010; Marcolli, 2014; Mason et al., 2016; Mahrt et al., 2018; Nichman et al., 2019). Although the mechanism remains uncertain, one common theory is that ~~IN~~nucleation probability and rate are positively correlated to particle surface ~~area~~active sites density (Fletcher, 1960, 1969); therefore, an empirical parameter that is relevant to particle size (e.g., Connolly et al., 2009; Kiselev et al., 2017) ~~larger particles may offer more surface sites for nucleation. Similarly, the probability of a BC aggregate to contain a pore with the right properties (e.g., pore size and surface hydrophilicity) increases with increasing aggregate diameter, which would favor PCF for larger particles~~ (Mahrt et al., 2018). The IN ability of monodisperse BC particles with the size range of 100-800 nm has previously been characterized (Koehler et al., 2009; Friedman et al., 2011; Kulkarni et al., 2016; Mahrt et al., 2018; Nichman et al., 2019). The lower size limit at which BC particles act as active ~~deposition~~-INPs below -38 °C varied between 100 nm and 400 nm. However, the size threshold below which BC cannot nucleate ice ~~in~~at thermodynamic conditions relevant to classical deposition mode at cirrus temperature and the underlying mechanism is still uncertain.

Laboratory experiments and field observations confirmed that BC morphology and surface chemistry may change significantly during ~~the~~-atmospheric aging-~~processes~~, leading to changes in particle surface area, shape, and chemical composition (e.g., Slowik et al., 2007; Khalizov et al., 2009; Tritscher et al., 2011; Fu et al., 2012; China et al., 2015b; Li et al., 2016; Moffet et al., 2016; Li et al., 2017; Wang et al., 2017; Bhandari et al., 2019). Commonly-used BC morphology characteristics are those derived from 2-D projected electron microscopy images, including fractal dimension (D_f), roundness, aspect ratio (AR), and convexity (e.g., Ramachandran and Reist, 1995; Lee and Kramer, 2004; China et al., 2013; China et al., 2014; China et al., 2015b; Kulkarni et al., 2016). Effective density and surface area have also been utilized to reflect BC morphology and mixing state (Tritscher et al., 2011; Kulkarni et al., 2016; Mahrt et al., 2018; Nichman et al., 2019).

Freshly emitted BC particles are typically hydrophobic, fractal, nanoscale (<200 nm) aggregates with a branched or chain-like structure (e.g., Kinsey et al., 2010; Beyersdorf et al., 2014; Liati et al., 2014; Vander Wal et al., 2014; Lobo et al., 2015; Moore et al., 2017). BC aggregate surface area is determined by primary particle sizes, number of primary particles, and the way primary particles are connected (Kittelson, 1998). ~~Mahrt et al. (2018)~~ and Nichman et al. (2019) reported a generally positive correlation between BC particle surface area and IN activity for particles with same size. For smaller particles, Mahrt et al. (2018) presented a complex dependence of BC IN activity on particle size, surface area, and BC surface hydrophilicity.

Field Code Changed

Field Code Changed

They attributed BC IN activity to ~~pore-condensation-and-freezing (PCF)~~ mechanism (Marcolli, 2014; David et al., 2019; David et al., 2020), in which ~~IN deposition-freezing~~ of BC ~~was-is~~ considered ~~essentially-as~~ homogeneous freezing of liquid water taken up in mesopores (2-50 nm) due to capillary effect (Fisher et al., 1981).

The surface chemistry of the emitted particles is governed by the source and the host environment in which the particles evolve. Nascent BC particles can interact with volatile species such as sulfates and unburnt hydrocarbons in the aircraft cooling exhaust plume and grow (e.g., Lefebvre, 1998; Onasch et al., 2009; Anderson et al., 2011; Kärcher, 2018). These particles can remain suspended in the atmosphere for days to weeks (Cape et al., 2012; Lund et al., 2018), ~~or even months in the tropopause~~ (Pusechel et al., 1992; Yu et al., 2019), during which the exposure to atmospheric biogenic and anthropogenic ~~species~~emissions, as well as oxidation, can lead to complex secondary organic aerosol (SOA) coatings (Jacobson, 2001; Zhang et al., 2008; China et al., 2015b; Kulkarni et al., 2016; Zhang et al., 2018b). Numerous experiments have been conducted to investigate the effects of surface coating on BC ~~deposition~~-IN ability. Hygroscopic BC particles (Koehler et al., 2009), or BC particles coated by hygroscopic materials, such as sulfuric acid (DeMott et al., 1999; Möhler et al., 2005b; Crawford et al., 2011), water-soluble organic acids (Friedman et al., 2011; Nichman et al., 2019) and SOA (Kulkarni et al., 2016), tended to enhance BC water uptake ability and form aqueous solutions on BC surface, moving IN onset SS_i towards the homogeneous freezing threshold. Hydrophobic organic coatings tended to impede surface interaction between BC and water molecules. Möhler et al. (2005b), Crawford et al. (2011), and Mahrt et al. (2018) reported a transition from heterogeneous to homogeneous freezing mode for combustion BC with increasing OC content. Ozone (Friedman et al., 2011) and hydroxyl (OH) radical (Chou et al., 2013; Kulkarni et al., 2016) oxidation can change surface functional groups of BC particles and enhance hydrophilicity, but no distinguishable BC IN activity change has been observed. Despite these previous efforts, the influence of particle morphology, chemistry, and aging, as well as the microphysical mechanism behind BC ~~deposition~~-IN ability, remains ambiguous.

In this work, we examine the effects of particle mobility diameter, morphology, and SOA coating on the IN ability of several aerosolized BC proxies as a function of SS_i in a cirrus relevant temperature regime (from -46 °C to -38 °C). Representative species of anthropogenic (toluene and *n*-dodecane) and biogenic (β -caryophyllene) volatile organic compounds were chosen to simulate potential photochemical atmospheric aging processes of BC. Different aging durations in equivalent atmospheric times were simulated by controlling the OH radical exposure. Our results help to clarify the effects of physicochemical properties and SOA formation on BC IN ability and cirrus formation in the upper troposphere.

2 Experimental: materials and methods

2.1 Materials

2.1.1 Black carbon samples

Three types of commercially available BC particles (Raven 2500 Ultra, hereafter R2500U, Birla Carbon U.S.A., Inc.; REGAL 330R, hereafter R330R, Cabot Corporation; and CAB-O-JET 300, hereafter COJ300, Cabot Corporation Inkjet Colorants Division), corresponding to different surface chemistry and morphology regimes were studied as proxies of atmospheric BC. Table 1 summarizes the characteristics of these BC proxies. R2500U and R330R are carbonaceous black pigment powder generated by incomplete combustion (Joyce and Henry, 2006; Cabot). COJ300 is a highly dispersible ink due to the 4-carboxyphenyl-modified surface (Johnson, 1999). COJ300 is selected for its high degree of oxidation, which is confirmed by the Particle Analysis by Laser Mass Spectrometry (PALMS) chemical analysis (see Fig. A1), classifying it as the most oxidized BC proxy in this study. R2500U and R330R are unoxidized but differ in morphology, which was confirmed by morphology characterization and PALMS analysis (see Sect. 3.1). R2500U, R330R, and COJ300 were chosen as proxies of freshly emitted BC, atmospheric compacted BC, and atmospheric oxidized BC, respectively. IN properties of 800 nm R330R and R2500U particles were previously studied (Nichman et al., 2019). This work addresses the remaining questions raised in the previous study and focuses on the impact of particle size, morphology, and surface oxidation.

2.1.2 SOA coating materials

Three organic species, toluene, *n*-dodecane, and β -caryophyllene, were selected to represent atmospheric SOA precursors from anthropogenic and biogenic sources (Table S1). Toluene and *n*-dodecane are often selected as surrogate jet fuel components to investigate combustion and emission characteristics because they have been proven well-suited to represent tens of hundreds of components found in mainstream jet fuels (e.g., Dooley et al., 2010; Dooley et al., 2012; Zhang et al., 2016; Zhao et al., 2017). Field aircraft emission studies also confirm the presence of these unburnt aliphatic and aromatic organic compounds in [particles of aircraft engine exhaust](#) (e.g., Pison and Menut, 2004; Kinsey et al., 2011; Beyersdorf et al., 2012; Timko et al., 2014). These organic compounds may coat BC particles, forming BC-containing aerosols in engine plume. Moreover, toluene is considered a dominant aromatic SOA precursor due to anthropogenic activities (e.g., Pandis et al., 1992) and serves as a proxy for other light aromatic species [\(such as xylenes, alkylbenzenes, naphthalene, etc.\)](#) in atmospheric aromatic-seeded SOA formation models (e.g., Hildebrandt Ruiz et al., 2015). *n*-dodecane is one of the most studied long-chain aliphatic SOA precursor (e.g., Presto et al., 2010; Yee et al., 2013; Loza et al., 2014) representing less volatile aliphatic species. [Modelling and field studies suggest that such less volatile organic species might be significant anthropogenic SOA precursors in highly populated area](#) (Hodzic et al., 2010; Tsimpidi et al., 2010; Lee-Taylor et al., 2011; Hodzic et al., 2016), [among which *n*-dodecane has relatively higher emission rate](#) (Lee-Taylor et al., 2011). [Terpenes are biogenic organics emitted by plants, among which \$\beta\$ -caryophyllene has been found to be one of the most atmospherically abundant sesquiterpenes originating from agricultural plants and pine trees, as well as other sources](#) (Arey et al., 1991; Ciccioli et al., 1999; Helmig et al., 2006;

Sakulyanontvittaya et al., 2008; Guenther et al., 2012; Henrot et al., 2017). Even though the atmospheric abundance of β -caryophyllene is not as significant as other biogenic organics, such as isoprene and α -pinene, Due to its high reactivity towards ozone and hydroxyl radical to form oxidized products with low volatility, makes β -caryophyllene has a strong potential to form an appreciable biogenic SOA source in the atmosphere (Shu and Atkinson, 1995; Calogirou et al., 1997; Hoffmann et al., 1997; Griffin et al., 1999; Helmig et al., 2006; Lee et al., 2006; Jaoui et al., 2007). An up to 7 ng m^{-3} atmospheric concentration of β -caryophyllene tracer during summer time was reported (Jaoui et al., 2007).

2.2 BC particle generation and characterization

2.2.1 BC particle generation

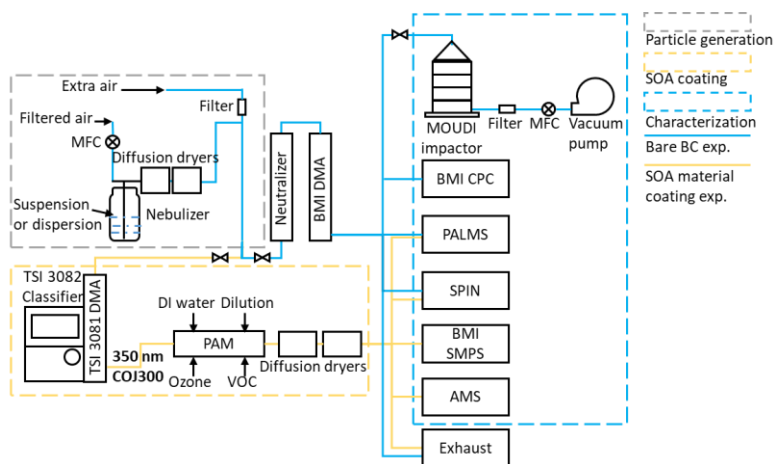


Figure 1. Schematic diagram of the experimental apparatus for bare BC particles (blue lines) and organic SOA coating experiments (yellow lines). The grey dashed box encloses the particle generation section, which is used for both bare BC and organic SOA coating experiments. The yellow dashed box denotes the SOA coating section. The blue dashed box is the aerosol characterization and test section.

Figure 1 shows a schematic diagram of the experimental apparatus used in this study. The particle generation setup is enclosed in the grey dashed box. Suspensions of R2500U and R330R, as well as a diluted COJ300 dispersion (dilution ratio 1:30) were atomized with a 3-jet collision nebulizer (CH Technologies (USA), Inc.), and bare BC experiments are marked by blue lines in Fig. 1. Suspensions of BC powder (R2500U and R330R) were prepared by mixing 1 g BC powder with 100 mL de-ionized (DI) water. The mixture was then sonicated for 10 minutes to make the suspension more uniform. The flow rates through the nebulizer was 1.5 SLPM (standard liters per minute) and 2.2 SLPM for bare BC experiments and BC-SOA mixing experiments, respectively, which is controlled by a mass flow controller (MFC, Model MC-2SLPM-D; ALICAT Scientific).

The atomized BC particles were dried by passing them through two consecutive 43 cm silica gel diffusion dryers (DDU 570/H, Topas). All samples were then neutralized and size selected. For bare BC experiments, by a BMI differential mobility analyzer (BMI DMA, Model 2002; Brechtel Manufacturing Inc.) was used to size-select particles, with a 500 nm cut-off size impactor installed at the DMA inlet to get rid of large particles. For BC-SOA mixing experiments, a TSI DMA (Model 3081, Classifier, Model 3082; TSI Inc.) was utilized for to select 350 nm COJ300 particles with no impactor applied bare BC and BC-SOA mixing experiments, respectively. The sheath-to-sample ratios for bare BC and BC-SOA mixing experiments were respectively ~6:1 and 4:1. Compared with the widely used sheath-to-sample ratio (10:1, Karlsson and Martinsson, 2003), the lower ratios in our experiments might broaden the BC particle size distribution, yet still offering satisfactory number concentration at the target particle size (Fig. 2) because of the large particle size being selected (Karlsson and Martinsson, 2003). The relative humidity (*RH*) of the aerosol stream entering the DMA measured by the BMI built-in *RH* sensor was ~16 %. During the bare BC ice nucleation experiments, the size-resolved particle number concentration was monitored with a BMI condensation particle counter (BMI CPC, Model 1700; Brechtel Manufacturing Inc.).

2.2.2 Characterization of BC morphology

The 200 nm, 300 nm and 400 nm R2500U, and 400 nm R330R and COJ300 BC particles were collected on 300-mesh carbon film copper grids (Ted Pella, Inc.) with a Micro-Orifice Uniform Deposit Impactor (MOUDI, MOUDI impactor (Model M135-10; TSI Inc.) for offline morphology analysis. The flow rate through the impactor was controlled by a MFC (Model MC-5SLPM-D; ALICAT Scientific) at 2 SLPM so that the cut-off size of the impactor was 100 nm. The samples were analyzed offline in a Zeiss Merlin High-resolution Scanning Electron Microscopy (HRSEM; Carl Zeiss Microscopy GmbH).

Table 1. Characteristics of selected BC proxies in this study. a_{BET-N_2} is the BET specific surface area based on N_2 adsorption isotherms; d_m is the particle mobility diameter; $\overline{d_a}$ denotes the mean 2-D projected area-equivalent aggregate diameter derived from SEM images; mean aspect ratio (\overline{AR}), roundness ($\overline{Roundness}$) and circularity ($\overline{Circularity}$) are the geometric mean morphology parameters derived from several aggregates and are defined in Sect. 2.2.2; $\overline{d_{pp}}$ denotes the mean geometric diameter of primary particles measured from SEM images, and N the number of primary particles analyzed for each BC type and size; D_f denotes the 3-D fractal dimension derived from 2-D SEM images; d_{va} is the particle vacuum aerodynamic diameter measured by the Particle Analysis by Laser Mass Spectrometry (PALMS) instrument; values in parenthesis-parentheses are the corresponding one standard deviations; values in brackets are the 95% confidence intervals of D_{eq} .

BC type	R2500U	COJ300	R330R
Composition	Furnace black	(4-carboxyphenyl)-modified carbon black ^a	Furnace black
CAS No.	1333-86-4	1106787-35-2	1333-86-4

Specific gravity (20 °C)	1.7-1.9 ^a			1.07 (dispersion) ^a	1.7-1.9 ^a
Bulk density (g/cm ³)	20-380			-	20-380
pH	7.0 ^b ; 4-11 ^c			7.0-8.6 ^a	6.9 ^b ; 2-11 ^c
Solubility	Insoluble			Insoluble but dispersible	Insoluble
α_{BET-N_2} (m ² /g) ^{a,d}	270			200	90
d_m (nm)	200	300	400	400	400
\overline{d}_a (nm)	316.9	403.5	343.5	629.4	816.6
<u>(± 1σ)</u>	(109.3)	(82.5)	(106.3)	(308.3)	(355.3)
\overline{AR}	1.22	1.36	1.44	1.19	1.33
<u>(± 1σ)</u>	(0.16)	(0.27)	(0.29)	(0.17)	(0.28)
<u>Roundness</u>	0.81	0.77	0.73	0.84	0.75
<u>(± 1σ)</u>	(0.06)	(0.08)	(0.09)	(0.08)	(0.10)
<u>Circularity</u>	0.78	0.64	0.61	0.72	0.53
<u>(± 1σ)</u>	(0.18)	(0.14)	(0.15)	(0.20)	(0.16)
\overline{d}_{pp} (nm)	41.9	35.5	34.5	34.2	45.4
<u>(± 1σ)</u>	(12.4)	(9.9)	(11.4)	(9.9)	(13.6)
N	242	256	343	139	251
D_f	2.02	1.92	1.92	2.34	2.31
<u>[95% confidence interval]</u>	<u>[1.85, 2.18]</u>	<u>[1.30, 2.53]</u>	<u>[1.68, 2.16]</u>	<u>[2.12, 2.56]</u>	<u>[2.01, 2.61]</u>
Median d_{va} ^e	-	-	608.7	610.6	-
Effective density (g/cm ³) ^f	-	-	1.52	1.44	-
<u>Spectra percentage exhibiting m/z = 16 signal</u>	=	=	<u>2.8</u>	<u>21.0</u>	=
<u>Median-Mean O:C ratio</u> ^g	-	-	<u>0.008</u>	<u>0.024</u>	-

Formatted: Font: Not Bold

Formatted: Font: Not Bold

Formatted: Font: Not Bold

Formatted: Font: Not Bold

Formatted: Font: Not Bold

Formatted: Font: Not Bold, Not Italic, Not Superscript/ Subscript

Formatted: Font: Not Bold, Not Italic

($\pm 1\sigma$)

(0.024)

(0.036)

Formatted: Font: Not Bold, Not Superscript/ Subscript

Formatted: Font: Not Bold

^aInformation offered by manufacturer datasheet. ^bMeasured by Nichman et al. (2019) using VWR pH meter. ^cMeasured by manufacturer in [compliant-compliance](#) with ASTM 1512. ^dBET specific surface area measured by manufacturers using N₂ adsorption in [compliant-compliance](#) with ASTM D-4820. ^eConverted from the measured time of flight. ^fCalculated from dividing median d_m by d_m (400 nm in this study) and times the reference density 1 g/m³ (Cziczo et al., 2006). ^gCalculated from PALMS spectra area.

Table 1 summarizes the morphological characteristics, including the projected area-equivalent diameter (d_a), aspect ratio (AR), roundness, circularity, and 3-D fractal dimension (D_f), for different BC types and sizes derived from high resolution SEM images ($\times 30,000$ to $\times 150,000$). Primary particle diameter ($\overline{d_{pp}}$) is the geometric average of the length and width of a clear primary particle ([see Fig. A2-A3 and A3A4 as well as the text in appendix A for more details](#)). $d_a = \sqrt{4A_a/\pi}$ is the diameter of a spherical aggregate that has the same projected area (A_a) as the BC aggregate (China et al., 2014). $AR = L_{max}/W_{max}$ is the ratio between the longest dimension (L_{max}) of an aggregate periphery to the perpendicular maximum width (W_{max} , Fig. A2). $Roundness = \sqrt{4A_a/\pi L_{max}^2}$ is used as a BC aggregate shape descriptor (e.g., China et al., 2013; China et al., 2015b; Kulkarni et al., 2016). Both AR and roundness are used to represent shape deviation from a circle, whose AR and roundness equal 1. $Circularity = 4\pi A_a/p^2$ is a parameter used to describe the rugged level of an aggregate periphery, with rugged irregular periphery causing circularity smaller than 1. D_f depends on primary particle number (N) and radius of gyration (R_g) of the aggregate (Mandelbrot, 1982). By using an ensemble approach, N is found to be scaled with $(A_a/A_p)^{1.09}$, where A_a and A_p are projected area of aggregate and primary particles, respectively (Samson et al., 1987; Köylü et al., 1995; Oh and Sorensen, 1997; China et al., 2014). The approximate relation $L_{max}/2R_g = 1.50 \pm 0.05$ is used to substitute R_g , (Brasil et al., 1999), and yield $k(L_{max}/\overline{d_p})^{D_f} = (A_a/A_p)^{1.09}$. D_f can then be derived by a power law fit of scattered points between $L_{max}/\overline{d_p}$ and $(A_a/A_p)^{1.09}$ for each aggregate (Fig. A4). [400 nm R2500U is more fractal than COJ300 and R330R with the same \$d_m\$, as well as 300 nm R2500U, which is indicated by \$D_f\$. Project area, as well as the derived \$d_a\$, are significantly affected by the degree of fractal, since highly fractal particles can have voids affecting project area. COJ300 and R330R, as well as 300 nm R2500U particles, are more spherical and compact than the fractal 400 nm R2500U, leading to larger \$d_a\$ in comparison with 400 nm R2500U.](#)

2.2.3 Chemical composition characterization of single BC particle

Qualitative chemical composition of [monodisperse-size-selected](#) BC particles was determined by PALMS. The detailed description of PALMS can be found elsewhere in literature (Cziczo et al., 2006; Zawadowicz et al., 2015). PALMS is an online single particle mass spectrometer in which inlet particles are first aligned by an aerodynamic lens. Two Nd:YAG green (532 nm) laser beams separated by 33.6 mm are arranged at the bottom of the inlet, measuring particle velocity based on time gap

between the scattering signals. The velocity can be converted into vacuum aerodynamic diameter (d_{va}) from the measured time of flight (Cziczo et al., 2006, Fig. A5). A 193 nm ultraviolet (UV) excimer laser is then triggered, ablating and ionizing the particle. The ions of both refractory and volatile particle components are classified based on their mass to charge (m/z) ratio. PALMS provides either positive or negative polarity spectra for each particle. Particle ionization is often not quantitative. However, average ion ratios across many spectra allows a qualitative compositional comparison between two similar aerosol populations. Hundreds of spectra were collected for each soot sample to account for ionization difference caused by particle orientation difference (Murphy et al., 1998).

Chemical composition of the SOA-coated BC particle stream was analyzed online by PALMS and an [High-Resolution Time-of-Flight Aerosol Mass Spectrometry \(HR-ToF-AMS; Aerodyne Research Inc.\)](#). [More details about the AMS can be found in literatures](#) (DeCarlo et al., 2006; Onasch et al., 2012), [here a brief introduction will be given](#). The AMS offers quantitative average mass spectrum of an ensemble of aerosols. Particles entering AMS first go through an aerodynamic lens inlet to form a particle beam. A mechanical chopper is used downstream the inlet to control sampling particle or particle free period. The AMS employs a heated 600 °C tungsten surface to vaporize nonrefractory aerosols. Ionization is achieved using a universal 70 eV electron ionization technique. Ionized species are detected by time of flight mass spectrometry. [More details about AMS can be found in literatures](#) (Jayne et al., 2000; Onasch et al., 2012).

Field Code Changed

Field Code Changed

2.3 SOA material coating on BC particles

The 350 nm COJ300 BC was chosen to be the seed particle in all SOA coating experiments because of its effective IN activity as well as its higher particle concentration ($\sim 1 \times 10^6 \text{ \# L}^{-1}$) at the selected size in comparison with other BCs ($1\text{--}3 \times 10^4 \text{ \# L}^{-1}$).

Particle generation during the SOA coating experiments was identical to bare BC experiments. The SOA coating experimental setup section is enclosed in the yellow dashed box of Fig. 1. [As stated above](#), COJ300 BC particles were nebulized in an air flow of 2.2 SLPM and dried in two consecutive 43 cm silica gel diffusion dryers, and then 350 nm BC particles were size-selected by a TSI 3081 DMA [with no impactor applied](#), and [were](#) directed to a potential aerosol mass (PAM) oxidation flow chamber (Kang et al., 2007; Lambe et al., 2011a; Liu et al., 2018). In the PAM reactor, gas phase volatile organic compound (VOC) reacts with OH radical and/or O₃ (Lambe et al., 2011a; Zhang et al., 2018a), and subsequently form SOA-coated BC particles. All flow rates were controlled by MFCs. The PAM chamber was operated at 4.4 SLPM total flow rate, including 2.2 SLPM BC aerosol flow, 1.0 SLPM O₃ carrier flow, 0.7 SLPM VOC carrier flow and 0.5 SLPM humidified air. The residence time of particles in PAM under such flow condition was approximately 260 s. O₃ was generated by irradiating 1.0 SLPM dry air through an external mercury lamp ($\lambda = 185 \text{ nm}$, AnaLamp low pressure Hg lamp; BHK Inc.) with a concentration of 110 ppm inside the PAM chamber in our study (Lambe et al., 2011b). [The typical O₃ mixing ratio in tropopause ranges between 0.1 to 1 ppm](#) (Fioletov, 2008; Gettelman et al., 2011). [The ozone concentration in this study was](#)

higher than ambient concentration to expediate the reaction given the short residence time of SOA within the PAM reactor
 (Lambe et al., 2011b; Zhang et al., 2015). (Fioletov, 2008; Gettelman et al., 2011) 0.5 SLPM humidified air was introduced
 into the chamber to react with the oxygen radical and produce OH radicals, with four mercury lamps ($\lambda = 254$ nm; BHK Inc.)
 mounted in Teflon-coated quartz cylinders inside the chamber to irradiate O_3 and produce oxygen radical ($O(^1D)$) via the UV
 photolysis reaction of O_3 first: $O_3 + h\nu \rightarrow O_2 + O(^1D)$, $O(^1D) + H_2O \rightarrow 2OH$. The OH radical concentration can be varied by
 changing the four lamps' voltage. Two voltage levels, i.e. 10 V and 3V, were tested in this study (indicated in Table 2 as
 suffixes -10 and -3), corresponding to different OH exposure levels and atmospheric aging time, ~10-15 days and ~70-90 days
 based on previous calculation (Lambe et al., 2011a). The equivalent atmospheric aging time t_{eq} were calculated using the OH
 concentration of the PAM reactor $c_{OH, PAM}$, the residence time of the particles within the PAM, t , and the ambient OH
 concentration $c_{OH, amb} = 1.0 \times 10^6 \text{ cm}^{-3}$ (Li et al., 2018) following the equation $t = c_{OH, PAM} \times t / c_{OH, amb}$ was calculated based on
 O_3 concentration and UV intensity, and RH measured real-time from the PAM reactor (Lambe et al., 2011a; Zhang et al.,
 2018a) (Lambe, 2011 #2055) (Zhang, 2018 #2347). The VOC was injected into a heated bulb by a syringe pump and mixed
 with 0.7 SLPM dry air. The particle size distributions downstream of the PAM were measured by a BMI scanning mobility
 particle sizer (BMI SMPS, comprising a Model 2002 DMA and a Model 1700 CPC; Brechtel Manufacturing Inc.). The
 injection rate was controlled so that the mode-modal sizediameter of the particles shifted from 350 nm bare BC particles to
 400 nm SOA-coated BC particles, as illustrated in Fig. 2. The 400 nm SOA-coated BC particles were then dried to ~16% RH
 and kept below 25% by passing through two consecutive 43 cm silica gel diffusion dryers (DDU 570/H, Topas). The PAM
 chamber was cleaned by flushing 10 SLPM clean air overnight after each experiment. In order to confirm the cleanliness of
 the chamber, particle concentration was measured before and after each experiment. The particle concentrations measured
 each day before experiments were below 70 \# cc^{-1} .

Formatted: Font: 8 pt
 Formatted: Font: Italic
 Formatted: Font: 8 pt, Italic

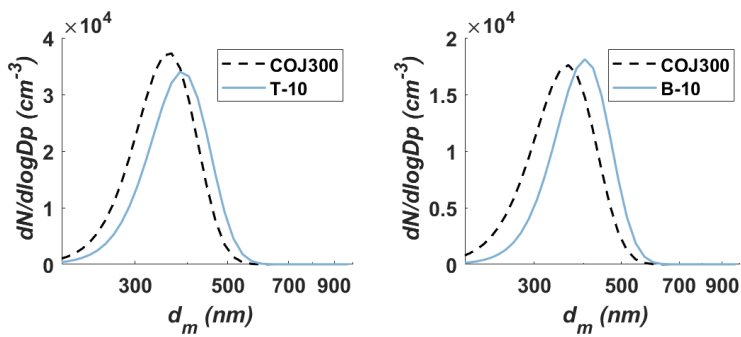


Figure 2. The ~~mode-modal~~ **modal** diameter shift of 350 nm COJ300 BC particles after toluene (left panel) and β -caryophyllene (right panel) SOA coating. The dashed and solid lines are fitted curves ~~to~~**for** bare uncoated and coated particles, respectively.

Table 2 summarizes all the SOA mixing IN experiments and the operating conditions. A peak shift from 350 nm to 400 nm and an increase of the 400 nm particle concentrations was observed for all experiments (Fig. 2 and Fig. B1), implying SOA coating on BC particles. The name prefixes *BG*, *T*, *D*, *B* in Table 2 stand for background test, toluene SOA coating experiments, *n*-dodecane SOA coating experiments, and β -caryophyllene SOA coating experiments, respectively. The name suffixes *BC*, *0*, *3*, *10*, and *s* denote seed BC only, O₃ oxidation only, low OH exposure level (3 V), high OH exposure level (10 V) and SOA self-nucleation experiments, respectively. All three organic species were exposed to both low and high OH concentrations to investigate the effect of oxidation level on SOA formation and IN activity. An extra O₃ oxidation experiment (*B-0*) was performed for β -caryophyllene because it is highly reactive towards O₃ and may form SOA absent of OH. Self-nucleation IN experiments (*-s*) were performed for pure SOAs generated from each organic species to exclude the effect of nucleated pure SOAs mixing with SOA-coated BC particles.

Table 2. Experiment conditions of BC and SOA coating experiments. The name prefixes *BG*, *T*, *D*, *B* stand for background test, toluene SOA coating experiments, *n*-dodecane SOA coating experiments, and β -caryophyllene SOA coating experiments, respectively. The name suffixes *BC*, *0*, *3*, *10*, and *s* denote seed BC only, O₃ oxidation only, low OH exposure level, high OH exposure level and SOA self-nucleation experiments, respectively.

Exp. Name	O ₃ (ppm)	OH UV Lamp Voltage (V)	Equivalent Atmospheric Exposure (days)	BC Seed	VOC concentration (ppb) ^a	
<i>BG-BC</i>	0	0	0	Y	-	-
<i>BG-0</i>	110	0	0	Y	-	-
<i>BG-10</i>	110	10	70-90	Y	-	-
<i>T-10</i>	110	10	70-90	Y	toluene	6000
<i>T-3</i>	110	3	10-15	Y	toluene	2000
<i>T-s^b</i>	110	10	70-90	N	toluene	4000
<i>D-10</i>	110	10	70-90	Y	<i>n</i> -dodecane	2000
<i>D-3</i>	110	3	10-15	Y	<i>n</i> -dodecane	500
<i>D-s^b</i>	110	10	70-90	N	<i>n</i> -dodecane	2000
<i>B-10</i>	110	10	70-90	Y	β -caryophyllene	5000
<i>B-3</i>	110	3	10-15	Y	β -caryophyllene	2300

<i>B-0</i>	110	0	0	Y	β -caryophyllene	5000
<i>B-s^b</i>	110	10	70-90	N	β -caryophyllene	5000

^aEstimated base on VOC volume injection rate. ^bSOA self-nucleation experiments kept the same OH exposure level and SOA size distribution as corresponding SOA coating experiments

2.4 Ice nucleation measurement

BC IN properties, including thermodynamic conditions at ice-nucleation IN onset and activation fraction (*AF*) as a function of *SS_i* and temperature, were measured with the SPIN, Droplet Measurement Technologies). The structuretheory, dimension and operating principles of SPIN can be found in previous studies (Garimella et al., 2016), and a brief description is given here.

SPIN is a continuous flow diffusion chamber style instrument comprising two flat parallel stainless-steel walls whose temperatures are controlled independently. The sampling flow rate of SPIN is 1.0 SLPM. Particles fed into SPIN are constrained by a ~9.0 SLPM sheath gas within a lamina near the centerline of SPIN chamber. Turbulent mixing at the injection point causes some particles to spread outside of the aerosol lamina centerline. Since particles experience lower *RH* as they spread outside of the lamina, correction factors ranging from ~1.9 to 8.0 were considered in previous studies (Garimella et al., 2017; Nichman et al., 2019; Wolf et al., 2019). Both walls are coated with ~1 mm ice prior to experiments. At the beginning of each experiment, a linear temperature gradient and water vapor partial pressure field are established between the warm and cold walls. Supersaturation with respect to ice is achieved because of the exponential relationship between temperature and saturation vapor pressure (Borgnakke and Sonntag, 2013; Steane, 2016). For all the experiments in this study, SPIN was operated in a *SS_i* scanning mode (1.0 to 1.6) while keeping the lamina temperature (-46 to -38 °C) constant for each scan. The *SS_i* increased from 1.0 at a rate of 0.03 per minute by increasing temperature gradient between the walls above homogeneous IN threshold and then lowered to ice saturation.

An optical particle counter (OPC) collects scattering signals for number counting and sizing, and a forward scattering depolarized signal for phase discrimination at SPIN chamber outlet. The size detection range of the OPC is 0.5 to 15 μ m. A machine learning algorithm using the OPC scattering and laser depolarization signal (Garimella et al., 2016) was used to classify each particle as an inactivated aerosol or ice crystal over the course of an experiment.

We define the IN onset as 1% of particles activating, i.e. *AF* = 1%, for a period of 10 seconds as activation. To account for aerosol spreading outside of the lamina where *SS_i* is the highest (Garimella et al., 2016), correction factors of 3.4 and 2.2 were applied for R2500U and R330R (Wolf et al., 2019). The correction factor was determined by taking the effect of morphology on particle behavior within SPIN lamina into consideration. Here the *AF* is defined as the number concentration of ice crystals identified by the machine learning algorithm divided by the total particle number concentration entering SPIN.

330 For the size-selected bare BC experiments, the total particle number concentration was measured by a CPC operating simultaneously with SPIN, while for the SOA coating experiments, the total particle number concentration was integrated from the SMPS measurement.

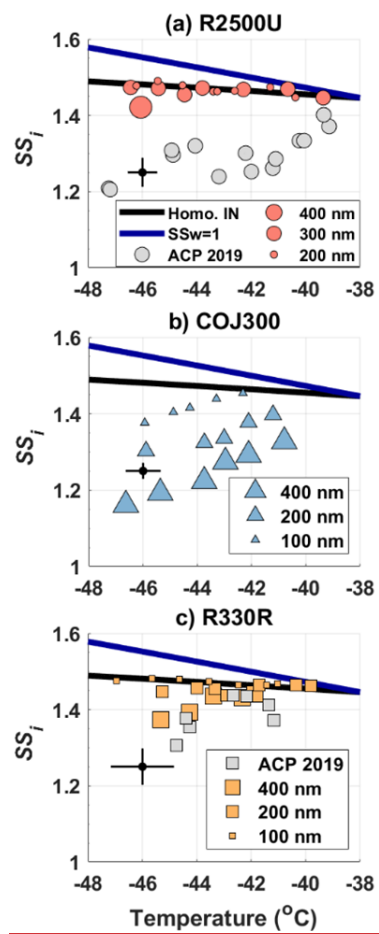
3 Results and discussion

3.1 Ice nucleation on bare BC particles

335 Figure 3 summarizes ~~(A) deposition-IIN onset temperature versus SS_i for 100-400 nm (a) R2500U, (b) COJ300 and (c) R330R BC particles; (B) SEM images of bare monodisperse ~400 nm BC particles; (C) representative negative ion PALMS mass spectra of bare monodisperse ~400 nm BC particles,~~ respectively. Representative error bars in black lines show one standard deviation of variability for SPIN lamina temperature and SS_i ~~derived from experimental data, respectively separately for each panel~~ (Kulkarni and Kok, 2012).

340 As shown in Table 1 and Fig. 3, the three test BC types ~~are substantially exhibit~~ different in-particle morphology. 400 nm R2500U has the smallest D_f (~1.92), and COJ300 and R330R have larger D_f (~2.34 and 2.31, respectively); R2500U is the most fractal BC while COJ300 and R330R are more spherical and compact. Meanwhile, R2500U and COJ300 have similar $\overline{d_{pp}}$ (34-35 nm), and R330R has larger (~45 nm) primary particles. The larger $\overline{d_{pp}}$ of 200 nm R2500U (Table 1) might result from the ~~blurringfusion~~ of primary particles under high magnification. Single particle surface area can be inferred by combining fractal level and $\overline{d_{pp}}$ together, and the decreasing order of single particle surface area is R2500U > COJ300 > R330R, which is in agreement with BET specific surface area data. Negative polarity mass spectra collected for 400 nm BC particles with PALMS are presented in Fig. ~~3C~~A2. The spectra of all three BC types exhibit typical consecutive carbon peaks ($m/z = 12, 24, 36$, etc.). The spectra of COJ300 shows presence of oxidized ions, such as O^+ ($m/z = 16$), OH^+ ($m/z = 17$), and $COOH^+$ ($m/z = 45$), which are highlighted in red in Fig. ~~A3C~~A(b). The frequency of $m/z = 16$ signal (Table 1) and PALMS O:C ratio result (Fig. A1) confirms that COJ300 is more oxidized than R2500U ~~(Fig. A1)~~.

Formatted: Font: Italic



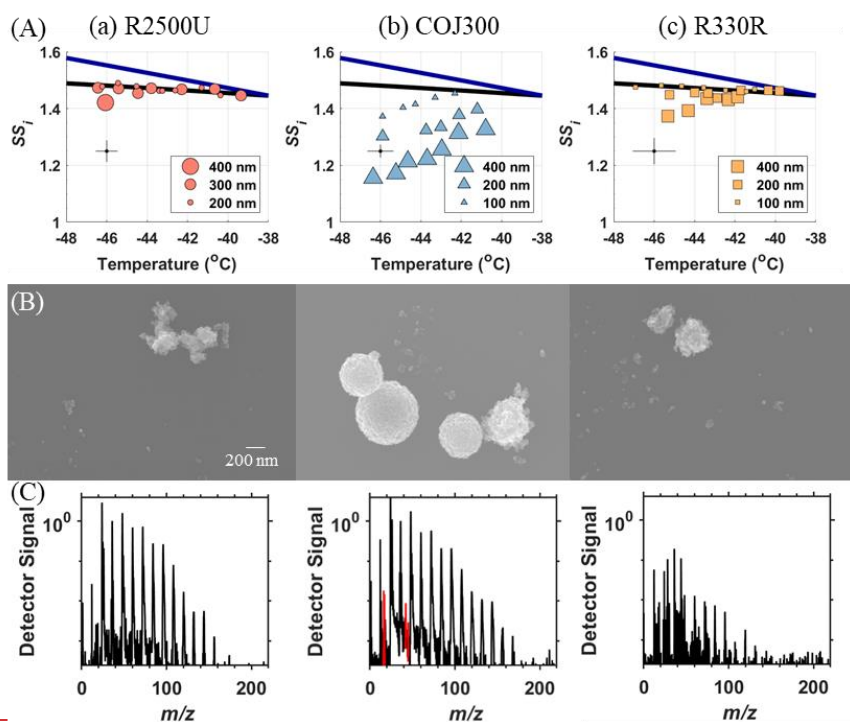


Figure 3. (A) IN onset SS_i ($AF = 1\%$) phase diagram, (B) SEM images, (C) representative negative mass spectrum obtained from PALMS of bare (a) R2500U (pink circles ●), (b) COJ300 (blue triangles ▲), and (c) Regal-330R (yellow squares ■), respectively. IN onset data for 800 nm R2500U and R330R from previous study is included and denoted in grey markers (Nichman et al., 2019). Different marker sizes in this study in row (A) corresponds to different d_m . Solid blue lines in row A are the water saturation lines, and black lines are homogeneous freezing lines of 200 nm aqueous droplets (Koop et al., 2000). A representative temperature and SS_i error bar of SPIN lamina temperature and SS_i is given on the left for each panel.

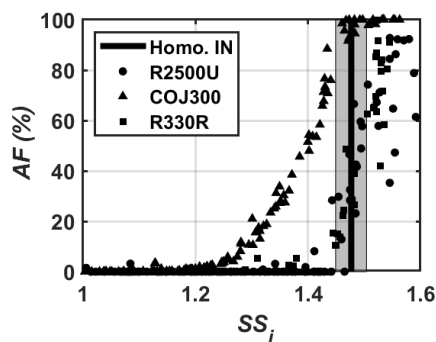


Figure 4. -45 °C SS_i scan of 400 nm bare BC particles, showing AF as a function of SS_i . The black line is the homogeneous freezing threshold for 200 nm aqueous droplets at -45 °C (Koop et al., 2000). The grey shading indicates one standard deviation of variability for SPIN lamina SS_i .

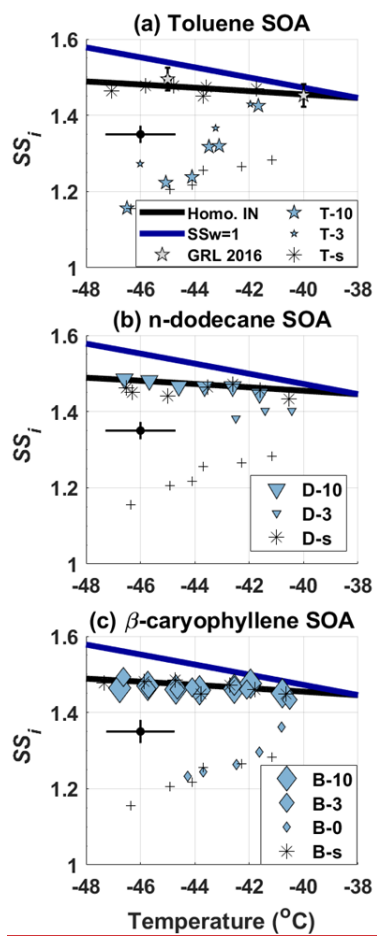
The results in Fig. 3A-3(a) demonstrate that the particle size is relevant to the particle IN ability, consistent with the BC heterogeneous IN ability enhancement triggered by increasing particle size in previous studies (Mahrt et al., 2018; Nichman et al., 2019). The 400 nm R2500U and R330R BC particles were able to nucleate ice below the homogeneous freezing threshold within the representative uncertainty range of SPIN lamina SS_i in the temperature range of -46 to -38 °C. The most spherical and oxidized COJ300 BC particles exhibited deposition-IN activity below homogeneous freezing threshold regardless of particle size and temperature in this study. The IN onset SS_i of all depositional active BC particles increases with increasing temperature. The trend is in agreement with previous studies on in cirrus temperature regime (DeMott et al., 1999; Möhler et al., 2005a; Koehler et al., 2009; Chou et al., 2013; Kulkarni et al., 2016; Mahrt et al., 2018; Nichman et al., 2019). The IN onset SS_i of 200 and 300 nm R2500U, as well as 100 and 200 nm R330R, falls into the homogeneous freezing regime. The sharp AF increase of 400 nm R2500U and R330R along the expected homogeneous freezing threshold in Fig. 4 confirm that these two BC types nucleate ice via homogeneous freezing. We conclude that the lower size threshold where the BC particles exhibit IN activity below homogeneous freezing threshold at thermodynamic conditions relevant to cirrus IN-mode transitions from heterogeneous IN to homogeneous freezing may well lie between 300-400 nm and 200-400 nm for R2500U and R330R around -46 °C, respectively. The IN ability of different size R330R particles at warmer-higher temperature (above -45 °C) shows little difference, indicating that the lower size threshold for R330R is likely between 400-800 nm for temperature between -44 to -40 °C (Nichman et al., 2019). The COJ300 BC is more IN active compared with R2500U and R330R. The COJ300 particles show deposition IN ability below homogeneous freezing threshold down to 100 nm within the temperature range in this study; the lower size threshold for COJ300 is below 100 nm. This finding agrees with the lower size limit between 100 nm and 200 nm for BC particles to act as an active INP reported by Mahrt et al. (2018).

Formatted: Font: Italic

The IN onset results show no clear dependence on particle fractal level and surface area. Even though the more fractal and branching feature of R2500U BC particles ~~may imply that there are more potential surface defects to initiate IN with larger surface area, the R2500U particles~~ do not clearly exhibit superior IN activity over R330R. Koehler et al. (2009) showed that IN was favored for oxidized hydrophilic BC, but too many hydrophilic active sites may bond water molecules, impeding ice embryo formation and thus impair IN (Pruppacher and Klett, 2010). The ~~surface-surface-~~modified, highly dispersible and spherical COJ300 with smaller $\overline{d_{pp}}$ shows better IN efficiency than fractal BC, which is consistent with the results of Mahrt et al. (2018) and Nichman et al. (2019) based on PCF mechanism. The ~~physio-chemical properties of COJ300 particles, including oxidized surface, smaller-appropriate $\overline{d_{pp}}$ offers-, and compacted spherical morphology, may result in higher probability to have smaller-cavities with appropriate size and hydrophilicity~~ on particle surfaces (Mahrt et al., 2020). ~~Such cavities that can~~ accommodate liquid water below bulk water saturation ~~by the inverse Kelvin effect and initiate homogeneous freezing of liquid water via PCF pathway~~ (Marcolli, 2014; David et al., 2019; David et al., 2020). ~~Water saturation pressure drop as a function of cavity radius is shown in Fig. C1.~~

3.2 Ice nucleation on BC coated with SOA material

Figure 5 shows the IN onset SS_i at which 1% of 400 nm SOA-coated COJ300 particles nucleate ice within the temperature range of -46 to -38 °C. The IN onset data of the bare 350 nm COJ300 particles (marked as + symbol) are also included to highlight the effect of SOA coating. IN onset SS_i of pure SOA particles are shown as an asterisk separately to rule out the possible ~~deposition IN~~ice formation below homogeneous freezing threshold induced by pure SOA.



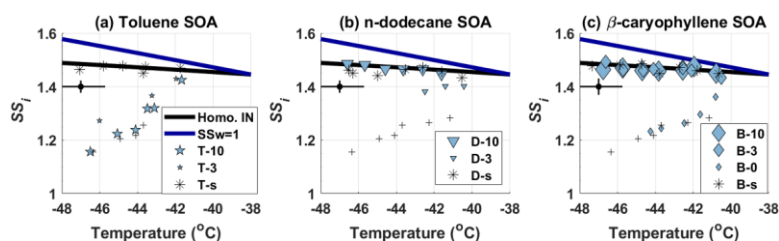


Figure 5. IN onset SS_i phase diagram of 350 nm COJ300 BC particles coated with (a) toluene SOA; (b) *n*-dodecane SOA; (c) β -caryophyllene SOA. Different symbol sizes denote different OH exposure level. IN onset SS_i of 350 nm bare COJ300 is shown in black plus (+) symbol for comparison. Pure SOA IN onset SS_i are presented as an asterisk (*) symbol for each organic species, respectively. The solid blue and black lines are water saturation lines and homogeneous lines for 200 nm aqueous droplets (Koop et al., 2000), respectively. A representative SPIN lamina temperature and SS_i error bar is given on the left side for each panel. [The toluene-SOA coated diesel BC IN data from Kulkarni et al. \(2016\) is also included for comparison.](#)

There exists no distinguishable difference between bare COJ300 and BC coated with highly oxidized toluene SOA (*T-10* in Table 2) from -46 to -44 °C. [The toluene SOA mass spectrum in Fig. 6\(a\) exhibits higher \$m/z = 44\$ \(\$\text{COO}^-\$ \) and lower \$m/z = 43\$ \(\$\text{C}_3\text{H}_7^-\$ \) fraction signal, indicating more oxidized organic species were generated during *T-10* and *T-3* experiments \(Lambe et al., 2011b\), agreeing with the previous study on toluene SOA \(Liu et al., 2018\). the higher O/C ratio \(Fig. 7\) of toluene-derived SOA when compared with the other two types of SOA may enhance the hygroscopicity of the particle \(Lambe et al., 2011b; Zhao et al., 2016; Liu et al., 2018\) and thus may reduce the deposition IN ability of BC particles. Volkamer et al. \(2001\)\(Murray et al., 2010; Berkemeier et al., 2014; Zhang et al., 2019c\)Ice crystals may form on the carbonaceous part of partially-coated particles, whose IN-onset \$SS_i\$ should be the same as bare COJ300. At temperatures above -43 °C, toluene SOA-coated BC particles nucleate ice at \$SS_i \sim 0.1\$ to 0.15 above bare 350 nm COJ300, but still \$\sim 0.15\$ below the homogeneous freezing threshold. This is in agreement with Wang et al. \(2012\) that pure aromatic SOA nucleate ice at \$SS_i \sim 0.1\$ to 0.15 below the homogeneous freezing limit. BC coated by \$\sim 10\$ –15 equivalent days atmospherically-oxidized toluene SOA \(*T-3* in Table 2\) particles nucleate ice in deposition mode at higher \$SS_i\$ than highly oxidized toluene SOA-coated BC within the investigated temperature range. Previous studies reported a molar weight range of 58–135 g mol⁻¹ for toluene SOA \(e.g., Bohn, 2001; Ji et al., 2017\). The toluene SOA mass spectrum in Fig. 6\(a\) exhibits higher \$m/z = 44\$ and lower \$m/z = 43\$ fraction signal, indicating more oxidized organic species were generated during *T-10* and *T-3* experiments \(Lambe et al., 2011b\), agreeing with the previous study on toluene SOA \(Liu et al., 2018\). On the one hand, the higher O/C ratio \(Fig. 7\) of toluene-derived SOA when compared with the other two types of SOA may enhance the hygroscopicity of the particle \(Lambe et al., 2011b; Zhao et al., 2016; Liu et al., 2018\) and thus may reduce the deposition IN ability of BC particles. On the other hand, Hinks et al. \(2018\) shows that toluene-derived SOA also contains a significant amount of oligomers under dry-laboratory conditions, similar to what we conducted in the PAM chamber in this study, potentially reducing the hygroscopicity and altering the phase state of](#)

Field Code Changed

the SOA to be semi-solid or solid (Zhang et al., 2018c; Li et al., 2020), under which the SOA can still nucleate ice (Zhang et al., 2019c). Overall, these two competing factors make our toluene SOA coating IN onset move towards but not fully in the homogeneous freezing regime, agreeing with the results of Kulkarni et al. (2016).

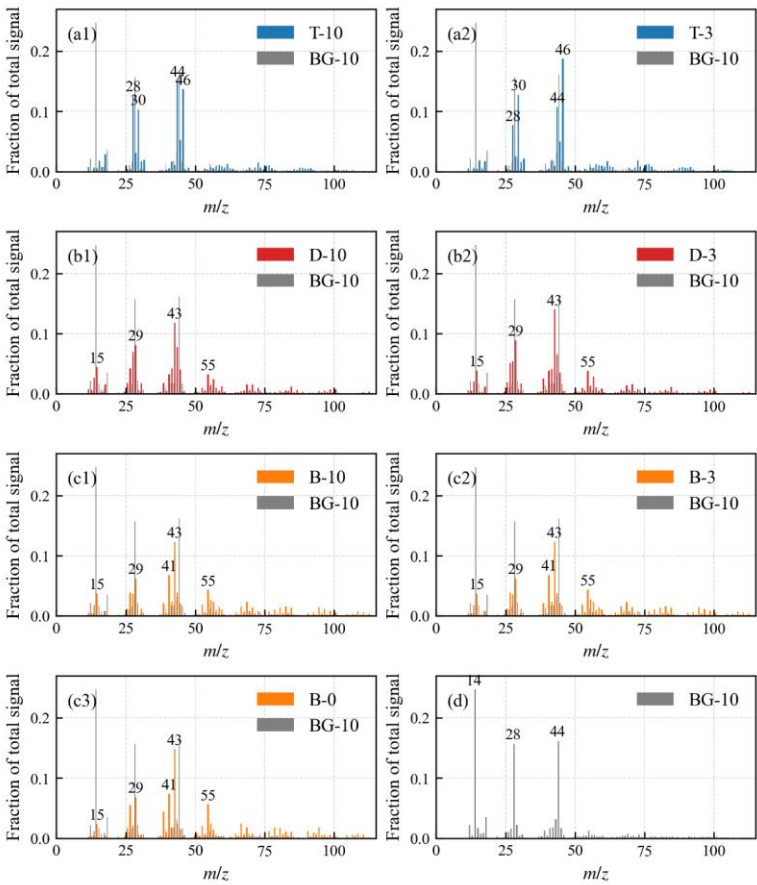


Figure 6. Normalized AMS mass spectra of COJ300 BC particles coated with (a) toluene SOA; (b) *n*-dodecane SOA; (c) β -caryophyllene SOA; and (d) bare COJ300 BC particles. More oxidized SOA is generated when toluene act as precursor, while less

Formatted: Caption, Indent: First line: 0 ch, Space After: 0 pt

oxidized SOAs are generated when *n*-dodecane and β -caryophyllene act as precursors in this study, as indicated by the different fractions of $m/z = 43$ and 44 , respectively (Lambe et al., 2011b; Ng et al., 2011; Canagaratna et al., 2015). The absolute organic mass loading present in the bare COJ300 BC experiment is less than 1% of the organic mass loading from the other three types of SOA coating experiments.

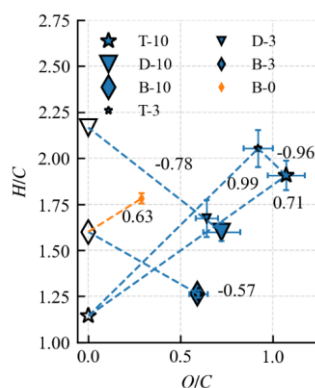


Figure 7. Elemental H/C ratio as a function of O/C ratio for three pure organic precursors (hollow symbols) and corresponding COJ300 BC particles seeded SOA inside the PAM reactor (filled symbols). Different symbol sizes denote different OH exposure level. The negative slopes SOA coating experiments are consistent with simultaneous carboxylic acid group addition and C-C single bond breakage (Heald et al., 2010; Lambe et al., 2011b).

The higher O/C ratio (Fig. 7) of toluene-derived SOA may enhance the hygroscopicity of the particle (Lambe et al., 2011b; Zhao et al., 2016; Liu et al., 2018) with a potential to form aqueous film on BC surface and reduce the IN ability of BC particles. On the other hand, Hinks et al. (2018) showed that toluene-derived SOA contained a significant amount of oligomers under dry laboratory conditions similar to what we conducted in the PAM chamber in this study. Volkamer et al. (2001) proved that glyoxal, which could facilitate the oligomerization as described by Hinks et al. (2018), can be produced from toluene reaction with OH as highly oxidized products. The slopes of T-10 and T-3 in Fig. 7 lie between 0-1 (0.71 and 0.99 for T-10 and T-3, respectively), suggests that oxygen and hydrogen atom addition accompanied by carbon-carbon double bond as well as benzene ring breakage might have happened during the toluene photooxidation experiments. These large oligomers could potentially reduce the hygroscopicity and alter the phase state of toluene SOA to be semi-solid or solid within the temperature range we investigated in this work (DeRieux et al., 2018; Zhang et al., 2018c; Li et al., 2020), under which the SOA can still nucleate ice (Murray et al., 2010; Berkemeier et al., 2014; Zhang et al., 2019c). The toluene SOA in T-10 with O:C ratio over 1 (Fig. 7) has most likely already transited into solid or semi-solid glassy state at the temperature range we investigated before entering SPIN (DeRieux et al., 2018). Therefore, it is very likely that BC particles are mostly stucked with or embedded in these glassy SOA with some bare BC part exposure. Ice crystals may therefore form on the carbonaceous part of partially coated particles, whose IN onset SS_0 should be the same as bare COJ300. At temperatures above -43°C , toluene SOA-coated

BC particles nucleate ice at $SS_i \sim 0.1$ to 0.15 above bare 350 nm COJ300, but still ~ 0.15 below the homogeneous freezing threshold. This might be due to the hygroscopicity enhancement of the toluene SOA-coated BC in *T-10*. BC coated by ~ 10 - 15 equivalent days atmospherically oxidized toluene SOA (*T-3* in Table 2) is less IN active than those coated by highly oxidized toluene SOA (*T-10*) at around $-46\text{ }^{\circ}\text{C}$ and $-43\text{ }^{\circ}\text{C}$. This might also be attributed the oxidation level and the corresponding phase state difference between the SOA generated from *T-10* and *T-3* experiments, which is beyond the scope of this study and requires further detailed phase transition study for toluene SOA. Overall, two competing effects, i.e. the hygroscopicity enhancement deactivating BC IN ability, together with toluene SOA glass phase transition producing sticked or partly coated BC, may make our toluene SOA coating IN onset move towards but not fully in the homogeneous freezing regime. The toluene SOA coated diesel combustion BC (Kulkarni et al., 2016), however, nucleate ice near the homogeneous threshold, as indicated in Fig. 3(a). This might be due to the much thicker (90 nm) organic coating in their study compared to the 25 nm coating of this work, leading to a complete coverage of BC surface.

The IN onset SS_i of highly oxidized *n*-dodecane SOA-coated COJ300 particles (*D-10* in Table 2) in Fig. 5(b) show that these particles nucleates ice homogeneously between -46 and $-42\text{ }^{\circ}\text{C}$. BC coated by slightly oxidized *n*-dodecane SOA (*D-3* in Table 2) nucleates ice nominally lower than homogeneous freezing threshold between -43 and $-40\text{ }^{\circ}\text{C}$. As shown in Fig. 5(c), the IN onset SS_i of OH-oxidized β -caryophyllene SOA-coated COJ300 particles (*B-10* and *B-3* in Table 2) is in the homogeneous freezing regime. However, O_3 -oxidized β -caryophyllene SOA shows no significantly alternation of IN ability. The mass spectra in Fig. 6(b) and Fig. 6(c) exhibit large fraction of signals at $m/z = 15$ (CH_3^+), 29 (C_2H_5^+), 43 (C_3H_7^+), and 55 (C_4H_7^+) for *n*-dodecane and β -caryophyllene SOA coating experiments in this study, implying formation of less oxidized aliphatic fragments during these experiments (Lambe et al., 2011b). The H/C and O/C values of *n*-dodecane and β -caryophyllene SOA coating in Fig. 7-7 are smaller than that of toluene SOA, which are in agreement with previous studies (Simonen et al., 2017; Li et al., 2019; Pereira et al., 2019). The slopes of H/C and O/C values of these two types of SOA and their respective two precursors (Fig. 7B2) are in the range between -1 and 0 , which is consistent with the simultaneous formation of carboxylic acid functional groups and C-C bond breakage (Heald et al., 2010; Lambe et al., 2011b). Addition of carboxylic acid group may enhance the hygroscopicity of *n*-dodecane and β -caryophyllene SOA, and the hygroscopicity is further enhanced with more OH exposure (Frosch et al., 2013; Yee et al., 2013; Schilling et al., 2015; Bé et al., 2017). We conclude that BC with OH oxidized *n*-dodecane and β -caryophyllene SOA coatings, regardless of oxidation level, may condense on BC surface and forms organic films, leading to nucleation in the homogeneous regime. However, COJ300 BC coated with O_3 oxidized β -caryophyllene SOA (*B-0* in Table 1) shows no significantly alternation of IN ability, as shown in Fig. 5(c). Unlike OH oxidation of β -caryophyllene where fragmentation happens, O_3 -addition is very likely to happen first on the carbon-carbon double bond of β -caryophyllene in *B-0*, leading to formation of semi-solid or solid SOA (Nguyen et al., 2009; Winterhalter et al., 2009), as illustrated in Fig. B2 with a slope between 0 - 1 . As with the case of *T-10*, such semi-solid or solid SOA might collide and stick with BC particles, leaving some bare carbonaceous surface that can nucleate ice following the IN pattern of COJ300 BC.

The experimental results are attributed to two factors: organic coating and ~~volatility~~SOA phase state. Previous studies controlling the combustion fuel-air-ratio produced BC particles occupying different organic content fractions, with higher organic content resulting in amorphous organic surfaces (Möhler et al., 2005b; Crawford et al., 2011; Mahrt et al., 2018). In these studies, shifts from heterogeneous to homogeneous freezing with increasing organic content have been observed. Kulkarni et al. (2016) reported that an 80 nm α -pinene SOA coating can suppress the ice nucleation ability of 120 nm diesel BC particles. However, studies show that as the ~~volatility-phase state~~ of the organic coating ~~decreases-changes~~ below certain threshold, especially near glass transition temperature, these organic coatings might be able to heterogeneously nucleate ice (Murray et al., 2010; Berkemeier et al., 2014; Zhang et al., 2019c). The suppression of BC IN ability by organic coating was attributed to coverage of surface-active sites and filling of pores on BC surface when the volatility of the organic coating is relatively high and might present in liquid phase. Certain SOA coatings in this study are less oxidized and thus may similarly impair BC IN ability due to their relatively high volatility, as Docherty et al. (2018) and Hildebrandt Ruiz et al. (2015) showed an inverse correlation between the volatility and oxidation state. Our results suggest that less oxidized SOA (*n*-dodecane and β -caryophyllene derived SOA from photooxidation), despite with 200 to 4000 folds of typical tropospheric SOA (Tsigaridis and Kanakidou, 2003; Heald et al., 2008; Hodzic et al., 2016) mass loading their high mass loadings in PAM chamber (~ 2000 to $4000 \mu\text{g m}^{-3}$ (Tsigaridis and Kanakidou, 2003; Heald et al., 2008)), are more likely to condense on seed particle and forms fully coated BC particles, moving IN onset *SS*_i to the homogeneous regime, while β -caryophyllene SOA oxidized by O₃ did not alter the *SS*_i of the soot particles. In addition, more oxidized SOA (toluene derived SOA from photooxidation) with potentially more oligomer formation, moving IN onset *SS*_i towards, but still below, homogeneous freezing.

4 Atmospheric implications

BC particles emitted from combustion sources (such as aero-engines) are carbonaceous nanoscale fractal aggregates with primary particle diameter of 20-50 nm (Bockhorn et al., 2009; Vander Wal et al., 2014). These BC particles can remain suspended in the atmosphere for days, and might undergo compaction and atmospheric aging, such as oxidation and mixing with atmospheric organic species/aerosols. This study focuses on the impact of morphology, particle size and mixing state on the IN ability of BC-containing aerosols. Three BC proxies were chosen to represent freshly emitted (in other words, unoxidized and more fractal) BC (R2500U), unoxidized compacted BC (R330R), and atmospheric chemically aged BC (COJ300). The morphological characteristics, such as d_{pys} , circularity, roundness, and D_f , are within the value range of typical BC emitted from aircraft engines, vehicles, biomass burning, laboratory flames/combustion sources, and those collected in field observations (e.g., Lapuerta et al., 2007; China et al., 2013; China et al., 2014; Vander Wal et al., 2014; China et al., 2015b; Zhang et al., 2019b). BC primary particle size range in this study lies between 10 to 70 nm with a modal size around 25 to 40 nm, being consistent with previous primary particle studies on combustion BC (e.g., Smekens et al., 2005; Liati et al., 2016; Joo et al., 2018). Previous field observations of transportation emissions and biomass burning reported that ambient BC occupied d_g , circularity, and roundness in the range of 130 to 940 nm, 0.19 to 0.55, and 0.32 to 0.6, respectively (China et al.,

Formatted: Font: (Default) 宋体, (Asian) 宋体, (Asian) Chinese (China)

2013; China et al., 2014; China et al., 2015a; China et al., 2015b), overlapping with the range in this work. Findings in this study can be relevant to airborne aircraft emissions and ground emissions carried by updrafts to tropopause. R2500U is similar to the fresh BC emitted from B737 at medium power burning conventional jet fuel in terms of morphology characteristics (Vander Wal et al., 2014). The primary particle size is consistent with BC emitted from prevalent gas turbine engines (Huang and Vander Wal, 2013). Findings in this study can be relevant to airborne aircraft emissions and ground emissions carried by updrafts to tropopause.

The IN results for bare BC particles show dependence on particle size and surface chemistry, but the role of fractal level seems to be of limited importance. The lower size limit of bare BC to exhibit IN activity is between 300-400 nm for R2500U at -46 °C. This is important for freshly emitted BC from aircraft engines and ground transportation vehicles, which are usually generally fractal and smaller than with $d_m < 200$ nm with modal size ranging from 20 to 100 nm (Kittelson, 1998; Wey et al., 2006; Anderson et al., 2011; Wang et al., 2016; Moore et al., 2017; Raza et al., 2018; Awad et al., 2020). It is unlikely that small, freshly emitted BC will activate as INP in aircraft plumes below the homogeneous freezing threshold if they possess similar physicochemical properties as R2500U. The smallest size for compacted BC (R330R) to activate as INPs lies between 200-400 nm at -46 °C. This means that the However, IN ability of small BC particles may be enhanced after cloud cycles, during which fractal BC geometries may collapse, and forms forming PCF favoring morphology (Mahrt et al., 2020). The COJ300 IN results imply that ice crystal formation may favor oxidized hydrophilic surfaces. The Apart from the most spherical morphology, the smaller d_{pp} of COJ300 may also offer higher probability to form appropriate for smaller mesopores with appropriate size to accommodate ice crystal formation below water saturation. Particles, with particles down to 100 nm can act as efficient INP. Pores formed by BC with larger d_{pp} might be too wide to accommodate liquid water at our experimental conditions. Besides, the COJ300 IN results imply that ice crystal formation may favor oxidized hydrophilic surfaces, confirming the importance of surface hydrophilicity for pore filling in PCF mechanism (David et al., 2019; David et al., 2020). This implies suggests that for long-lived atmospheric BC particles, after being oxidized and compacted, may act as efficient INP.

To simulate atmospheric aging, toluene, *n*-dodecane and β -caryophyllene were chosen to represent anthropogenic and biogenic SOA precursors (Atkinson and Arey, 2003; Hu et al., 2008; Ding et al., 2014). Toluene-derived SOA coatings impede BC heterogeneous IN activity slightly while *n*-dodecane and β -caryophyllene-derived SOA coatings caused BC particles to nucleate ice homogeneously. BC emitted from aircraft and vehicles are likely to be coated by toluene and *n*-dodecane derived SOA (e.g., Beyersdorf et al., 2012; Beyersdorf et al., 2014; Timko et al., 2014). According to our experimental results, even though such coating can facilitate particle growth, SOA-coated particles are more likely to nucleate ice near the homogeneous freezing threshold.

The conclusions drawn here for BC proxies may deviate from genuine BC collected-emitted from combustion sources. Nonetheless, BC surrogates are often used in research to mimic aircraft emitted BC for their similarity and availability (e.g.,

Persiantseva et al., 2004). Additional IN studies, over a wider temperature range would also be required for the proxies to firmly verify the PCF mechanism; the question whether the studied IN is depositional or in fact homogeneous IN of liquid water in pores and cavities, remains to be answered due to the limited temperature range investigated in this study.

5 Summary

The IN ability of size-selected (100-400 nm) ~~monodisperse~~ BC particles with different morphologies and surface chemistry and BC particles coated with toluene, *n*-dodecane, and β -caryophyllene-derived SOA has been systematically investigated in the cirrus temperature regime (-46 to -38 °C). Three aerosolized BC proxies were selected to represent particle morphology at different atmospheric aging stages, i.e. freshly emitted (R2500U), atmospheric compacted (R330R), and atmospheric compacted and oxidized (COJ300). The IN activity was investigated in relation to particle size, morphology, surface chemistry, SOA precursor type and OH exposure level.

The results show the lower size limit for BC particles to exhibit IN activity varies between BC type. 400 nm freshly emitted and compacted BC particles nucleate ice near the homogeneous freezing threshold. Ice crystals form on most spherical, surface-surface-modified hydrophilic BC at SS; as low as 1.15. The onset of some ~~deposition-nucleation~~ IN below the homogeneous freezing threshold, as opposed to purely homogeneous freezing, occurs for some BC types between 100-200 nm, in some cases below 100 nm. We conclude that BC IN favors larger, spherical particles and-with oxidized hydrophilic surfaces. The highly fractal BC particles did not necessarily act as superior ~~deposition~~-INP over more spherical ones as would normally be anticipated from surface ~~active-density-area~~ theory. This ~~might could be caused-by~~ attributed to PCF occurring in the pores and cavities ~~with appropriate size of-offered by more~~ compacted BC particles.

Toluene-derived SOA coatings increase bare BC IN onset SS; by 0.1-0.15, but still below the homogeneous freezing threshold. Slightly oxidized toluene SOA coatings seem to have a stronger deactivation effect on BC IN ability than highly oxidized toluene SOA, which might be caused by oligomer formation and phase state transition of toluene SOA material under different oxidation levels. The larger molar ~~weight-masses~~ of OH oxidized *n*-dodecane and β -caryophyllene SOA enhances the coating thickness and further elevates the IN onset SS; into the homogeneous freezing regime. This might be due to SOA material filling the pores on BC surfaces and leading to IN near the homogeneous regime. O₃ oxidized β -caryophyllene SOA ~~does not seem to~~ not affect BC IN activity. OH exposure levels of *n*-dodecane and β -caryophyllene SOA coating experiments, from an equivalent atmospheric 10 to 90 days, OH exposure levels of all SOA coating experiments from 10-15 up to 90 equivalent atmospheric days shows no significant difference. Our study broadens aging processes of atmospheric BC particles and may offer the basis to better predict their IN activity and contribution to cirrus cloud formation. We suggest future studies should focus on IN activity of realistic combustion particles (aircraft, vehicles, and biomass burning, etc.) and advanced single particle characterization for validation of the PCF mechanism.

Appendix A: BC morphology-physio-chemical properties characterization

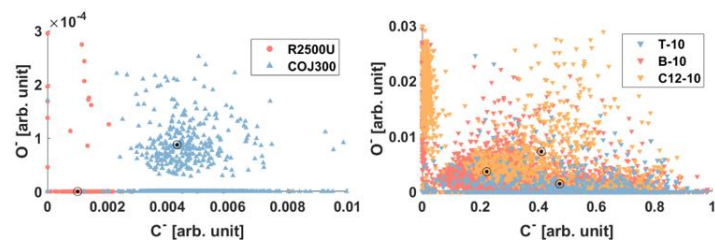
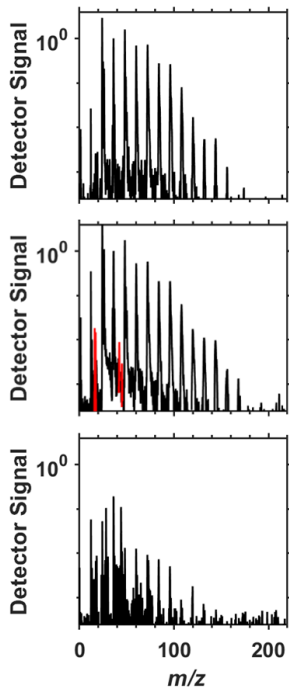


Figure A1. Negative polarity oxygen and carbon peak areas from PALMS for (left panel) 400 nm R2500U and COJ300 BC; (right panel) SOA-coated BC particles. Cluster centroid denoted as \odot . Generally, the probability of O⁻ signal presence in COJ300 occupies is an order of magnitude higher O⁻ signal than R2500U.



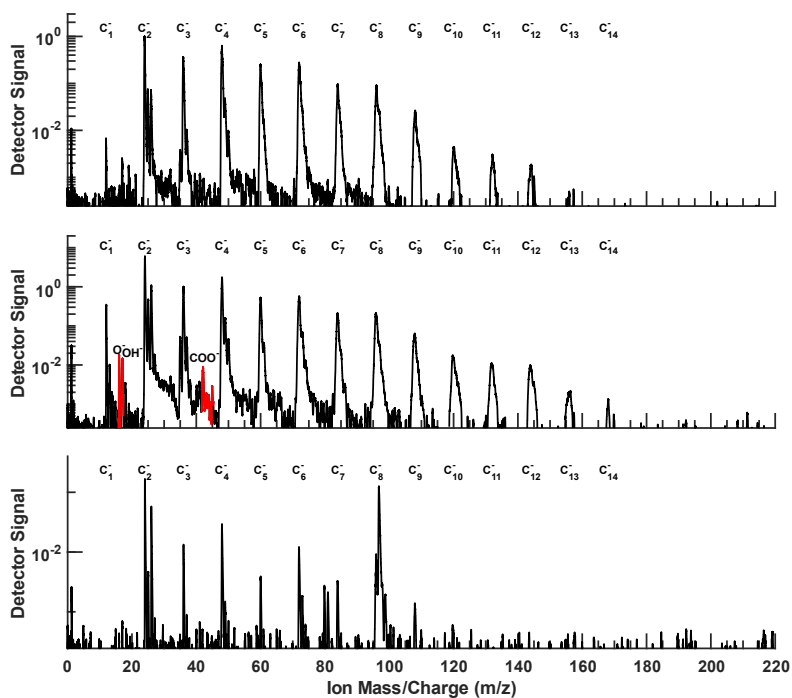


Figure A21. Negative polarity oxygen and carbon peak areas from PALMS for (left panel) 400-nm R2500U and COJ300 BC; (right panel) SOA-coated BC particles. Cluster centroid denoted as \odot . Generally, COJ300 occupies a higher O-signal than R2500U. Representative negative-ion PALMS mass spectra of bare size selected (a) R2500U, (b) COJ300, and (c) R330R BC particles with a modal size around 400 nm. The ions indicative of oxidized material ($m/z = 16, 17$, and 45) are highlighted in red.

Formatted: Caption

Formatted: Font: Italic

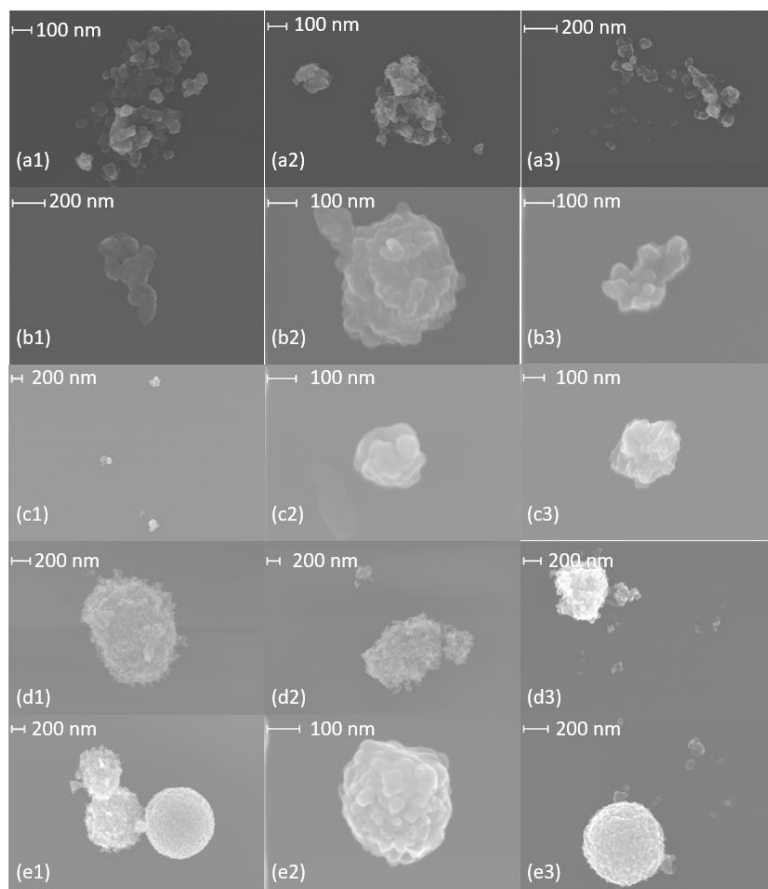


Figure A3. SEM images of (a) 400 nm R2500U, (b) 300 nm R2500U, (c) 200 nm R2500U, (d) 400 nm R330R, and (e) 400 nm COJ300.

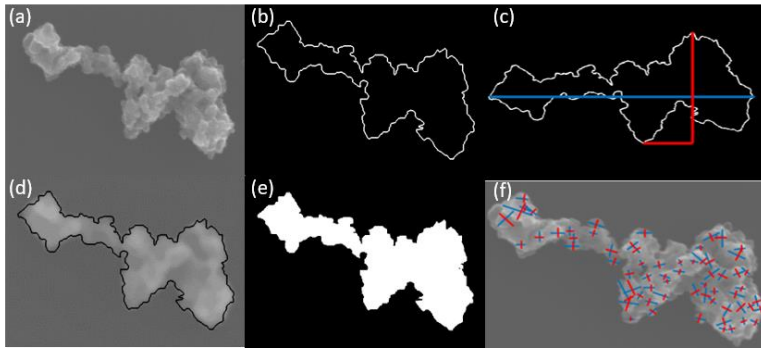


Figure A42. Example of processing of SEM images. (a) original image; (b) manually draw an approximate aggregate outline; (c) obtain the longest dimension (L_{max}) of an aggregate periphery to the perpendicular maximum width (W_{max}); (d) validation of the periphery; (e) use binary figure to obtain project aggregate area (A_a); (f) measurement of primary particle diameter (d_{pp}).

BC aggregate parameters, including L_{max} and W_{max} , perimeter, and project area, are determined by manually drawing the periphery of the aggregate, as shown in Fig. A4 (a-e). The primary particle diameter is determined by identifying the boundary of BC primary particle in the SEM image. After manual selection of the start and end points of a primary particle's length and width respectively, the distance between these points are calculated automatically and recorded. The primary particle diameter equals to the geometric mean of the length and width. Primary particle size distribution of a specific BC type and size can then be obtained by categorizing primary particle diameters into different size bins and count the frequency, as shown in Fig. A5. BC primary particle size distribution obeys normal distribution. The coefficients and goodness of normal distribution fittings are shown in Table A1.

Table A1. Coefficients and goodness for the normal primary particle size distribution fitting. 95% confidence intervals are enclosed in brackets.

BC type and size	Geometric mean diameter (nm)	Geometric standard deviation (nm)	R^2
200 nm R2500U	36.85 [35.97, 37.73]	14.30 [13.05, 15.55]	0.98
300 nm R2500U	30.50 [29.43, 31.56]	12.70 [11.20, 14.21]	0.96
400 nm R2500U	29.06 [28.25, 29.97]	12.70 [11.55, 13.85]	0.98
400 nm COJ300	30.41 [29.54, 31.29]	12.11 [10.88, 13.35]	0.97
400 nm R330R	40.39 [33.44, 47.34]	16.32 [15.06, 17.58]	0.95

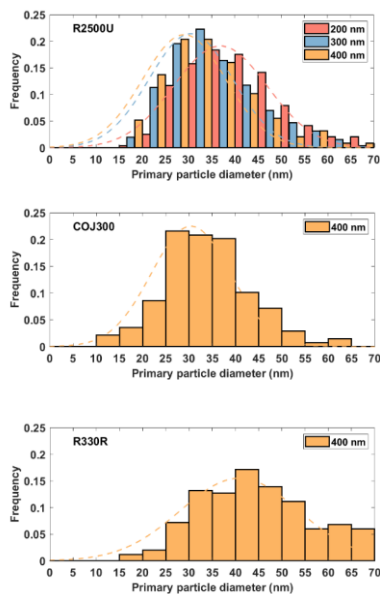


Figure A53. Primary particle size distributions for select BC particle types. The dashed lines are fitted normal distribution curves.

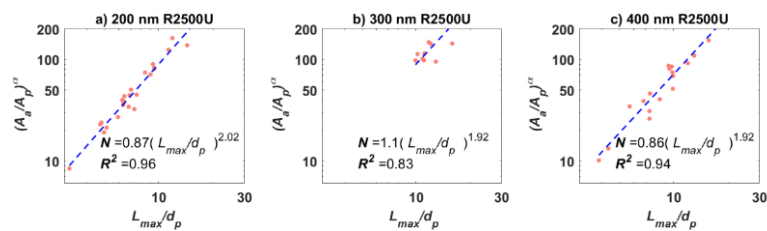


Figure A64. Power law fit to obtain 3-D fractal dimensions of (a) 200 nm ($N=25$), (b) 300 nm ($N=12$), (c) 400 nm ($N=21$) R2500U BC particles. More than 10 aggregates were analyzed for each size.

Formatted: Font: (Default) Times New Roman

Formatted: Normal

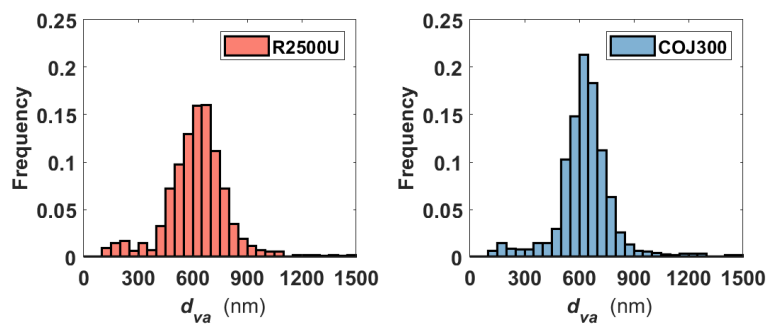
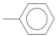

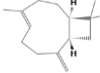


Figure A75. Vacuum aerodynamic diameter (d_{va}) derived from PALMS for 400 nm R2500U and COJ300 (Cziczo et al., 2006).

Formatted: Normal

Table B1. Organic compounds engaged in this study. The parameters are taken from room temperature data.

Compound	Structure	Formula (m/z)	SOA mass yields (%) ^a	Rate constants×10 ¹² [cm ³ /molecule·s]	
Toluene		C ₇ H ₈ (92)	8 - 49 (Hildebrandt et al., 2009)	<i>k</i> _{OH}	6.36 (Tully et al., 1981)
<i>n</i> -dodecane		C ₁₂ H ₂₆ (170)	9 (Presto et al., 2010)	<i>k</i> _{OH}	13.3 (Lamkaddam et al., 2019)
<i>β</i> -caryophyllene		C ₁₅ H ₂₄ (205)	17 - 63 (Griffin et al., 1999)	<i>k</i> _{OH}	200 (Shu and Atkinson, 1995)
			53 ^b (Jaoui et al., 2013)	<i>k</i> _{O3}	1.16 × 10 ⁻² (Shu and Atkinson, 1994)

^aMeasured at organic particle concentration of 10 µg/m³; ^bMeasured at organic particle concentration of 26 µg/m³.

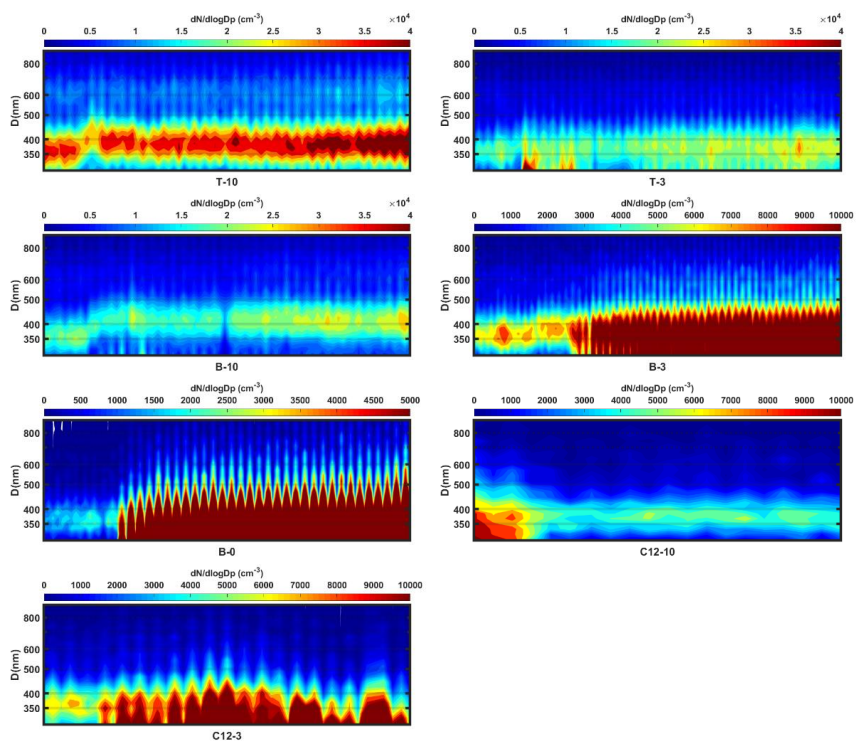


Figure B1. Temporal Particle-particle size distribution evolution for different BC and SOA mixing experiments. The x axis is the number of scans, equivalent to experiment time. Together with the color map, y axis shows the size distribution for a certain time. A size shift from 350 nm to 400 nm can be observed for each experiment.

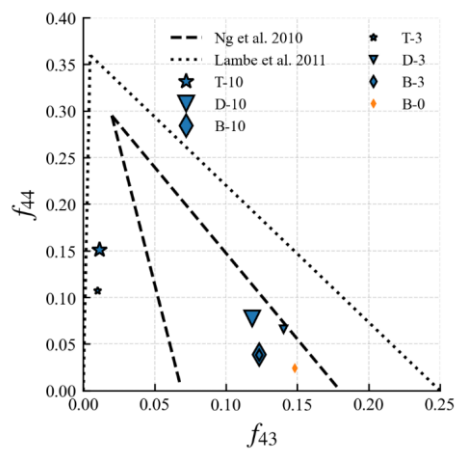


Figure B2 The measured fraction of AMS signals at $m/z = 43$ (f_{43}) and $m/z = 44$ (f_{44}). SOA generated from *n*-dodecane and β -caryophyllene in this study are within the ambient SOA- f_{44} and f_{43} range measured by Ng et al. (2010). Toluene-derived SOA in this study exhibits similar f_{44} and f_{43} signal range to the laboratory measurement of glyoxal-derived SOA (Lambe et al., 2011b).

650

Data availability

Data inquires can be directed to the corresponding author (Longfei Chen, chenlongfei@buaa.edu.cn).Appendix C: Pressure drop due to the presence of pores and cavities

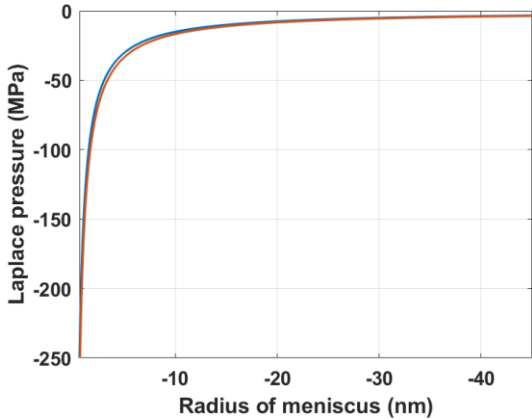


Figure C1. Saturation pressure drop (Laplace pressure) as a function of the radius of the meniscus

Formatted: Normal

Formatted: Caption, Space After: 0 pt

Author Contributions

CZ, YZ, MJW, LN, TBO and DJC designed the experiments and methodology. CZ collected black carbon samples and performed morphology characterization. CZ, YZ, MJW and CS performed chemical analyses, and measured ice nucleation activity. CZ, YZ, MJW, LN, LC, and DJC prepared manuscript with input from all coauthors.

Acknowledgments

The authors declare no competing interests. We thank [our peer reviewers for their valuable comments and suggestions to make our paper scientifically improved and more concise](#). We thank Andrew Lambe and other colleagues at Aerodyne Research Inc. for their help with the PAM reactor and SOA coating experiment. This work was supported by National Natural Science Foundation of China (Grant No. 51922019) and Chinese Government Scholarship (Grant No. 201806020052). YZ was supported by the NSF Postdoctoral Fellowship under AGS Grant No. 1524731 and the National Institutes of Health (NIH) Grant No. T32ES007018.

References

- Anderson, B. E., Beyersdorf, A. J., Hudgins, C. H., Plant, J. V., Thornhill, K. L., Winstead, E. L., Ziemba, L. D., Howard, R., Corporan, E., Miake-Lye, R. C., Herndon, S. C., Timko, M., Woods, E., Dodds, W., Lee, B., Santoni, G., Whitefield, P., Hagen, D., Lobo, P., Knighton, W. B., Bulzan, D., Tacina, K., Wey, C., VanderWal, R., and Bhargava, A.: Alternative Aviation Fuel Experiment (Aafex), National Aeronautics and Space Administration, Langley Research Center. NASA/TM-2011-217059., Hanover, 2011.
- Arey, J., Winer, A. M., Atkinson, R., Aschmann, S. M., Long, W. D., Morrison, C. L., and Olszyk, D. M.: Terpenes Emitted from Agricultural Species Found in California's Central Valley, *Journal of Geophysical Research: Atmospheres*, 96, 9329-9336, 10.1029/91JD00447, 1991.
- Atkinson, R., and Arey, J.: Gas-Phase Tropospheric Chemistry of Biogenic Volatile Organic Compounds: A Review, *Atmospheric Environment*, 37, 197-219, [https://doi.org/10.1016/S1352-2310\(03\)00391-1](https://doi.org/10.1016/S1352-2310(03)00391-1), 2003.
- Awad, O. I., Ma, X., Kamil, M., Ali, O. M., Zhang, Z., and Shuai, S.: Particulate Emissions from Gasoline Direct Injection Engines: A Review of How Current Emission Regulations Are Being Met by Automobile Manufacturers, *Science of The Total Environment*, 718, 137302, <https://doi.org/10.1016/j.scitotenv.2020.137302>, 2020.
- Bé, A. G., Upshur, M. A., Liu, P., Martin, S. T., Geiger, F. M., and Thomson, R. J.: Cloud Activation Potentials for Atmospheric A-Pinene and B-Caryophyllene Ozonolysis Products, *ACS Central Science*, 3, 715-725, 10.1021/acscentsci.7b00112, 2017.
- Berkemeier, T., Shiraiwa, M., Pöschl, U., and Koop, T.: Competition between Water Uptake and Ice Nucleation by Glassy Organic Aerosol Particles, *Atmospheric Chemistry and Physics*, 14, 12513-12531, 10.5194/acp-14-12513-2014, 2014.
- Beyersdorf, A. J., Thornhill, K. L., Winstead, E. L., Ziemba, L. D., Blake, D. R., Timko, M. T., and Anderson, B. E.: Power-Dependent Speciation of Volatile Organic Compounds in Aircraft Exhaust, *Atmospheric Environment*, 61, 275-282, <https://doi.org/10.1016/j.atmosenv.2012.07.027>, 2012.
- Beyersdorf, A. J., Timko, M. T., Ziemba, L. D., Bulzan, D., Corporan, E., Herndon, S. C., Howard, R., Miake-Lye, R., Thornhill, K. L., Winstead, E., Wey, C., Yu, Z., and Anderson, B. E.: Reductions in Aircraft Particulate Emissions Due to the Use of Fischer-Tropsch Fuels, *Atmospheric Chemistry and Physics*, 14, 11-23, 10.5194/acp-14-11-2014, 2014.
- Bhandari, J., China, S., Chandrakar, K. K., Kinney, G., Cantrell, W., Shaw, R. A., Mazzoleni, L. R., Giroto, G., Sharma, N., Gorkowski, K., Gilardoni, S., Decesari, S., Facchini, M. C., Zanca, N., Pavese, G., Esposito, F., Dubey, M. K., Aiken, A. C., Chakrabarty, R. K., Moosmüller, H., Onasch, T. B., Zaveri, R. A., Scarnato, B. V., Fialho, P., and Mazzoleni, C.: Extensive Soot Compaction by Cloud Processing from Laboratory and Field Observations, *Scientific Reports*, 9, 11824, 10.1038/s41598-019-48143-y, 2019.

Formatted: Font: 10 pt

Formatted: Left, Indent: Left: 0 cm, Hanging: 1.27 cm, Line spacing: 1.5 lines

Formatted: Font: 10 pt

Formatted: Font: 10 pt

Formatted: Font: 10 pt

Formatted: Font: 10 pt

Formatted: Font: 10 pt

Formatted: Font: 10 pt

Bockhorn, H., D'Anna, A., and Sarofim, A. F.: Combustion Generated Fine Carbonaceous Particles, edited by: Wang, H.,
Universitätsverlag Karlsruhe, Karlsruhe, 2009.

700 Bond, T. C., Doherty, S. J., Fahey, D. W., Forster, P. M., Bernsten, T., DeAngelo, B. J., Flanner, M. G., Ghan, S., Kärcher,
B., Koch, D., Kinne, S., Kondo, Y., Quinn, P. K., Sarofim, M. C., Schultz, M. G., Schulz, M., Venkataraman, C.,
Zhang, H., Zhang, S., Bellouin, N., Guttikunda, S. K., Hopke, P. K., Jacobson, M. Z., Kaiser, J. W., Klimont, Z.,
Lohmann, U., Schwarz, J. P., Shindell, D., Storelvmo, T., Warren, S. G., and Zender, C. S.: Bounding the Role of
705 Black Carbon in the Climate System: A Scientific Assessment, *Journal of Geophysical Research: Atmospheres*,
118, 5380-5552, 10.1002/jgrd.50171, 2013.

Bond, T. C., Streets, D. G., Yarber, K. F., Nelson, S. M., Woo, J.-H., and Klimont, Z.: A Technology-Based Global
Inventory of Black and Organic Carbon Emissions from Combustion, *Journal of Geophysical Research:*
Atmospheres, 109, 10.1029/2003jd003697, 2004.

Borgnakke, C., and Sonntag, R. E.: *Thermodynamic Relations*, in: *Fundamentals of Thermodynamics*, 8th ed., Wiley, New
710 York, 557, 2013.

Brasil, A. M., Farias, T. L., and Carvalho, M. G.: A Recipe for Image Characterization of Fractal-Like Aggregates, *Journal*
of Aerosol Science, 30, 1379-1389, [https://doi.org/10.1016/S0021-8502\(99\)00026-9](https://doi.org/10.1016/S0021-8502(99)00026-9), 1999.

Brooks, S. D., Suter, K., and Olivarez, L.: Effects of Chemical Aging on the Ice Nucleation Activity of Soot and Polycyclic
Aromatic Hydrocarbon Aerosols, *The Journal of Physical Chemistry A*, 118, 10036-10047, 10.1021/jp508809y,
715 2014.

Burkhardt, U., and Kärcher, B.: Global Radiative Forcing from Contrail Cirrus, *Nature Climate Change*, 1, 54,
10.1038/nclimate1068, 2011.

Cabot Corporation: <https://www.cabotcorp.com/search/?query=regal+330R>, last access: 9 October, 2020.

Calogirou, A., Kotzias, D., and Kettrup, A.: Product Analysis of the Gas-Phase Reaction of B-Caryophyllene with Ozone,
720 *Atmospheric Environment*, 31, 283-285, [https://doi.org/10.1016/1352-2310\(96\)00190-2](https://doi.org/10.1016/1352-2310(96)00190-2), 1997.

Canagaratna, M. R., Jimenez, J. L., J. H. Kroll, Chen, Q., Kessler, S. H., Massoli, P., Ruiz, L. H., Fortner, E., Williams, L.
R., Wilson, K. R., Surratt, J. D., Donahue, N. M., Jayne, J. T., and Worsnop, D. R.: Elemental Ratio Measurements
of Organic Compounds Using Aerosol Mass Spectrometry: Characterization, Improved Calibration, and
Implications, *Atmospheric Chemistry and Physics*, 253-272, 2015.

725 Cape, J. N., Coyle, M., and Dumitrean, P.: The Atmospheric Lifetime of Black Carbon, *Atmospheric Environment*, 59, 256-
263, <https://doi.org/10.1016/j.atmosenv.2012.05.030>, 2012.

China, S., Kulkarni, G., Scarnato, B. V., Sharma, N., Pekour, M., Shilling, J. E., Wilson, J., Zelenyuk, A., Chand, D., Liu, S.,
Aiken, A. C., Dubey, M., Laskin, A., Zaveri, R. A., and Mazzoleni, C.: Morphology of Diesel Soot Residuals from
Supercooled Water Droplets and Ice Crystals: Implications for Optical Properties, *Environmental Research Letters*,
730 10, 114010, 10.1088/1748-9326/10/11/114010, 2015a.

Formatted: Font: 10 pt

Formatted: Font: 10 pt

Formatted: Font: 10 pt

Formatted: Font: 10 pt

Formatted: Font: 10 pt

Formatted: Font: 10 pt

Formatted: Font: 10 pt

Formatted: Font: 10 pt

- China, S., Mazzoleni, C., Gorkowski, K., Aiken, A. C., and Dubey, M. K.: Morphology and Mixing State of Individual Freshly Emitted Wildfire Carbonaceous Particles, *Nature communications*, 4, 2122, 10.1038/ncomms3122, 2013.
- China, S., Salvadori, N., and Mazzoleni, C.: Effect of Traffic and Driving Characteristics on Morphology of Atmospheric Soot Particles at Freeway on-Ramps, *Environmental Science & Technology*, 48, 3128-3135, 10.1021/es405178n, 2014.
- China, S., Scarnato, B., Owen, R. C., Zhang, B., Ampadu, M. T., Kumar, S., Dzepina, K., Dziobak, M. P., Fialho, P., Perlinger, J. A., Hueber, J., Helmig, D., Mazzoleni, L. R., and Mazzoleni, C.: Morphology and Mixing State of Aged Soot Particles at a Remote Marine Free Troposphere Site: Implications for Optical Properties, *Geophysical Research Letters*, 42, 1243-1250, doi:10.1002/2014GL062404, 2015b.
- Chou, C., Kanji, Z. A., Stetzer, O., Tritscher, T., Chirico, R., Heringa, M. F., Weingartner, E., Prévôt, A. S. H., Baltensperger, U., and Lohmann, U.: Effect of Photochemical Ageing on the Ice Nucleation Properties of Diesel and Wood Burning Particles, *Atmos. Chem. Phys.*, 13, 761-772, 10.5194/acp-13-761-2013, 2013.
- Ciccioli, P., Brancaleoni, E., Frattoni, M., Di Palo, V., Valentini, R., Tirone, G., Seufert, G., Bertin, N., Hansen, U., Csiky, O., Lenz, R., and Sharma, M.: Emission of Reactive Terpene Compounds from Orange Orchards and Their Removal by within-Canopy Processes, *Journal of Geophysical Research: Atmospheres*, 104, 8077-8094, 10.1029/1998jd100026, 1999.
- Connolly, P. J., Möhler, O., Field, P. R., Saathoff, H., Burgess, R., Choularton, T., and Gallagher, M.: Studies of Heterogeneous Freezing by Three Different Desert Dust Samples, *Atmos. Chem. Phys.*, 9, 2805-2824, 10.5194/acp-9-2805-2009, 2009.
- Crawford, I., Möhler, O., Schnaiter, M., Saathoff, H., Liu, D., McMeeking, G., Linke, C., Flynn, M., Bower, K. N., Connolly, P. J., Gallagher, M. W., and Coe, H.: Studies of Propane Flame Soot Acting as Heterogeneous Ice Nuclei in Conjunction with Single Particle Soot Photometer Measurements, *Atmospheric Chemistry and Physics*, 11, 9549-9561, 10.5194/acp-11-9549-2011, 2011.
- Cziczo, D. J., Thomson, D. S., Thompson, T. L., DeMott, P. J., and Murphy, D. M.: Particle Analysis by Laser Mass Spectrometry (Palms) Studies of Ice Nuclei and Other Low Number Density Particles, *International Journal of Mass Spectrometry*, 258, 21-29, 10.1016/j.ijms.2006.05.013, 2006.
- David, R. O., Fahrni, J., Marcolli, C., Mahrt, F., Brühwiler, D., and Kanji, Z. A.: The Role of Contact Angle and Pore Width on Pore Condensation and Freezing, *Atmos. Chem. Phys.*, 20, 9419-9440, 10.5194/acp-20-9419-2020, 2020.
- David, R. O., Marcolli, C., Fahrni, J., Qiu, Y., Perez Sirkin, Y. A., Molinero, V., Mahrt, F., Brühwiler, D., Lohmann, U., and Kanji, Z. A.: Pore Condensation and Freezing Is Responsible for Ice Formation Below Water Saturation for Porous Particles, *Proceedings of the National Academy of Sciences*, 116, 8184-8189, 10.1073/pnas.1813647116, 2019.
- DeCarlo, P. F., Kimmel, J. R., Trimborn, A., Northway, M. J., Jayne, J. T., Aiken, A. C., Gonin, M., Fuhrer, K., Horvath, T., Docherty, K. S., Worsnop, D. R., and Jimenez, J. L.: Field-Deployable, High-Resolution, Time-of-Flight Aerosol Mass Spectrometer, *Analytical Chemistry*, 78, 8281-8289, 10.1021/ac061249n, 2006.

765 DeMott, P. J., Chen, Y., Kreidenweis, S. M., Rogers, D. C., and Sherman, D. E.: Ice Formation by Black Carbon Particles, *Geophysical Research Letters*, 26, 2429-2432, doi:10.1029/1999GL900580, 1999.

DeMott, P. J., Cziczo, D. J., Prenni, A. J., Murphy, D. M., Kreidenweis, S. M., Thomson, D. S., Borys, R., and Rogers, D. C.: Measurements of the Concentration and Composition of Nuclei for Cirrus Formation, *Proceedings of the National Academy of Sciences*, 100, 14655-14660, 10.1073/pnas.2532677100, 2003.

770 DeRieux, W. S. W., Li, Y., Lin, P., Laskin, J., Laskin, A., Bertram, A. K., Nizkorodov, S. A., and Shiraiwa, M.: Predicting the Glass Transition Temperature and Viscosity of Secondary Organic Material Using Molecular Composition, *Atmos. Chem. Phys.*, 18, 6331-6351, 10.5194/acp-18-6331-2018, 2018.

Diehl, K., and Mitra, S. K.: A Laboratory Study of the Effects of a Kerosene-Burner Exhaust on Ice Nucleation and the Evaporation Rate of Ice Crystals, *Atmospheric Environment*, 32, 3145-3151, [https://doi.org/10.1016/S1352-2310\(97\)00467-6](https://doi.org/10.1016/S1352-2310(97)00467-6), 1998.

775 Ding, X., He, Q.-F., Shen, R.-Q., Yu, Q.-Q., and Wang, X.-M.: Spatial Distributions of Secondary Organic Aerosols from Isoprene, Monoterpenes, B-Caryophyllene, and Aromatics over China During Summer, *Journal of Geophysical Research: Atmospheres*, 119, 8177-8181, 10.1002/2014jd021748, 2014.

Docherty, K. S., Corse, E. W., Jaoui, M., Offenberg, J. H., Kleindienst, T. E., Krug, J. D., Riedel, T. P., and Lewandowski, M.: Trends in the Oxidation and Relative Volatility of Chamber-Generated Secondary Organic Aerosol, *Aerosol Science and Technology*, 52, 992-1004, 10.1080/02786826.2018.1500014, 2018.

780 Dooley, S., Won, S. H., Chaos, M., Heyne, J., Ju, Y., Dryer, F. L., Kumar, K., Sung, C.-J., Wang, H., Oehlschlaeger, M. A., Santoro, R. J., and Litzinger, T. A.: A Jet Fuel Surrogate Formulated by Real Fuel Properties, *Combustion and Flame*, 157, 2333-2339, <https://doi.org/10.1016/j.combustflame.2010.07.001>, 2010.

785 Dooley, S., Won, S. H., Jahangirian, S., Ju, Y., Dryer, F. L., Wang, H., and Oehlschlaeger, M. A.: The Combustion Kinetics of a Synthetic Paraffinic Jet Aviation Fuel and a Fundamentally Formulated, Experimentally Validated Surrogate Fuel, *Combustion and Flame*, 159, 3014-3020, 10.1016/j.combustflame.2012.04.010, 2012.

Dymarska, M., Murray, B. J., Sun, L., Eastwood, M. L., Knopf, D. A., and Bertram, A. K.: Deposition Ice Nucleation on Soot at Temperatures Relevant for the Lower Troposphere, *Journal of Geophysical Research: Atmospheres*, 111, doi:10.1029/2005JD006627, 2006.

790 Fioletov, V. E.: Ozone Climatology, Trends, and Substances That Control Ozone, *Atmosphere-Ocean*, 46, 39-67, 10.3137/ao.460103, 2008.

Fisher, L. R., Gamble, R. A., and Middlehurst, J.: The Kelvin Equation and the Capillary Condensation of Water, *Nature*, 290, 575-576, 10.1038/290575a0, 1981.

795 Fletcher, N. H.: Nucleation and Growth of Ice Crystals Upon Crystalline Substrates, *Australian Journal of Physics*, 13, 408-418, 1960.

Fletcher, N. H.: Active Sites and Ice Crystal Nucleation, *Journal of the Atmospheric Sciences*, 26, 1266-1271, 10.1175/1520-0469(1969)026<1266:asaicn>2.0.co;2, 1969.

Formatted: Font: 10 pt

Formatted: Font: 10 pt

Formatted: Font: 10 pt

Formatted: Font: 10 pt

- Fornea, A. P., Brooks, S. D., Dooley, J. B., and Saha, A.: Heterogeneous Freezing of Ice on Atmospheric Aerosols Containing Ash, Soot, and Soil, *Journal of Geophysical Research: Atmospheres*, 114, doi:10.1029/2009JD011958, 2009.
- Friedman, B., Kulkarni, G., Beránek, J., Zelenyuk, A., Thornton, J. A., and Cziczo, D. J.: Ice Nucleation and Droplet Formation by Bare and Coated Soot Particles, *Journal of Geophysical Research*, 116, 10.1029/2011jd015999, 2011.
- Frosch, M., Bilde, M., Nenes, A., Praplan, A. P., Jurányi, Z., Dommen, J., Gysel, M., Weingartner, E., and Baltensperger, U.: Ccn Activity and Volatility of B-Caryophyllene Secondary Organic Aerosol, *Atmos. Chem. Phys.*, 13, 2283-2297, 10.5194/acp-13-2283-2013, 2013.
- Fu, H., Zhang, M., Li, W., Chen, J., Wang, L., Quan, X., and Wang, W.: Morphology, Composition and Mixing State of Individual Carbonaceous Aerosol in Urban Shanghai, *Atmos. Chem. Phys.*, 12, 693-707, 10.5194/acp-12-693-2012, 2012.
- Garimella, S., Kristensen, T. B., Ignatius, K., Welts, A., Voigtländer, J., Kulkarni, G. R., Sagan, F., Kok, G. L., Dorsey, J., Nichman, L., Rothenberg, D. A., Rösch, M., Kirchgäßner, A. C. R., Ladkin, R., Wex, H., Wilson, T. W., Ladino, L. A., Abbatt, J. P. D., Stetzer, O., Lohmann, U., Stratmann, F., and Cziczo, D. J.: The Spectrometer for Ice Nuclei (Spin): An Instrument to Investigate Ice Nucleation, *Atmospheric Measurement Techniques*, 9, 2781-2795, 10.5194/amt-9-2781-2016, 2016.
- Garimella, S., Rothenberg, D. A., Wolf, M. J., David, R. O., Kanji, Z. A., Wang, C., Rösch, M., and Cziczo, D. J.: Uncertainty in Counting Ice Nucleating Particles with Continuous Flow Diffusion Chambers, *Atmos. Chem. Phys.*, 17, 10855-10864, 10.5194/acp-17-10855-2017, 2017.
- Gottelman, A., Hoor, P., Pan, L. L., Randel, W. J., Hegglin, M. I., and Birner, T.: The Extratropical Upper Troposphere and Lower Stratosphere, *Reviews of Geophysics*, 49, 10.1029/2011RG000355, 2011.
- Griffin, R. J., Cocker III, D. R., Seinfeld, J. H., and Dabdub, D.: Estimate of Global Atmospheric Organic Aerosol from Oxidation of Biogenic Hydrocarbons, *Geophysical Research Letters*, 26, 2721-2724, 10.1029/1999gl900476, 1999.
- Guenther, A. B., Jiang, X., Heald, C. L., Sakulyanontvittaya, T., Duhl, T., Emmons, L. K., and Wang, X.: The Model of Emissions of Gases and Aerosols from Nature Version 2.1 (Megan2.1): An Extended and Updated Framework for Modeling Biogenic Emissions, *Geosci. Model Dev.*, 5, 1471-1492, 10.5194/gmd-5-1471-2012, 2012.
- Heald, C. L., Henze, D. K., Horowitz, L. W., Feddes, J., Lamarque, J. F., Guenther, A., Hess, P. G., Vitt, F., Seinfeld, J. H., Goldstein, A. H., and Fung, I.: Predicted Change in Global Secondary Organic Aerosol Concentrations in Response to Future Climate, Emissions, and Land Use Change, *Journal of Geophysical Research: Atmospheres*, 113, 10.1029/2007JD009092, 2008.
- Heald, C. L., Kroll, J. H., Jimenez, J. L., Docherty, K. S., DeCarlo, P. F., Aiken, A. C., Chen, Q., Martin, S. T., Farmer, D. K., and Artaxo, P.: A Simplified Description of the Evolution of Organic Aerosol Composition in the Atmosphere, *Geophysical Research Letters*, 37, 10.1029/2010gl042737, 2010.

Helmig, D., Ortega, J., Guenther, A., Herrick, J. D., and Geron, C.: Sesquiterpene Emissions from Loblolly Pine and Their Potential Contribution to Biogenic Aerosol Formation in the Southeastern Us, *Atmospheric Environment*, 40, 4150-4157, <https://doi.org/10.1016/j.atmosenv.2006.02.035>, 2006.

835 Henrot, A. J., Stanelle, T., Schröder, S., Siegenthaler, C., Taraborrelli, D., and Schultz, M. G.: Implementation of the Megan (V2.1) Biogenic Emission Model in the Echam6-Hammoz Chemistry Climate Model, *Geosci. Model Dev.*, 10, 903-926, 10.5194/gmd-10-903-2017, 2017.

Heymsfield, A. J., Krämer, M., Luebke, A., Brown, P., Cziczo, D. J., Franklin, C., Lawson, P., Lohmann, U., McFarquhar, G., Ulanowski, Z., and Van Tricht, K.: Cirrus Clouds, *Meteorological Monographs*, 58, 2.1-2.26, 10.1175/amsmonographs-d-16-0010.1, 2017.

840 Hildebrandt, L., Donahue, N. M., and Pandis, S. N.: High Formation of Secondary Organic Aerosol from the Photo-Oxidation of Toluene, *Atmos. Chem. Phys.*, 9, 2973-2986, 10.5194/acp-9-2973-2009, 2009.

Hildebrandt Ruiz, L., Paciga, A. L., Cerully, K. M., Nenes, A., Donahue, N. M., and Pandis, S. N.: Formation and Aging of Secondary Organic Aerosol from Toluene: Changes in Chemical Composition, Volatility, and Hygroscopicity, *Atmos. Chem. Phys.*, 15, 8301-8313, 10.5194/acp-15-8301-2015, 2015.

845 Hinks, M. L., Montoya-Aguilera, J., Ellison, L., Lin, P., Laskin, A., Laskin, J., Shiraiwa, M., Dabdub, D., and Nizkorodov, S. A.: Effect of Relative Humidity on the Composition of Secondary Organic Aerosol from the Oxidation of Toluene, *Atmos. Chem. Phys.*, 18, 1643-1652, 10.5194/acp-18-1643-2018, 2018.

Hodzic, A., Jimenez, J. L., Madronich, S., Canagaratna, M. R., DeCarlo, P. F., Kleinman, L., and Fast, J.: Modeling Organic Aerosols in a Megacity: Potential Contribution of Semi-Volatile and Intermediate Volatility Primary Organic Compounds to Secondary Organic Aerosol Formation, *Atmos. Chem. Phys.*, 10, 5491-5514, 10.5194/acp-10-5491-2010, 2010.

850 Hodzic, A., Kasibhatla, P. S., Jo, D. S., Cappa, C. D., Jimenez, J. L., Madronich, S., and Park, R. J.: Rethinking the Global Secondary Organic Aerosol (Soa) Budget: Stronger Production, Faster Removal, Shorter Lifetime, *Atmos. Chem. Phys.*, 16, 7917-7941, 10.5194/acp-16-7917-2016, 2016.

855 Hoffmann, T., Odum, J. R., Bowman, F., Collins, D., Klockow, D., Flagan, R. C., and Seinfeld, J. H.: Formation of Organic Aerosols from the Oxidation of Biogenic Hydrocarbons, *Journal of Atmospheric Chemistry*, 26, 189-222, 10.1023/A:1005734301837, 1997.

Hu, D., Bian, Q., Li, T. W. Y., Lau, A. K. H., and Yu, J. Z.: Contributions of Isoprene, Monoterpenes, B-Caryophyllene, and Toluene to Secondary Organic Aerosols in Hong Kong During the Summer of 2006, *Journal of Geophysical Research: Atmospheres*, 113, 10.1029/2008jd010437, 2008.

860 Huang, C.-H., and Vander Wal, R. L.: Effect of Soot Structure Evolution from Commercial Jet Engine Burning Petroleum Based Jp-8 and Synthetic H₂ and Ft Fuels, *Energy & Fuels*, 27, 4946-4958, 10.1021/ef400576c, 2013.

IPCC: Ipcc, 2013: Climate Change 2013: The Physical Science Basis. Contribution of Working Group I to the Fifth Assessment Report of the Intergovernmental Panel on Climate Change [Stocker, T.F., D. Qin, G.-K. Plattner, M.

865

Formatted: Font: 10 pt

Formatted: Font: 10 pt

Tignor, S.K. Allen, J. Boschung, A. Nauels, Y. Xia, V. Bex and P.M. Midgley (Eds.)). Cambridge University Press, Cambridge, United Kingdom and New York, NY, USA., 2013.

Jacobson, M. Z.: Strong Radiative Heating Due to the Mixing State of Black Carbon in Atmospheric Aerosols, *Nature*, 409, 695-697, 10.1038/35055518, 2001.

870 Jaoui, M., Kleindienst, T. E., Docherty, K. S., Lewandowski, M., and Offenberg, J. H.: Secondary Organic Aerosol Formation from the Oxidation of a Series of Sesquiterpenes: A-Cedrene, B-Caryophyllene, A-Humulene and A-Farnesene with O₃, OH and NO₃ Radicals, *Environmental Chemistry*, 10, 178-193, <https://doi.org/10.1071/EN13025>, 2013.

Jaoui, M., Lewandowski, M., Kleindienst, T. E., Offenberg, J. H., and Edney, E. O.: B-Caryophyllenic Acid: An Atmospheric Tracer for B-Caryophyllene Secondary Organic Aerosol, *Geophysical Research Letters*, 34, 10.1029/2006GL028827, 2007.

875 Joo, P. H., Gigone, B., Griffin, E. A., Christensen, M., and Gülder, Ö. L.: Soot Primary Particle Size Dependence on Combustion Pressure in Laminar Ethylene Diffusion Flames, *Fuel*, 220, 464-470, <https://doi.org/10.1016/j.fuel.2018.02.025>, 2018.

880 Joyce, G. A., and Henry, W. M.: Modeling the Equilibrium Compressed Void Volume of Carbon Black, *Rubber Chemistry and Technology*, 79, 735-764, 10.5254/1.3547964, 2006.

Kang, E., Root, M. J., Toohey, D. W., and Brune, W. H.: Introducing the Concept of Potential Aerosol Mass (Pam), *Atmos. Chem. Phys.*, 7, 5727-5744, 10.5194/acp-7-5727-2007, 2007.

Kanji, Z. A., and Abbatt, J. P. D.: Laboratory Studies of Ice Formation Via Deposition Mode Nucleation onto Mineral Dust and N-Hexane Soot Samples, *Journal of Geophysical Research*, 111, 10.1029/2005jd006766, 2006.

885 Kanji, Z. A., DeMott, P. J., Möhler, O., and Abbatt, J. P. D.: Results from the University of Toronto Continuous Flow Diffusion Chamber at Icis 2007: Instrument Intercomparison and Ice Onsets for Different Aerosol Types, *Atmospheric Chemistry and Physics*, 11, 31-41, 10.5194/acp-11-31-2011, 2011.

Kanji, Z. A., Ladino, L. A., Wex, H., Boose, Y., Burkert-Kohn, M., Cziczo, D. J., and Krämer, M.: Overview of Ice Nucleating Particles, *Meteorological Monographs*, 58, 1.1-1.33, 10.1175/amsmonographs-d-16-0006.1, 2017.

890 Kärcher, B.: Formation and Radiative Forcing of Contrail Cirrus, *Nature communications*, 9, 1824, 10.1038/s41467-018-04068-0, 2018.

Kärcher, B., Möhler, O., DeMott, P. J., Pechtl, S., and Yu, F.: Insights into the Role of Soot Aerosols in Cirrus Cloud Formation, *Atmos. Chem. Phys.*, 7, 4203-4227, 10.5194/acp-7-4203-2007, 2007.

895 Karlsson, M. N. A., and Martinsson, B. G.: Methods to Measure and Predict the Transfer Function Size Dependence of Individual Dmas, *Journal of Aerosol Science*, 34, 603-625, [https://doi.org/10.1016/S0021-8502\(03\)00020-X](https://doi.org/10.1016/S0021-8502(03)00020-X), 2003.

Khalizov, A. F., Zhang, R., Zhang, D., Xue, H., Pagels, J., and McMurry, P. H.: Formation of Highly Hygroscopic Soot Aerosols Upon Internal Mixing with Sulfuric Acid Vapor, *Journal of Geophysical Research: Atmospheres*, 114, 10.1029/2008JD010595, 2009.

Formatted: Font: 10 pt

Formatted: Font: 10 pt

Formatted: Font: 10 pt

Formatted: Font: 10 pt

Formatted: Font: 10 pt

Formatted: Font: 10 pt

900 Kinsey, J. S., Dong, Y., Williams, D. C., and Logan, R.: Physical Characterization of the Fine Particle Emissions from
Commercial Aircraft Engines During the Aircraft Particle Emissions Experiment (Apex) 1–3, Atmospheric
Environment, 44, 2147-2156, 10.1016/j.atmosenv.2010.02.010, 2010.

Kinsey, J. S., Hays, M. D., Dong, Y., Williams, D. C., and Logan, R.: Chemical Characterization of the Fine Particle
Emissions from Commercial Aircraft Engines During the Aircraft Particle Emissions Experiment (Apex) 1 to 3,
905 Environmental Science & Technology, 45, 3415-3421, 10.1021/es103880d, 2011.

Kiselev, A., Bachmann, F., Pedevilla, P., Cox, S. J., Michaelides, A., Gerthsen, D., and Leisner, T.: Active Sites in
Heterogeneous Ice Nucleation-the Example of K-Rich Feldspars, Science, 355, 367-371, 10.1126/science.aai8034,
2017.

Kittelson, D. B.: Engines and Nanoparticles: A Review, Journal of Aerosol Science, 29, 575-588,
910 [https://doi.org/10.1016/S0021-8502\(97\)10037-4](https://doi.org/10.1016/S0021-8502(97)10037-4), 1998.

Koehler, K. A., DeMott, P. J., Kreidenweis, S. M., Popovicheva, O. B., Petters, M. D., Carrico, C. M., Kireeva, E. D.,
Khokhlova, T. D., and Shonija, N. K.: Cloud Condensation Nuclei and Ice Nucleation Activity of Hydrophobic and
Hydrophilic Soot Particles, Physical Chemistry Chemical Physics, 11, 7906-7920, 10.1039/B905334B, 2009.

Koop, T., Luo, B., Tsias, A., and Peter, T.: Water Activity as the Determinant for Homogeneous Ice Nucleation in Aqueous
915 Solutions, Nature, 406, 611, 10.1038/35020537, 2000.

Köylü, Ü. Ö., Faeth, G. M., Farias, T. L., and Carvalho, M. G.: Fractal and Projected Structure Properties of Soot
Aggregates, Combustion and Flame, 100, 621-633, [https://doi.org/10.1016/0010-2180\(94\)00147-K](https://doi.org/10.1016/0010-2180(94)00147-K), 1995.

Kulkarni, G., China, S., Liu, S., Nandasiri, M., Sharma, N., Wilson, J., Aiken, A. C., Chand, D., Laskin, A., Mazzoleni, C.,
Pekour, M., Shilling, J., Shutthanandan, V., Zelenyuk, A., and Zaveri, R. A.: Ice Nucleation Activity of Diesel Soot
920 Particles at Cirrus Relevant Temperature Conditions: Effects of Hydration, Secondary Organics Coating, Soot
Morphology, and Coagulation, Geophysical Research Letters, 43, 3580-3588, 10.1002/2016gl068707, 2016.

Kulkarni, G. R., and Kok, G. L.: Mobile Ice Nucleus Spectrometer, ; Pacific Northwest National Lab. (PNNL), Richland,
WA (United States)PNNL-21384; Other: 600306000 United States 10.2172/1071991 Other: 600306000 PNNL
English, Medium: ED; Size: PDFN, 2012.

925 Lambe, A. T., Ahern, A. T., Williams, L. R., Slowik, J. G., Wong, J. P. S., Abbatt, J. P. D., Brune, W. H., Ng, N. L., Wright,
J. P., Croasdale, D. R., Worsnop, D. R., Davidovits, P., and Onasch, T. B.: Characterization of Aerosol
Photooxidation Flow Reactors: Heterogeneous Oxidation, Secondary Organic Aerosol Formation and Cloud
Condensation Nuclei Activity Measurements, Atmos. Meas. Tech., 4, 445-461, 10.5194/amt-4-445-2011, 2011a.

Lambe, A. T., Onasch, T. B., Massoli, P., Croasdale, D. R., Wright, J. P., Ahern, A. T., Williams, L. R., Worsnop, D. R.,
930 Brune, W. H., and Davidovits, P.: Laboratory Studies of the Chemical Composition and Cloud Condensation Nuclei
(Ccn) Activity of Secondary Organic Aerosol (Soa) and Oxidized Primary Organic Aerosol (Opoa), Atmos. Chem.
Phys., 11, 8913-8928, 10.5194/acp-11-8913-2011, 2011b.

Formatted: Font: 10 pt

Formatted: Font: 10 pt

Formatted: Font: 10 pt

Formatted: Font: 10 pt

935 Lamkaddam, H., Gratien, A., Ropion, M., Pangui, E., and Doussin, J.-F.: Kinetic Study of the Temperature Dependence of
Oh-Initiated Oxidation of N-Dodecane, *The Journal of Physical Chemistry A*, 123, 9462-9468,
10.1021/acs.jpca.9b07704, 2019.

Lapuerta, M., Martos, F. J., and Herreros, J. M.: Effect of Engine Operating Conditions on the Size of Primary Particles
Composing Diesel Soot Agglomerates, *Journal of Aerosol Science*, 38, 455-466,
<https://doi.org/10.1016/j.jaerosci.2007.02.001>, 2007.

940 Lee-Taylor, J., Madronich, S., Aumont, B., Baker, A., Camredon, M., Hodzic, A., Tyndall, G. S., Apel, E., and Zaveri, R.
A.: Explicit Modeling of Organic Chemistry and Secondary Organic Aerosol Partitioning for Mexico City and Its
Outflow Plume, *Atmos. Chem. Phys.*, 11, 13219-13241, 10.5194/acp-11-13219-2011, 2011.

Lee, A., Goldstein, A. H., Kroll, J. H., Ng, N. L., Varutbangkul, V., Flagan, R. C., and Seinfeld, J. H.: Gas-Phase Products
and Secondary Aerosol Yields from the Photooxidation of 16 Different Terpenes, *Journal of Geophysical Research:*
Atmospheres, 111, 10.1029/2006jd007050, 2006.

945 Lee, C., and Kramer, T. A.: Prediction of Three-Dimensional Fractal Dimensions Using the Two-Dimensional Properties of
Fractal Aggregates, *Advances in Colloid and Interface Science*, 112, 49-57,
<https://doi.org/10.1016/j.cis.2004.07.001>, 2004.

Lee, D. S., Fahey, D. W., Forster, P. M., Newton, P. J., Wit, R. C. N., Lim, L. L., Owen, B., and Sausen, R.: Aviation and
Global Climate Change in the 21st Century, *Atmospheric Environment*, 43, 3520-3537,
950 10.1016/j.atmosenv.2009.04.024, 2009.

Lee, D. S., Pitari, G., Grewe, V., Gierens, K., Penner, J. E., Petzold, A., Prather, M. J., Schumann, U., Bais, A., Bernsten, T.,
Iachetti, D., Lim, L. L., and Sausen, R.: Transport Impacts on Atmosphere and Climate: Aviation, *Atmospheric*
Environment, 44, 4678-4734, <https://doi.org/10.1016/j.atmosenv.2009.06.005>, 2010.

Lefebvre, A. H.: *Gas Turbine Combustion*, CRC press, 1998.

955 Li, K., Chen, L., Han, K., Lv, B., Bao, K., Wu, X., Gao, X., and Cen, K.: Smog Chamber Study on Aging of Combustion
Soot in Isoprene/So2/Nox System: Changes of Mass, Size, Effective Density, Morphology and Mixing State,
Atmospheric Research, 184, 139-148, <https://doi.org/10.1016/j.atmosres.2016.10.011>, 2017.

Li, K., Liggio, J., Lee, P., Han, C., Liu, Q., and Li, S. M.: Secondary Organic Aerosol Formation from A-Pinene, Alkanes,
and Oil-Sands-Related Precursors in a New Oxidation Flow Reactor, *Atmos. Chem. Phys.*, 19, 9715-9731,
960 10.5194/acp-19-9715-2019, 2019.

Li, M., Karu, E., Brenninkmeijer, C., Fischer, H., Lelieveld, J., and Williams, J.: Tropospheric Oh and Stratospheric Oh and
Cl Concentrations Determined from CH₄, CH₃Cl, and Sf₆ Measurements, *npj Climate and Atmospheric Science*, 1,
29, 10.1038/s41612-018-0041-9, 2018.

965 Li, W., Shao, L., Zhang, D., Ro, C.-U., Hu, M., Bi, X., Geng, H., Matsuki, A., Niu, H., and Chen, J.: A Review of Single
Aerosol Particle Studies in the Atmosphere of East Asia: Morphology, Mixing State, Source, and Heterogeneous
Reactions, *Journal of Cleaner Production*, 112, 1330-1349, <https://doi.org/10.1016/j.jclepro.2015.04.050>, 2016.

Formatted: Font: 10 pt

Formatted: Font: 10 pt

Formatted: Font: 10 pt

Formatted: Font: 10 pt

Formatted: Font: 10 pt

Formatted: Font: 10 pt

Formatted: Font: 10 pt

Formatted: Font: 10 pt

Formatted: Font: 10 pt

Formatted: Font: 10 pt

- Li, Y., Day, D. A., Stark, H., Jimenez, J. L., and Shiraiwa, M.: Predictions of the Glass Transition Temperature and Viscosity of Organic Aerosols from Volatility Distributions, *Atmos. Chem. Phys.*, 20, 8103-8122, 10.5194/acp-20-8103-2020, 2020.
- 970 Liati, A., Brem, B. T., Durdina, L., Vogtli, M., Dasilva, Y. A., Eggenschwiler, P. D., and Wang, J.: Electron Microscopic Study of Soot Particulate Matter Emissions from Aircraft Turbine Engines, *Environmental science & technology*, 48, 10975-10983, 10.1021/es501809b, 2014.
- Liati, A., Schreiber, D., Dimopoulos Eggenschwiler, P., Arroyo Rojas Dasilva, Y., and Spiteri, A. C.: Electron Microscopic Characterization of Soot Particulate Matter Emitted by Modern Direct Injection Gasoline Engines, *Combustion and Flame*, 166, 307-315, 10.1016/j.combustflame.2016.01.031, 2016.
- 975 Liu, T., Huang, D. D., Li, Z., Liu, Q., Chan, M., and Chan, C. K.: Comparison of Secondary Organic Aerosol Formation from Toluene on Initially Wet and Dry Ammonium Sulfate Particles at Moderate Relative Humidity, *Atmos. Chem. Phys.*, 18, 5677-5689, 10.5194/acp-18-5677-2018, 2018.
- Lobo, P., Durdina, L., Smallwood, G. J., Rindlisbacher, T., Siegerist, F., Black, E. A., Yu, Z., Mensah, A. A., Hagen, D. E., 980 Miake-Lye, R. C., Thomson, K. A., Brem, B. T., Corbin, J. C., Abegglen, M., Sierau, B., Whitefield, P. D., and Wang, J.: Measurement of Aircraft Engine Non-Volatile Pm Emissions: Results of the Aviation-Particle Regulatory Instrumentation Demonstration Experiment (a-Pride) 4 Campaign, *Aerosol Science and Technology*, 49, 472-484, 10.1080/02786826.2015.1047012, 2015.
- Loza, C. L., Craven, J. S., Yee, L. D., Coggon, M. M., Schwantes, R. H., Shiraiwa, M., Zhang, X., Schilling, K. A., Ng, N. 985 L., Canagaratna, M. R., Ziemann, P. J., Flagan, R. C., and Seinfeld, J. H.: Secondary Organic Aerosol Yields of 12-Carbon Alkanes, *Atmos. Chem. Phys.*, 14, 1423-1439, 10.5194/acp-14-1423-2014, 2014.
- Lund, M. T., Samset, B. H., Skeie, R. B., Watson-Parris, D., Katich, J. M., Schwarz, J. P., and Weinzierl, B.: Short Black Carbon Lifetime Inferred from a Global Set of Aircraft Observations, *npj Climate and Atmospheric Science*, 1, 31, 10.1038/s41612-018-0040-x, 2018.
- 990 L    nd, F., Stetzer, O., Welti, A., and Lohmann, U.: Experimental Study on the Ice Nucleation Ability of Size-Selected Kaolinite Particles in the Immersion Mode, *Journal of Geophysical Research: Atmospheres*, 115, 10.1029/2009jd012959, 2010.
- Mahrt, F., Kilchhofer, K., Marcolli, C., Gr  nquist, P., David, R. O., R  sch, M., Lohmann, U., and Kanji, Z. A.: The Impact of Cloud Processing on the Ice Nucleation Abilities of Soot Particles at Cirrus Temperatures, *Journal of Geophysical Research: Atmospheres*, 125, e2019JD030922, 10.1029/2019jd030922, 2020.
- 995 Mahrt, F., Marcolli, C., David, R. O., Gronquist, P., Meier, E. J. B., Lohmann, U., and Kanji, Z. A.: Ice Nucleation Abilities of Soot Particles Determined with the Horizontal Ice Nucleation Chamber, *Atmospheric Chemistry and Physics*, 18, 13363-13392, 10.5194/acp-18-13363-2018, 2018.
- Mandelbrot, B. B.: *The Fractal Geometry of Nature*, W. H. Freeman and Company, San Francisco, 1982.

- 1000 Marcolli, C.: Deposition Nucleation Viewed as Homogeneous or Immersion Freezing in Pores and Cavities, *Atmospheric Chemistry and Physics*, 14, 2071-2104, 10.5194/acp-14-2071-2014, 2014.
- Mason, R. H., Si, M., Chou, C., Irish, V. E., Dickie, R., Elizondo, P., Wong, R., Brintnell, M., Elsasser, M., Lassar, W. M., Pierce, K. M., Leaitch, W. R., MacDonald, A. M., Platt, A., Toom-Sauntry, D., Sarda-Estève, R., Schiller, C. L., Suski, K. J., Hill, T. C. J., Abbatt, J. P. D., Huffman, J. A., DeMott, P. J., and Bertram, A. K.: Size-Resolved
1005 Measurements of Ice-Nucleating Particles at Six Locations in North America and One in Europe, *Atmos. Chem. Phys.*, 16, 1637-1651, 10.5194/acp-16-1637-2016, 2016.
- Moffet, R. C., O'Brien, R. E., Alpert, P. A., Kelly, S. T., Pham, D. Q., Gilles, M. K., Knopf, D. A., and Laskin, A.: Morphology and Mixing of Black Carbon Particles Collected in Central California During the Cares Field Study, *Atmos. Chem. Phys.*, 16, 14515-14525, 10.5194/acp-16-14515-2016, 2016.
- 1010 Möhler, O., Büttner, S., Linke, C., Schnaiter, M., Saathoff, H., Stetzer, O., Wagner, R., Krämer, M., Mangold, A., Ebert, V., and Schurath, U.: Effect of Sulfuric Acid Coating on Heterogeneous Ice Nucleation by Soot Aerosol Particles, *Journal of Geophysical Research: Atmospheres*, 110, doi:10.1029/2004JD005169, 2005a.
- Möhler, O., Linke, C., Saathoff, H., Schnaiter, M., Wagner, R., Mangold, A., Krämer, M., and Schurath, U.: Ice Nucleation on Flame Soot Aerosol of Different Organic Carbon Content, *Meteorologische Zeitschrift*, 14, 477-484,
1015 10.1127/0941-2948/2005/0055, 2005b.
- Moore, R. H., Thornhill, K. L., Weinzierl, B., Sauer, D., D'Ascoli, E., Kim, J., Lichtenstern, M., Scheibe, M., Beaton, B., Beyersdorf, A. J., Barrick, J., Bulzan, D., Corr, C. A., Crosbie, E., Jurkat, T., Martin, R., Riddick, D., Shook, M., Slover, G., Voigt, C., White, R., Winstead, E., Yasky, R., Ziemba, L. D., Brown, A., Schlager, H., and Anderson, B. E.: Biofuel Blending Reduces Particle Emissions from Aircraft Engines at Cruise Conditions, *Nature*, 543, 411-415,
1020 10.1038/nature21420, 2017.
- Murphy, D. M., Thomson, D. S., Middlebrook, A. M., and Schein, M. E.: In Situ Single-Particle Characterization at Cape Grim, *Journal of Geophysical Research: Atmospheres*, 103, 16485-16491, 10.1029/97JD03281, 1998.
- Murray, B. J., Wilson, T. W., Dobbie, S., Cui, Z., Al-Jumr, S. M. R. K., Möhler, O., Schnaiter, M., Wagner, R., Benz, S., Niemand, M., Saathoff, H., Ebert, V., Wagner, S., and Kärcher, B.: Heterogeneous Nucleation of Ice Particles on
1025 Glassy Aerosols under Cirrus Conditions, *Nature Geoscience*, 3, 233-237, 10.1038/ngeo817, 2010.
- Ng, N. L., Canagaratna, M. R., Jimenez, J. L., Chhabra, P. S., Seinfeld, J. H., and Worsnop, D. R.: Changes in Organic Aerosol Composition with Aging Inferred from Aerosol Mass Spectra, *Atmos. Chem. Phys.*, 11, 6465-6474,
10.5194/acp-11-6465-2011, 2011.
- Ng, N. L., Canagaratna, M. R., Zhang, Q., Jimenez, J. L., Tian, J., Ulbrich, I. M., Kroll, J. H., Docherty, K. S., Chhabra, P. S., Bahreini, R., Murphy, S. M., Seinfeld, J. H., Hildebrandt, L., Donahue, N. M., DeCarlo, P. F., Lanz, V. A., Prévôt, A. S. H., Dinar, E., Rudich, Y., and Worsnop, D. R.: Organic Aerosol Components Observed in Northern
1030 Hemispheric Datasets from Aerosol Mass Spectrometry, *Atmos. Chem. Phys.*, 10, 4625-4641, 10.5194/acp-10-4625-2010, 2010.

1035 Nguyen, T. L., Winterhalter, R., Moortgat, G., Kanawati, B., Peeters, J., and Vereecken, L.: The Gas-Phase Ozonolysis of B-Caryophyllene (C₁₅H₂₄). Part II: A Theoretical Study, *Physical Chemistry Chemical Physics*, 11, 4173-4183, 10.1039/B817913A, 2009.

Nichman, L., Wolf, M., Davidovits, P., Onasch, T. B., Zhang, Y., Worsnop, D. R., Bhandari, J., Mazzoleni, C., and Cziczo, D. J.: Laboratory Study of the Heterogeneous Ice Nucleation on Black-Carbon-Containing Aerosol, *Atmos. Chem. Phys.*, 19, 12175-12194, 10.5194/acp-19-12175-2019, 2019.

1040 Oh, C., and Sorensen, C. M.: The Effect of Overlap between Monomers on the Determination of Fractal Cluster Morphology, *Journal of Colloid and Interface Science*, 193, 17-25, <https://doi.org/10.1006/jcis.1997.5046>, 1997.

Onasch, T. B., Jayne, J. T., Herndon, S., Worsnop, D. R., Miake-Lye, R. C., Mortimer, I. P., and Anderson, B. E.: Chemical Properties of Aircraft Engine Particulate Exhaust Emissions, *Journal of Propulsion and Power*, 25, 1121-1137, 10.2514/1.36371, 2009.

1045 Onasch, T. B., Trimborn, A., Fortner, E. C., Jayne, J. T., Kok, G. L., Williams, L. R., Davidovits, P., and Worsnop, D. R.: Soot Particle Aerosol Mass Spectrometer: Development, Validation, and Initial Application, *Aerosol Science and Technology*, 46, 804-817, 10.1080/02786826.2012.663948, 2012.

Pandis, S. N., Harley, R. A., Cass, G. R., and Seinfeld, J. H.: Secondary Organic Aerosol Formation and Transport, *Atmospheric Environment. Part A. General Topics*, 26, 2269-2282, [https://doi.org/10.1016/0960-1686\(92\)90358-R](https://doi.org/10.1016/0960-1686(92)90358-R), 1992.

1050 Pereira, K. L., Rovelli, G., Song, Y. C., Mayhew, A. W., Reid, J. P., and Hamilton, J. F.: A New Aerosol Flow Reactor to Study Secondary Organic Aerosol, *Atmos. Meas. Tech.*, 12, 4519-4541, 10.5194/amt-12-4519-2019, 2019.

Persiantseva, N. M., Popovicheva, O. B., and Shonija, N. K.: Wetting and Hydration of Insoluble Soot Particles in the Upper Troposphere, *Journal of Environmental Monitoring*, 6, 939-945, 10.1039/B407770A, 2004.

1055 Petzold, A., Ström, J., Ohlsson, S., and Schröder, F. P.: Elemental Composition and Morphology of Ice-Crystal Residual Particles in Cirrus Clouds and Contrails, *Atmospheric Research*, 49, 21-34, [https://doi.org/10.1016/S0169-8095\(97\)00083-5](https://doi.org/10.1016/S0169-8095(97)00083-5), 1998.

Pison, I., and Menut, L.: Quantification of the Impact of Aircraft Traffic Emissions on Tropospheric Ozone over Paris Area, *Atmospheric Environment*, 38, 971-983, <https://doi.org/10.1016/j.atmosenv.2003.10.056>, 2004.

1060 Popovicheva, O. B., Persiantseva, N. M., Lukhovitskaya, E. E., Shonija, N. K., Zubareva, N. A., Demirdjian, B., Ferry, D., and Suzanne, J.: Aircraft Engine Soot as Contrail Nuclei, *Geophysical Research Letters*, 31, doi:10.1029/2003GL018888, 2004.

Presto, A. A., Miracolo, M. A., Donahue, N. M., and Robinson, A. L.: Secondary Organic Aerosol Formation from High-Nox Photo-Oxidation of Low Volatility Precursors: N-Alkanes, *Environmental Science & Technology*, 44, 2029-2034, 10.1021/es903712r, 2010.

1065 Pruppacher, H. R., and Klett, J. D.: *Microphysics of Clouds and Precipitation*, 2 ed., Atmospheric and Oceanographic Sciences Library, 18, Springer Netherlands, XXII, 954 pp., 2010.

Formatted: Font: 10 pt

Formatted: Font: 10 pt

Formatted: Font: 10 pt

Formatted: Font: 10 pt

Formatted: Font: 10 pt

Formatted: Font: 10 pt

Formatted: Font: 10 pt

Formatted: Font: 10 pt

1070 Pusechel, R. F., Blake, D. F., Snetsinger, K. G., Hansen, A. D. A., Verma, S., and Kato, K.: Black Carbon (Soot) Aerosol in the Lower Stratosphere and Upper Troposphere, *Geophysical Research Letters*, 19, 1659-1662, 10.1029/92GL01801, 1992.

Ramachandran, G., and Reist, P. C.: Characterization of Morphological Changes in Agglomerates Subject to Condensation and Evaporation Using Multiple Fractal Dimensions, *Aerosol Science and Technology*, 23, 431-442, 10.1080/02786829508965326, 1995.

1075 Raza, M., Chen, L., Leach, F., and Ding, S.: A Review of Particulate Number (Pn) Emissions from Gasoline Direct Injection (Gdi) Engines and Their Control Techniques, *Energies*, 11, 10.3390/en11061417, 2018.

Sakulyanontvittaya, T., Duhl, T., Wiedinmyer, C., Helmig, D., Matsunaga, S., Potosnak, M., Milford, J., and Guenther, A.: Monoterpene and Sesquiterpene Emission Estimates for the United States, *Environmental Science & Technology*, 42, 1623-1629, 10.1021/es702274e, 2008.

1080 Samson, R. J., Mulholland, G. W., and Gentry, J. W.: Structural Analysis of Soot Agglomerates, *Langmuir*, 3, 272-281, 10.1021/la00074a022, 1987.

Schilling, K. A., Yee, L. D., Loza, C. L., Coggon, M. M., Schwantes, R., Zhang, X., Dalleska, N. F., and Seinfeld, J. H.: Secondary Organic Aerosol Composition from C12 Alkanes, *The Journal of Physical Chemistry A*, 119, 4281-4297, 10.1021/jp501779w, 2015.

Seinfeld, J. H.: Clouds, Contrails and Climate, *Nature*, 391, 837-838, 1998.

1085 Shu, Y., and Atkinson, R.: Rate Constants for the Gas-Phase Reactions of O₃ with a Series of Terpenes and Oh Radical Formation from the O₃ Reactions with Sesquiterpenes at 296 ± 2 K, *International Journal of Chemical Kinetics*, 26, 1193-1205, 10.1002/kin.550261207, 1994.

Shu, Y., and Atkinson, R.: Atmospheric Lifetimes and Fates of a Series of Sesquiterpenes, *Journal of Geophysical Research: Atmospheres*, 100, 7275-7281, 10.1029/95JD00368, 1995.

1090 Simonen, P., Saukko, E., Karjalainen, P., Timonen, H., Bloss, M., Aakko-Saksa, P., Rönkkö, T., Keskinen, J., and Dal Maso, M.: A New Oxidation Flow Reactor for Measuring Secondary Aerosol Formation of Rapidly Changing Emission Sources, *Atmos. Meas. Tech.*, 10, 1519-1537, 10.5194/amt-10-1519-2017, 2017.

Slowik, J. G., Cross, E. S., Han, J.-H., Kolucki, J., Davidovits, P., Williams, L. R., Onasch, T. B., Jayne, J. T., Kolb, C. E., and Worsnop, D. R.: Measurements of Morphology Changes of Fractal Soot Particles Using Coating and Denuding Experiments: Implications for Optical Absorption and Atmospheric Lifetime, *Aerosol Science and Technology*, 41, 734-750, 10.1080/02786820701432632, 2007.

1095 Smekens, A., Godoi, R. H. M., Berghmans, P., and Van Grieken, R.: Characterisation of Soot Emitted by Domestic Heating, Aircraft and Cars Using Diesel or Biodiesel, *Journal of Atmospheric Chemistry*, 52, 45-62, 10.1007/s10874-005-6903-7, 2005.

1100 Steane, A. M.: Phase Change, in: *Thermodynamics: A Complete Undergraduate Course*, Oxford University Press, 2016.

- Timko, M. T., Albo, S. E., Onasch, T. B., Fortner, E. C., Yu, Z., Miake-Lye, R. C., Canagaratna, M. R., Ng, N. L., and Worsnop, D. R.: Composition and Sources of the Organic Particle Emissions from Aircraft Engines, *Aerosol Science and Technology*, 48, 61-73, 10.1080/02786826.2013.857758, 2014.
- 1105 Tritscher, T., Jurányi, Z., Martin, M., Chirico, R., Gysel, M., Heringa, M. F., DeCarlo, P. F., Sierau, B., Prévôt, A. S. H., Weingartner, E., and Baltensperger, U.: Changes of Hygroscopicity and Morphology During Ageing of Diesel Soot, *Environmental Research Letters*, 6, 034026, 10.1088/1748-9326/6/3/034026, 2011.
- Tsigaridis, K., and Kanakidou, M.: Global Modelling of Secondary Organic Aerosol in the Troposphere: A Sensitivity Analysis, *Atmos. Chem. Phys.*, 3, 1849-1869, 10.5194/acp-3-1849-2003, 2003.
- 1110 Tsimpidi, A. P., Karydis, V. A., Zavala, M., Lei, W., Molina, L., Ulbrich, I. M., Jimenez, J. L., and Pandis, S. N.: Evaluation of the Volatility Basis-Set Approach for the Simulation of Organic Aerosol Formation in the Mexico City Metropolitan Area, *Atmos. Chem. Phys.*, 10, 525-546, 10.5194/acp-10-525-2010, 2010.
- Tully, F. P., Ravishankara, A. R., Thompson, R. L., Nicovich, J. M., Shah, R. C., Kreutter, N. M., and Wine, P. H.: Kinetics of the Reactions of Hydroxyl Radical with Benzene and Toluene, *The Journal of Physical Chemistry*, 85, 2262-2269, 10.1021/j150615a025, 1981.
- 1115 Vali, G., DeMott, P. J., Möhler, O., and Whale, T. F.: Technical Note: A Proposal for Ice Nucleation Terminology, *Atmos. Chem. Phys.*, 15, 10263-10270, 10.5194/acp-15-10263-2015, 2015.
- Vander Wal, R. L., Bryg, V. M., and Huang, C.-H.: Aircraft Engine Particulate Matter: Macro- Micro- and Nanostructure by Hrtm and Chemistry by Xps, Combustion and Flame, 161, 602-611, 10.1016/j.combustflame.2013.09.003, 2014.
- 1120 Volkamer, R., Platt, U., and Wirtz, K.: Primary and Secondary Glyoxal Formation from Aromatics: Experimental Evidence for the Bicycloalkyl–Radical Pathway from Benzene, Toluene, and P-Xylene, *The Journal of Physical Chemistry A*, 105, 7865-7874, 10.1021/jp010152w, 2001.
- Wang, Y., Liu, F., He, C., Bi, L., Cheng, T., Wang, Z., Zhang, H., Zhang, X., Shi, Z., and Li, W.: Fractal Dimensions and Mixing Structures of Soot Particles During Atmospheric Processing, *Environmental Science & Technology Letters*, 4, 487-493, 10.1021/acs.estlett.7b00418, 2017.
- 1125 Wang, Y., Liu, H., and Lee, C.-F. F.: Particulate Matter Emission Characteristics of Diesel Engines with Biodiesel or Biodiesel Blending: A Review, *Renewable and Sustainable Energy Reviews*, 64, 569-581, <https://doi.org/10.1016/j.rser.2016.06.062>, 2016.
- Welti, A., Lüönd, F., Stetzer, O., and Lohmann, U.: Influence of Particle Size on the Ice Nucleating Ability of Mineral Dusts, *Atmos. Chem. Phys.*, 9, 6705-6715, 10.5194/acp-9-6705-2009, 2009.
- 1130 Wey, C., Anderson, B., Hudgins, C., Wey, C., Li-Jones, X., Winstead, E., Thornhill, L., Lobo, P., Hagen, D., and Whitefield, P.: Aircraft Particle Emissions Experiment (Apex), 2006.
- Winterhalter, R., Herrmann, F., Kanawati, B., Nguyen, T. L., Peeters, J., Vereecken, L., and Moortgat, G. K.: The Gas-Phase Ozonolysis of B-Caryophyllene (C15h24). Part I: An Experimental Study, *Physical Chemistry Chemical Physics*, 11, 4152-4172, 10.1039/B817824K, 2009.

Formatted: Font: 10 pt

Formatted: Font: 10 pt

- 135 Wolf, M. J., Coe, A., Dove, L. A., Zawadowicz, M. A., Dooley, K., Biller, S. J., Zhang, Y., Chisholm, S. W., and Cziczo, D. J.: Investigating the Heterogeneous Ice Nucleation of Sea Spray Aerosols Using *Prochlorococcus* as a Model Source of Marine Organic Matter, *Environmental science & technology*, 53, 1139-1149, 10.1021/acs.est.8b05150, 2019.
- 140 Yee, L. D., Craven, J. S., Loza, C. L., Schilling, K. A., Ng, N. L., Canagaratna, M. R., Ziemann, P. J., Flagan, R. C., and Seinfeld, J. H.: Effect of Chemical Structure on Secondary Organic Aerosol Formation from C₁₂ Alkanes, *Atmos. Chem. Phys.*, 13, 11121-11140, 10.5194/acp-13-11121-2013, 2013.
- Yu, P., Toon, O. B., Bardeen, C. G., Zhu, Y., Rosenlof, K. H., Portmann, R. W., Thornberry, T. D., Gao, R.-S., Davis, S. M., Wolf, E. T., de Gouw, J., Peterson, D. A., Fromm, M. D., and Robock, A.: Black Carbon Lifts Wildfire Smoke High into the Stratosphere to Form a Persistent Plume, *Science*, 365, 587-590, 10.1126/science.aax1748, 2019.
- 145 Zawadowicz, M. A., Abdelmonem, A., Mohr, C., Saathoff, H., Froyd, K. D., Murphy, D. M., Leisner, T., and Cziczo, D. J.: Single-Particle Time-of-Flight Mass Spectrometry Utilizing a Femtosecond Desorption and Ionization Laser, *Analytical Chemistry*, 87, 12221-12229, 10.1021/acs.analchem.5b03158, 2015.
- Zhang, C., Hui, X., Lin, Y., and Sung, C.-J.: Recent Development in Studies of Alternative Jet Fuel Combustion: Progress, Challenges, and Opportunities, *Renewable and Sustainable Energy Reviews*, 54, 120-138, 10.1016/j.rser.2015.09.056, 2016.
- 150 Zhang, R., Khalizov, A. F., Pagels, J., Zhang, D., Xue, H., and McMurry, P. H.: Variability in Morphology, Hygroscopicity, and Optical Properties of Soot Aerosols During Atmospheric Processing, *Proc Natl Acad Sci U S A*, 105, 10291-10296, 10.1073/pnas.0804860105, 2008.
- Zhang, X., Chen, X., and Wang, J.: A Number-Based Inventory of Size-Resolved Black Carbon Particle Emissions by Global Civil Aviation, *Nature communications*, 10, 534, 10.1038/s41467-019-08491-9, 2019a.
- 155 Zhang, Y., Chen, Y., Lambe, A. T., Olson, N. E., Lei, Z., Craig, R. L., Zhang, Z., Gold, A., Onasch, T. B., Jayne, J. T., Worsnop, D. R., Gaston, C. J., Thornton, J. A., Vizuete, W., Ault, A. P., and Surratt, J. D.: Effect of the Aerosol-Phase State on Secondary Organic Aerosol Formation from the Reactive Uptake of Isoprene-Derived Epoxidiols (Iepox), *Environmental Science & Technology Letters*, 5, 167-174, 10.1021/acs.estlett.8b00044, 2018a.
- 160 Zhang, Y., Favez, O., Canonaco, F., Liu, D., Močnik, G., Amodeo, T., Sciare, J., Prévôt, A. S. H., Gros, V., and Albinet, A.: Evidence of Major Secondary Organic Aerosol Contribution to Lensing Effect Black Carbon Absorption Enhancement, *npj Climate and Atmospheric Science*, 1, 47, 10.1038/s41612-018-0056-2, 2018b.
- 165 Zhang, Y., Katira, S., Lee, A., Lambe, A. T., Onasch, T. B., Xu, W., Brooks, W. A., Canagaratna, M. R., Freedman, A., Jayne, J. T., Worsnop, D. R., Davidovits, P., Chandler, D., and Kolb, C. E.: Kinetically Controlled Glass Transition Measurement of Organic Aerosol Thin Films Using Broadband Dielectric Spectroscopy, *Atmos. Meas. Tech.*, 11, 3479-3490, 10.5194/amt-11-3479-2018, 2018c.

- Zhang, Y., Liu, F., Clavel, D., Smallwood, G. J., and Lou, C.: Measurement of Soot Volume Fraction and Primary Particle Diameter in Oxygen Enriched Ethylene Diffusion Flames Using the Laser-Induced Incandescence Technique, *Energy*, 177, 421-432, <https://doi.org/10.1016/j.energy.2019.04.062>, 2019b.
- 1170 Zhang, Y., Nichman, L., Spencer, P., Jung, J. I., Lee, A., Heffernan, B. K., Gold, A., Zhang, Z., Chen, Y., Canagaratna, M. R., Jayne, J. T., Worsnop, D. R., Onasch, T. B., Surratt, J. D., Chandler, D., Davidovits, P., and Kolb, C. E.: The Cooling Rate- and Volatility-Dependent Glass-Forming Properties of Organic Aerosols Measured by Broadband Dielectric Spectroscopy, *Environmental Science & Technology*, 53, 12366-12378, 10.1021/acs.est.9b03317, 2019c.
- 1175 Zhang, Y., Sanchez, M. S., Douet, C., Wang, Y., Bateman, A. P., Gong, Z., Kuwata, M., Renbaum-Wolff, L., Sato, B. B., Liu, P. F., Bertram, A. K., Geiger, F. M., and Martin, S. T.: Changing Shapes and Implied Viscosities of Suspended Submicron Particles, *Atmos. Chem. Phys.*, 15, 7819-7829, 10.5194/acp-15-7819-2015, 2015.
- 1180 Zhao, D. F., Buchholz, A., Kortner, B., Schlag, P., Rubach, F., Fuchs, H., Kiendler-Scharr, A., Tillmann, R., Wahner, A., Watne, Å. K., Hallquist, M., Flores, J. M., Rudich, Y., Kristensen, K., Hansen, A. M. K., Glasius, M., Kourtchev, I., Kalberer, M., and Mentel, T. F.: Cloud Condensation Nuclei Activity, Droplet Growth Kinetics, and Hygroscopicity of Biogenic and Anthropogenic Secondary Organic Aerosol (Soa), *Atmos. Chem. Phys.*, 16, 1105-1121, 10.5194/acp-16-1105-2016, 2016.
- 1185 Zhao, L., Yang, T., Kaiser, R. I., Troy, T. P., Ahmed, M., Ribeiro, J. M., Belisario-Lara, D., and Mebel, A. M.: Combined Experimental and Computational Study on the Unimolecular Decomposition of Jp-8 Jet Fuel Surrogates. Ii: N-Dodecane (N-C12h26), *The Journal of Physical Chemistry A*, 121, 1281-1297, 10.1021/acs.jpca.6b11817, 2017.

Formatted: Font: 10 pt

Formatted: Font: 10 pt